Studies of translation, on the ensemble level using *in vivo* techniques and on the single molecule level using optical tweezers.

Ph.D. thesis by
Cand. Scient. Thomas Møller Hansen

Advisors: Lene B. Oddershede, Niels Bohr Institute, and
Michael A. Sørensen, Institute of Molecular Biology and Fysiology.

University of Copenhagen 2007

Contents

Chapter 1.

Preface

Welcome to the world of biological macromolecules. It is a world at the scales of piconewtons and nanometers. Welcome to the world of protein synthesis in a living cell, in particular the mechanism of programmed ribosomal frameshifting.
For a person interested in molecular biology, an optical tweezers is a new tool to investigate biological macromolecules on the single molecule level. It is a tool which measures forces and distances at scales relevant to the motion and forces exerted by biological macromolecules. In this thesis the optical tweezers are used to investigate the unfolding of mRNA pseudoknots. Literally, the experimenter has holds on each side of the knot and pulls until it unwinds. The pseudoknots have a function in the stimulation of ribosomal frame shifting during the translation of certain mRNA's. The measurements of the unfolding of mRNA pseudoknots on the single molecule level are compared to ensemble measurements of the same pseudoknots ability to stimulate ribosomal frameshifting in living cells.

Thesis outline

One point is important to keep in mind while reading this thesis: When working toward the goal of unfolding the RNA pseudoknots, I started practicing by using a larger molecule. Gradually I made the molecule smaller in order to keep control of the experiment even though, at last the molecule was so small, that it was hard to see what I was doing.

The thesis starts with two chapters introducing important background knowledge before it goes on with the chapters more directly related to the experiments and results.

Chapter 2. Programmed Ribosomal Frameshifting.

This chapter introduces the concept of ribosomal frameshifting which occurs during the translation (protein synthesis) of certain genes. Current models of the mechanism are reviewed.

Chapter 3. Single Molecule Biophysics.

This chapter introduces the three topics from biophysics relevant for this thesis: Optical tweezers, elasticity of biopolymers, thermodynamic and kinetics in RNA pseudoknot unfolding experiments.

Chapter 4. Materials and methods

The Materials and Methods chapter gives a description of the different experimental procedures used. To get full value of this chapter, the reader is welcome to go back to relevant parts of the chapter while reading the results chapter.

Chapter 5. Results.

This chapter gives the results of the experiments. It describes measurements of frameshifting in *Escherichia coli* bacterial cells. Using the optical tweezers, single DNA molecules were stretched. These experiments gave valuable experience with this type of experiments, which made the final experimental goal possible. The goal was the unfolding of RNA pseudoknots.

Chapter 6. Discussion.

In the Discussion, the results of unfolding RNA pseudoknots using the optical tweezers are related to the biological function of the RNA pseudoknots.

Appendix

The appendix contains the scientific papers to which I contributed during my thesis work.

Acknowledgements

Many people have contributed to this project and helped me with their ideas, knowledge, and moral support. Without that support, this thesis would not have been possible. I would like to thank everybody, who has helped me with this Ph.D. project.

The idea of investigation of ribosomal frameshifting with optical tweezers appeared a day at the Department of Molecular Cell Biology University of Copenhagen when Stanley Brown showed me a paper by Michelle Wang. She exerted and measured the force able to stall active RNA polymerases. Wang used optical tweezers and single molecules of RNA polymerase. Back then, I was dealing with protein synthesis and ribosomal frameshifting in my master thesis, and the single molecule optical tweezers methods instantly seemed as the perfect tool for a study of protein synthesis and ribosomal frameshifting. The possibility of getting a handle on a single ribosome and measure forces and distances was very appealing to me. It was far from the experimental tools in genetics and molecular biology, I was familiar with. The idea of capturing particles in a laser beam sounded like science fiction but in some ways the experiment was: grap the thing and pull. Stanley also informed me of the newly formed optical tweezers group led by Lene Oddershede at the nearby Niels Bohr Institute.

The idea was presented to my master thesis supervisor, Steen Pedersen, who suggested me to do a Ph. D. project in collaboration with the optical tweezers group. Lene liked the idea and after finishing my masters, we went on to apply for money. During this process Steen got a new position as head of department and then I had to look for another supervisor within the biology side. This is where Michael Sørensen came in. He had been a former student of Steen and together they had had a close collaboration in the field of protein synthesis for several years. Michael told me he could supervise me in the molecular biology issues but the physics part was of my own risk.

Many of us biologists fear the heavy equations, which physicist seem to joggle along at ease. Still, I liked the equations that I actually did understand, and I decided to take the

risk trusting Lene would be able to guide me through the physics. After all, though molecular biology and biophysics are two different disciplines, they both study the same phenomena. Michael kept his promise. Lene rewarded my trust.
Lene and Michael, it has been some years of great learning for me in the field of science and we got some valuable experimental results. Sometimes the experiments gave me a hard time, and I lost my patience and positive spirit. Thank you for your moral support. Somewhere in the middle of the project, Nader too came along as a visiting post doc and joined our team. Nader, your contributions have really been decisive and I have enjoyed your company in the lab.

I'm very pleased to hear, that Lene and Michael wish to maintain their collaboration and plan to continue the studies of translation using optical tweezers.

Chapter 2.

Programmed Ribosomal Frameshifting

Synthesis of a protein in a living cell, involves two major steps. First, a working copy of a gene, an mRNA, is synthesized in the process of transcription. Second, protein is synthesized using the information read in mRNA in the process of translation. The subject of this chapter is programmed ribosomal frameshifting, which takes place during the translation process of some genes. The machinery that translates the RNA is the tRNA's, the ribosome, and related protein factors. The ribosome is a molecular motor and moves along the mRNA string, while reading the genetic information in a sequential manner and synthesizing the protein accordingly.

An mRNA is read in codons of three nucleotides and therefore it has in principle three reading frames. In the vast majority of genes only one reading frame, defined by the initiation codon, is exploited and translated into protein. The elongation phase of protein synthesis is a precise process and mechanisms exist to promote translational fidelity. The frequency of frameshift errors have been estimated to less than 3×10^{-5} (Atkins et al., 1972; Kurland, 1979). However, a growing number of highly efficient programmed frameshift sites have been described (Farabaugh, 1996; Gesteland and Atkins, 1996). Currently, close to 100 examples of -1 frameshifting and a similar number of +1 ribosomal frameshifting have been listed in the Recode database (URL: http://recode.genetics.utah.edu/ , (Baranov et al., 2003)). There is considerable interest in how ribosomal frameshift occurs, as this may provide insights into normal frame maintenance, tRNA movement and unwinding of mRNA secondary structures by ribosomes. The -1 frameshift sites is found in both eukaryotic and prokaryotic cellular genes, but the majority is in viruses, bacteriophages and mobile genetic elements. Typically, they comprise a heptameric slippery sequence, where the frameshifting occurs, and a stimulatory RNA element.

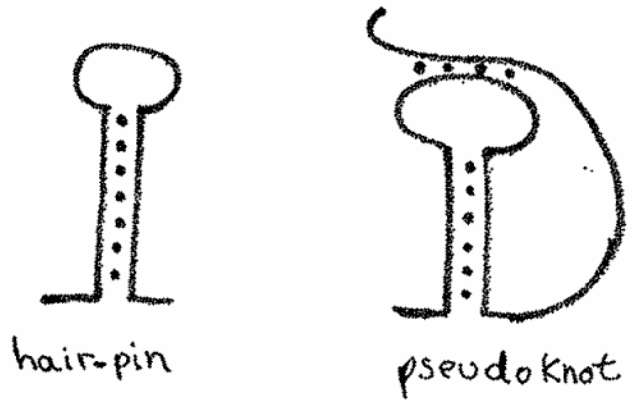

Figure 1. Schematic drawing of a RNA hairpin (stem loop) and pseudoknot. The dots symbolize the bonds in the basepairs. In a RNA hairpin the RNA strand loops back and forms basepairs to it self. The result is a double stranded helix (stem) and single strand loop on top. In a pseudoknot the singlestrand

folds back to the loop and forms basepairs with nucleotides in the loop, and this way a second helix forms. The pseudoknot in the drawing has two helixes and three loops. The pseudoknots in this thesis have two loops only, corresponding to the left and right loop in the drawing. With zero nucleotides to form the middle loop the stems form a qasicontinues helix.

Frameshifts are thought to happen by dual tRNA slippage. The slippery sequence can be written as X XXY YYZ. In the zero phase the P-site tRNA and A-site tRNA pair to XXY and YYZ, respectively. After the shift to the -1 phase they pair to XXX and YYY. Following the frameshift, the tRNAs remain paired to the mRNA at the two non-wobble anticodon bases. In the original model the dual slippage of the tRNAs was proposed to happen simultaneously (Jacks et al., 1988). However, it was recently argued that the frameshift certainly involves dual slippage but it is likely not simultaneously. P-site tRNA rearrangement relative to mRNA should first provide a space for A-site tRNA repositioning (Baranov et al., 2004). Examples of stimulatory elements include 5' Shine-Dalgarno like sequences as well as 3' stem loops and pseudoknots (Figure 1), which are placed at an optimal distance from the slippery sequence. In many viral frameshift sites the stimulatory element is a pseudoknot 3' of the slippery sequence, see Figure 2.

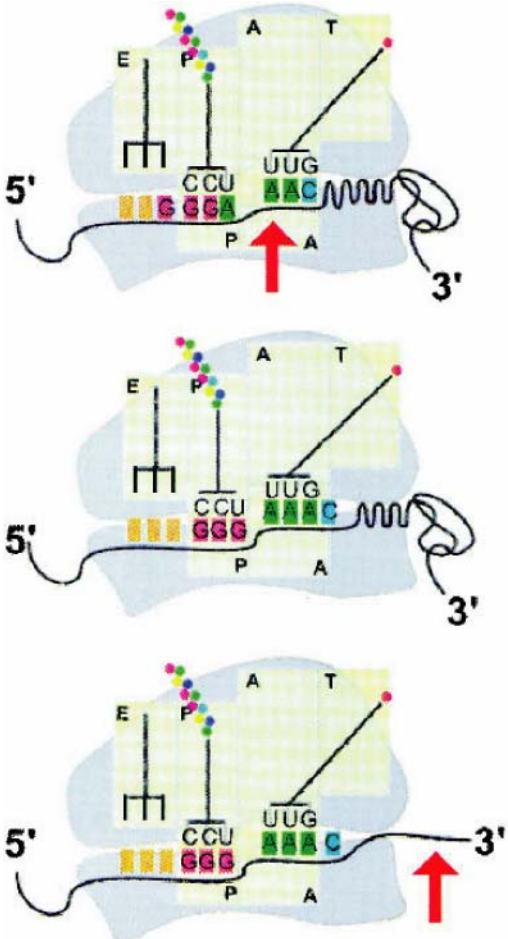

Figure 2. Overview of programmed –1 ribosomal frameshifting. (*Top*) The elongating ribosomes encounter an mRNA pseudoknot with their A- and P-site tRNAs positioned over the heptameric X XXYYYZ "slippery site" (red arrow). The incoming frame is indicated by spaces. (*Middle*) While at the slippery site, if the ribosome shifts by 1 base in the 5' direction, the non-wobble bases of both the A- and

P-site tRNAs can re-pair with the new −1 frame codons. (*Bottom*) The mRNA pseudoknot is denatured (arrow), and elongation continues in new reading frame. The illustration is from (Plant et al., 2003).

The mechanism of frameshift stimulation is not well understood. Involvement of protein factors binding to the RNA seems unlikely since in a competition experiment addition of excess RNA pseudoknots did not affect frameshift efficiencies (ten Dam et al., 1994). Furthermore, many pseudoknots stimulated programmed frameshifts function in heterologous organisms from different kingdoms of life and make it unlikely that the function requires trans-acting factors.

It has been suggested that the stimulatory structure pauses the ribosome while the slippery sequence is positioned in the decoding site of the ribosome, thereby increasing the chance of tRNA slippage. The data from measurements of ribosomal pausing with pseudoknots, mutated pseudoknots, and related stem-loops support the view that pausing alone is insufficient to mediate frameshifting and additional events are required (Kontos et al., 2001; Tu et al., 1992). In IBV (Infectious Bronchitis Virus) stem-loops and pseudoknots apparently induce the same amount of ribosomal pausing, while only the pseudoknot stimulate efficient frameshifting (Kontos et al., 2001).

A pseudoknot can be viewed as a stem-loop where nucleotides in the loop forms a second stem with 3' mRNA. This may lock or decrease the rotational freedom of the first stem, and induce super coiling while the ribosome unfolds the first stem. Experimental data support a role for torsional restraint in positioning the ribosome to pause with the slippery sequence in the A- and P-site when unfolding pseudoknots (Plant and Dinman, 2005). It is clear that an optimal spacing of 6-9 nt between the slippery sequence and the pseudoknot is crucial, and positions the pseudoknot close to the entrance of the mRNA tunnel of the ribosome.

The '9 Å model' was suggested for the mechanism of frameshift stimulation (Plant et al., 2003), see Figure 3. Movement of 9 Å by the anticodon loop of the aminoacyl-tRNA at the accommodation step normally pulls the downstream mRNA a similar distance along with it. The authors suggest that the downstream mRNA pseudoknot provides resistance to this movement by becoming wedged into the entrance of the ribosomal mRNA tunnel. These two opposing forces result in the creation of a local region of tension in the mRNA between the A-site codon and the mRNA pseudoknot. The tension can be relieved by one of two mechanisms; unwinding the pseudoknot, allowing the downstream region to move forward, or by slippage of the proximal region of the mRNA backwards by one base. Even if mRNA slips backwards one base, then still, afterwards, the ribosome will have to unwind the pseudoknot in order to move forward. After the -1 nt slip the next translational step will be correspond to + 3 nt as usual. The tension will be bigger than after previous translational step and hence the chance of unfolding the pseudoknot is bigger.

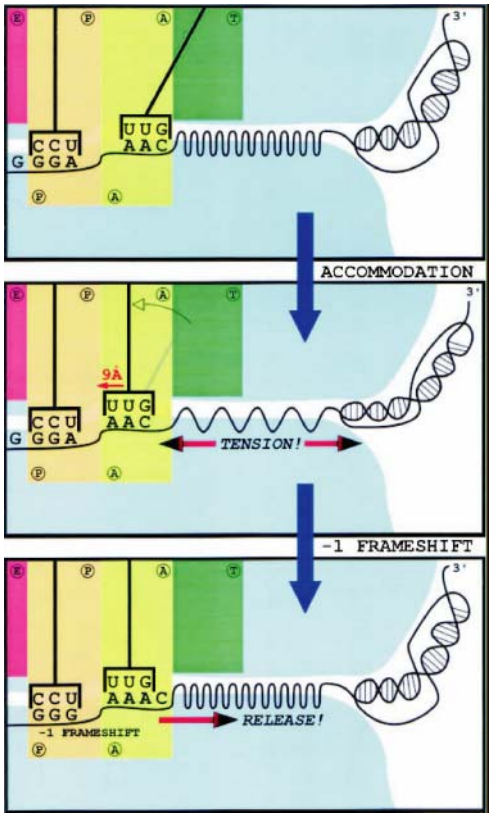

Figure 3. The 9-Å model. (*Top*) The 0-frame A- and P-site codons of a programmed −1 ribosomal frameshift signal are base paired to cognate peptidyl- and aa-tRNAs occupying the P/P and A/T hybrid states respectively. (*Middle*) Upon accommodation, the anticodon loop of the aa-tRNA moves 9 Å in the 5' direction, pulling the 3' mRNA sequence along with it. The mRNA pseudoknot is too large to enter the downstream tunnel, with the consequence that the linker region between the A-site codon and the mRNA pseudoknot is stretched, creating a localized region of tension in the linker mRNA. (*Bottom*) Decoupling of the A- and P-site codon:anticodon interactions from the 0-frame, and re-pairing in the −1 frame repositions the mRNA so as to relieve the tension. The illustration is from (Plant et al., 2003).

Support for this mechanical model for the stimulation of ribosomal frameshifting comes from the observation of a deformed t-RNA in the A-site of a ribosome interacting with a mRNA pseudoknot (Namy et al., 2006). Another important piece of information on the stimulation of ribosomal frameshifting emerge from a comparison of the programmed frameshifting in the *dnaX* and *prfB* genes of *Escherichia coli* (Atkins et al., 2001). A sequence upstream of the slippery sequence stimulates ribosomal frameshifting in these two mRNA. The upstream stimulatory sequence resembles the Shine-Dalgarno (SD) sequence known from initiation on bacterial mRNAs, and it forms bonds (basepairs) to the 16S ribosomal RNA (Larsen et al., 1994; Weiss et al., 1988). In *prfB* the frameshift is +1 and the spacer between the SD-like sequence and the P-site is three nucleotides. In *dnaX* the frameshift is -1 and the spacer is 12 nucleotides. This suggests that when the SD binds to the ribosome, in *prfB* the mRNA is pulled into the +1 frame, whereas in *dnaX* the mRNA is pushed into the -1 frame. At initiation sites the corresponding distance between SD and initiation codon are intermediary. The most common spacer is eight nucleotides. Intriguing, when the spacer in *dnaX* frameshiftsite is mutated down to three nucleotides the SD-like sequence inhibit -1 frameshifting (Larsen et al., 1994).

In a mechanical model, as in the pausing model, the unfolding kinetics and stability of pseudoknots might play an important role in stimulation of frameshift. A correlation has

not been found between frameshifting frequencies and the difference in Gibbs free energy (ΔG) between folded and unfolded pseudoknots measured from UV optical melting profiles (Giedroc et al., 2000). In the *dnaX* case the downstream stimulatory element is a hairpin rather than a pseudoknot. A correlation is seen between the Gibbs free energy (ΔG) difference of folded and unfolded hairpin and frameshifting efficiency (Larsen et al., 1997).

While the energy difference of the folded and unfolded states is an intrinsic property of the structure, the kinetics is dependent on the reaction coordinate. When the pseudoknot is opened by a ribosome, this might not happen in a reversible manner, i.e. the work performed by the ribosome might be larger than ΔG, and a substantial fraction of the work might be dissipated irreversibly. The unfolding process may not be an equilibrium process and hence the kinetics crucially depend on the actual work done, not just on ΔG for the process. The scope of this thesis was to resemble the action of a ribosome. We mechanically unfolded pseudoknot using optical tweezers. By applying a load on the structure it is forced to unfold.

Chapter 3.

Single Molecule Biophysics

This thesis is a cross-over of molecular biology and biophysics. This chapter is devoted to explain some basic concepts in biophysics, and thereby make it easier to understand experiments and discussion of results in the forthcoming chapters. The first section is about the optical tweezers, the instrument used in the single molecule experiments in this thesis. The second section considers the elasticity of RNA and DNA, which is important because most of the experiments involve stretching a single RNA or DNA molecule. In the third and fourth section the unfolding of RNA structures e.g. pseudoknots is introduced in terms of thermodynamics and kinetics.

3.1 Optical tweezers. Trapping, detection and calibration.

As the name implies, with an optical tweezers you can grap and hold an object using a beam of light. It might sound science fiction and it is certainly not a property of light that we are familiar with from our everyday life. Light has momentum. When a milli Watts intensity tightly focused laser beam is applied on the scale of a microscope, the forces exerted by the light beam are significant. Optical trapping, optical tweezers, laser traps or laser tweezers are synonyms for a versatile technique used to manipulate microscopic objects with light radiation.

The first optical tweezers was proposed by Ashkin and coworkers in the seventies and one particular trapping scheme demonstrated in 1986 is now used to study living cells and biological macromolecules (Svoboda and Block, 1994). The use of optical tweezers to study the macromolecules of living cells has been growing steadily for the last 15 years, and examples of the studies includes DNA, RNA, the package of DNA into virus particles, motors on DNA: polymerases and isomerases, motors on the cytoskeleton: kinesin, and muscle fibers: actin and myosin.

The optical tweezers can trap living cells, or beads of e.g. gold, sillica or polystyrene. In this work micron sized polystyrene beads were trapped. The forces exerted on the trapped bead are in the order of pN and with a proper detection scheme positions are measured on a nm scale. This allows the experimenter to probe mechanics on an energy scale close the thermal energy, k_BT, where many biological phenomena take place. This is the energy scale of many biochemical reactions and of phenomena related to biological macromolecules. Boltzmann's constant is $k_B = 1.38 \times 10^{-23}$ J/K and T is the absolute temperature. At room temperature, 25 °C, k_BT is $k_BT = 4.12 \times 10^{-21}$ J = 4.12 pN × nm. ATP (Adenosine-Tri-Phosphate) is often referred to as the energy coin of the living cell and the hydrolysis one molecule of ATP ($ATP \rightarrow ADP + P_i$) releases about 50 pN × nm of free energy.

The main components of the optical tweezers are an infrared laser (1064 nm) and an inverted microscope. The wave length of the laser suits experiments with biological

materials, since they absorb very little light of this wave length. The illustration in Figure 4 schematically shows the path of the laser beam. More technical details and a reference for the optical tweezers equipment are given in the Materials and Methods section. Here I'll try to explain the basic principles of trapping, detection and calibration.

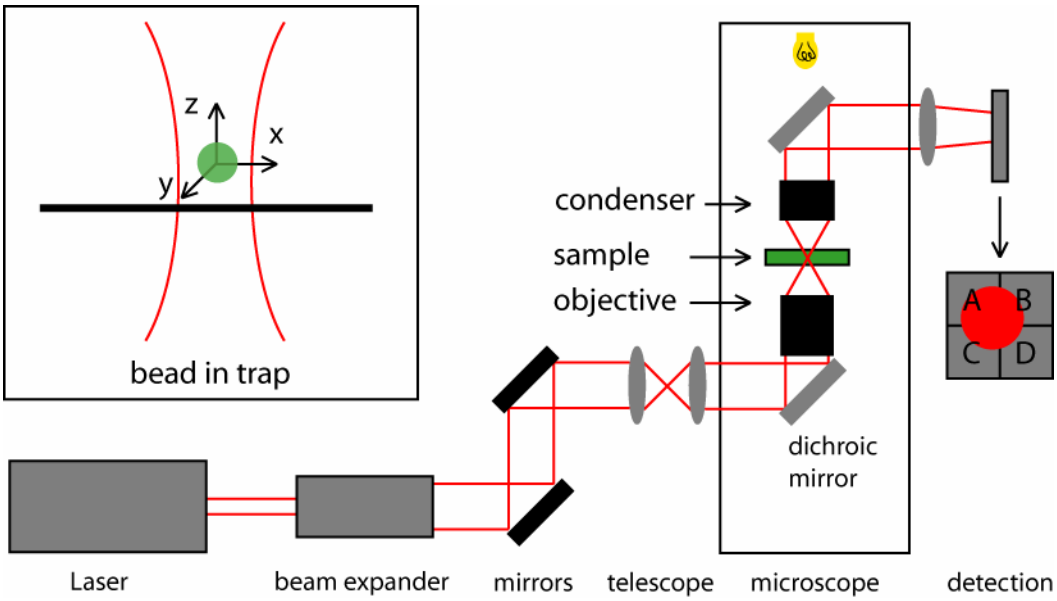

Figure 4. Optical tweezers setup. The laser emits an infrared beam (1064 nm), which is expanded (20X) in order to overfill bottom lens of the objective. The beam is directed into the microscope via two mirrors. Before entering the microscope the beam passes through a telescope consisting of two lenses. The first lens is moveable and serves to steer the position of the trap inside the sample. Inside the microscope, a dichroic mirror directs the beam into the objective, which focuses the beam inside the sample. The insert up left shows a bead positioned in the center of the trap which lies slightly above the focus of the laser beam. The x-y plane perpendicular to the direction of the beam is indicated as well as the z axis in the direction of the beam. The light leaving the sample is collected by the condenser and via another dichroic mirror and a lens; it is projected onto a quadrant photodiode for detection.

Inside the sample the bead is trapped close to center of the trap. How optical trapping works is intuitively understandable in a ray optics view, see Figure 5. The forces shown in Figure 5 are denoted the gradient force. In addition to the gradient force, the laser beam gives rise to another force, the scattering force. This force originates from the light which scatters from the bead and acts in the direction of the beam. The scattering force pushes the trap center slightly above the focus point. The scattering force has practical implications when you aim to trap a bead with the laser tweezers. Trapping a bead is most successful if you position the bead below the trap, and let the scattering force direct the bead towards the trap.

In the ray optics view it is assumed that the wave length of the light is much smaller than the size of the bead, that is however not true in reality. The trapped beads are of micron size and thereby of similar size as the wave length of the laser light used (the intermediate regime). Then the picture in Figure 5 is not valid. However optical trapping works, and when you consider particle properties of light (opposed to wave properties), as in the ray optics view, you intuitively understands how. A theory of optical trapping in the intermediate regime, have been resolved and proven by experimental results, see (Rohrbach, 2005).

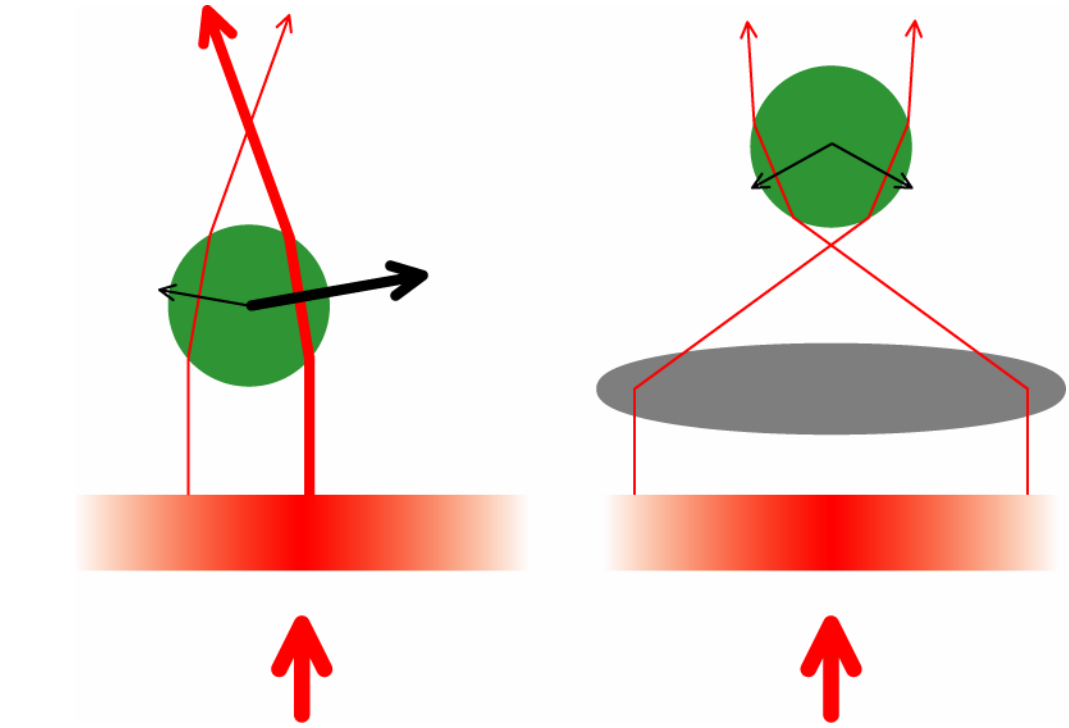

Figure 5. Ray-optical view of optical trapping. The intensity profile of the incoming laser beam is indicated in the red box, showing the highest intensity in the center of the beam. The left panel illustrates trapping in the plane perpendicular to the laser beam. The two rays are refracted as they pass through the bead. Since the ray has momentum, a momentum change counteracting the momentum change of the ray is experienced by the bead. The size of the force is proportional to the intensity of the rays. The right ray has the highest intensity, so the total force on the bead is pointing right towards the center of the laser beam. The right panel illustrates trapping along the axis of the laser beam. A lens focuses the beam. Above the focus point, conservation of momentum pushes the bead towards the focus point.

Detection of the bead positions relative to the trap are accomplished by a detection system in the back focal plane of the condenser. In this detection scheme, the interference pattern of the laser beam and trapped object is projected on a quadrant photodiode, see Figure 4. In this work, the position in the x-y plane perpendicular to the direction of the laser beam was considered. The quadrant photodiode is sketched in Figure 4. The detection principle builds on subtraction of pair vise sums of the light intensity in quadrants. The x-coordinate is calculated as (A+C)-(B+C) and the y-coordinate as (A+B)-(C+D). Detection of the position along the z axis (the direction of the beam) can be accomplished using the sum of the signal from all quadrants.

A key property of the optical trap is that the force exerted on the trapped bead is harmonic to a good approximation. Thus for positions on a coordinate axis (x), the restoring force on the bead is similar to that of a Hookian spring:

$$F(x) = -\kappa_x (x - x_0)$$

where κ_x denotes the spring constant and x_0 is the equilibrium position of the trap, or in other words, the center of the trap. So, by knowing the spring constant and the position of the bead relative to the center of the trap, you can calculate the force acting on the bead. To estimate the position, the signal from the photodiode is used. This is measured

in Volts and to convert to nanometers you need a conversion factor. In the calibration of an optical trap the conversion factor and the spring constant are the parameters you want to estimate.

Gravity and inertia are not significant for the micron sized beads in water. My observation is that the beads sediment slowly, maybe falling 100 μm in several minutes. Besides the forces originating from the laser beam, forces originating from the collisions of molecules of the surrounding media are significant. The molecules of the surrounding media moves around, they have thermal energy. The motion of the bead is denoted Brownian motion. Knowledge of Brownian motion and thermal energy is exploited in the calibration of the optical trap. The parameters to estimate in the procedure, the trap stiffness and conversion factor, depends on bead size and material, and hence the calibration procedure is initiated after a bead has been trapped. To calibrate the trap, a time series of bead positions is sampled, which subsequently is used to estimate the trap stiffness and conversion factor. The bead position is sampled at a certain frequency. In most of the experiments described in this thesis, the sampling frequency was 50 kHz, and hence the time series gives the bead position every 0.02 ms. The distribution of bead positions sampled in a time series is shown in Figure 6, left panel.

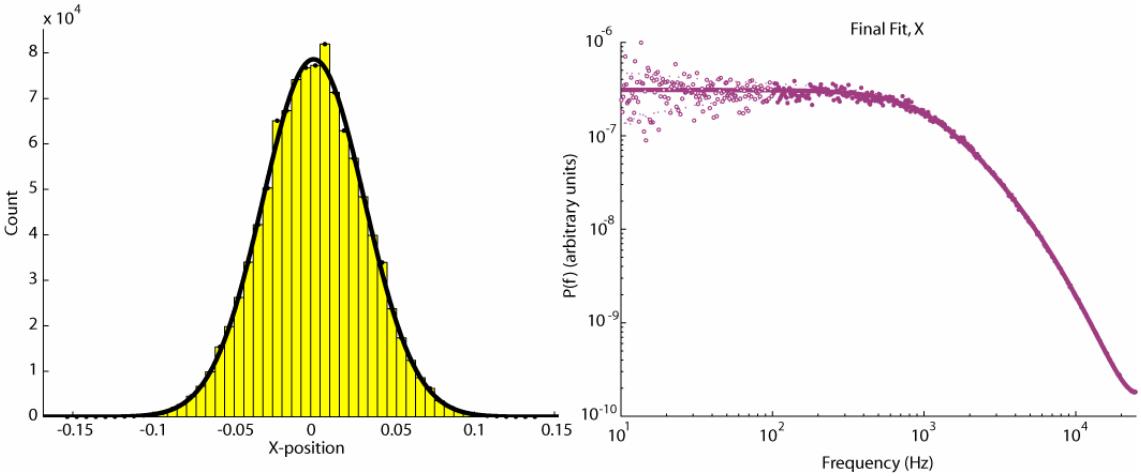

Figure 6. Data for Calibration of the optical trap. Left panel shows the histogram of bead positions along the x-axis (in volts) with a Gaussian curve fitted. Right panel shows the same data transformed to a power spectrum and a fit to the power spectrum. The corner frequency is 1135 Hz and diffusion constant is 7.9 v^2 (v^2 = arbitrary units in graph). Which then gives a spring constant κ_x= 0.141 pN/nm and conversion factor of 227 nm/v (2.1 μm bead diameter, T=20 °C).

The data in the time series is transformed to show the power spectral density as a function of frequency *S(f)*. This a practical way to evaluate the data since from the theory of Brownian motion it is known to have the following distribution (Berg-Sorensen et al., 2003; Svoboda and Block, 1994),

$$S(f) = \frac{k_B T}{\pi^2 \gamma (f^2 + f_c^2)},$$

where γ is the viscous friction and

$$f_c = \frac{\kappa}{2\pi\gamma}$$

The spring constant, κ, is found from the corner frequency, f_c. The viscous friction is found from Stokes law, $\gamma=6\pi\eta r$, where η is the fluid viscosity and r is the bead radius. In the calibration fits done in this work, fitting parameters are D_v and f_c in the following equation:

$$S_v(f) = \frac{D_v}{2\pi^2(f^2 + f_c^2)}$$

To find the conversion factor, A, for the units on the length scale we use:

$$S(f) = A^2 S_v(f) \Leftrightarrow A = \sqrt{\frac{k_B T}{\gamma D_v}}$$

Figure 6 right panel, shows a typical power spectrum for the trap used in this work. The spring constant was calculated to, κ_x= 0.141 pN/nm, and the conversion factor, A= 227 nm/v.

Before we got to the point where we were able to use the actual mechanical unfolding of the pseudoknots, we went through a lot of trial and error with different aspects of the laser trap equipment. Below, I will summarize two points that we learned in this process:

1. Removal of unwanted noise from the signal of bead positions in the optical trap. This is the signal detected by the quadrant photodiode. When we examined our first time series of a trapped bead, the data clearly represented the Brownian motion of the bead, but also another random fluctuation. It was much slower, with periods about seconds, and had significantly larger amplitude, in the order of 50 nm. Such fluctuations would distort our measurements, since we expected a rip length of 15-20 nm (rip length is the increase in end-to-end distance observed when a pseudoknot unfolds). We suspected some component in the optical path of the laser to be the cause of this noise. Mirrors and lenses were checked to ensure that all screws were tight. Even the laser had a service check. One night, after several weeks of searching for the reason of the noise, Nader Reihani turned of the microscope and after about half an hour, he observed the noise to slowly disappear. He reasoned that some of the electrical parts of the microscope produced heat and heated the air in the laser path. Since changing the temperature of the air changes its refractive index, this could bend the laser light and make it fluctuate. We've all seen this phenomenon on a hot summer day. After removing the power supply, which was placed below the beam path at the entrance to the microscope, this noise disappeared.

2. Re-alignment of the laser beam path to improve the trap stiffness. The trap stiffness was too low, to exert the forces that we speculated would unfold the RNA pseudoknots. We knew that a simple hairpin would unfold at 15-20 pN (Liphardt et al., 2001), which was also close to the maximal force we could

obtain. Since the pseudoknots had more hydrogen bonds than those hairpins, we expected force maybe up to 50 pN was needed. After a careful realignment of the components in the laser beam path, we achieved a 5-10 times stronger trap, suitable for our experiments. The realignment included moving the beam expander closer to the laser, which gave a thinner beam after expansion. Before this move, the beam was wider than the mirrors, resulting in the edges of the beam being cut off at the mirrors, and hence a loss of laser power.

3.2 Elasticity of nucleic acid biopolymers

This section will focus on the elasticity of RNA and DNA, but the concepts explained here are also relevant for other biopolymers e.g. the filamentous proteins of the cytoskeleton. Three length parameters, L_c (contour length), r_{ee} (end-to-end distance) and L_p (persistence length), are important in the description of biopolymer elasticity. L_c is the distance along the biopolymer backbone from one end to the other end. The r_{ee} is the shortest distance from one end to the other end of the polymer, see Figure 7.

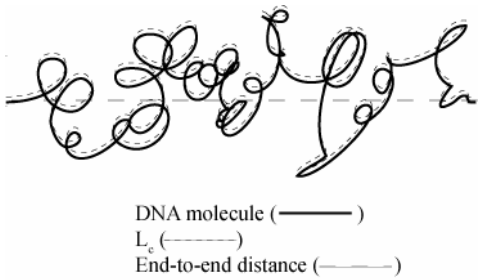

Figure 7. Schematic drawing of a DNA molecule illustrating contour length (L_c) and end-to-end distance (r_{ee}).

For a condensed biopolymer L_c is larger than r_{ee}, but when r_{ee} is increased by stretching of the polymer, r_{ee} approaches L_c. L_p describes the length scale where the biopolymer is a stiff object with regard to thermal fluctuations. $L_p << L_c$ for a soft polymer whereas for a stiff polymer L_c is equal to or smaller than L_p. L_p is independent on r_{ee} and L_c. As an example, imagine the elasticity of a 1 cm diameter steel wire. A piece of the wire only a few centimeters long is a quite stiff and unbendable object, whereas a piece a few meters long is a relatively soft and bendable object. Thus the actual elasticity of molecules made of a certain material depends on the length scale.
Physicists define the persistence length as $L_p = \kappa_f/k_BT$, where κ_f is the flexural rigidity and k_BT is Boltzmann's constant times absolute temperature. The flexural rigidity reflects both geometry and composition of the material. The more stiff the material, or in other words the more energy it costs to bend it, the higher the flexural rigidity is. The definition of persistence length shows the importance of temperature since the persistence length increase as temperature decrease. At zero temperature the polymer adopts a shape that minimizes its energy, which correspond to a straight conformation. With higher temperature the polymer exchange thermal energy with the surroundings making bended conformations more favorable, see Figure 8. For a polymer in water, one might imagine the water molecules shaking and moving around by thermal energy sometimes crashing into the polymer bending it into its condensed conformations. Thus at room temperature and $L_p << L_c$ the polymer is highly bended. This condensed

polymer is fluctuating between conformations with $r_{ee} << L_c$. When taking a statistical mechanics point of view, the polymer conformations have an r_{ee} distributed around a certain average or most probable r_{ee}, which at room temperature is smaller than L_c.

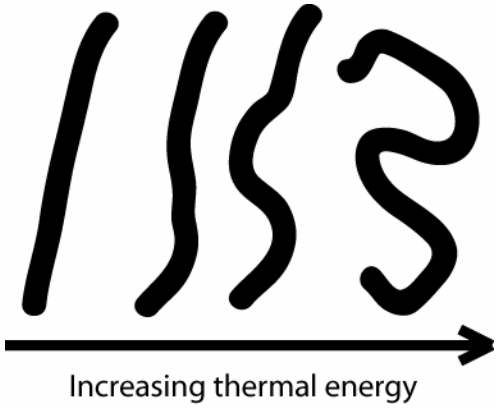

Figure 8. Influence of temperature on persistence length and polymer conformations. Persistence length decreases when temperature increases. The soft polymer exchange thermal energy with the surrounding media and as a result it adopts condensed conformations at higher temperatures.

For double stranded B-DNA at conditions relevant for biological systems, L_p is approximately 50 nm. The contour length is 0.34 nm/bp. Accordingly, the 48 kbp phage lambda DNA molecule has L_c = 16 µm, which is 320 times longer than L_p. This molecule is thus soft and bendable and r_{ee} is expected to be smaller than L_c. In other words, under conditions relevant to biological systems the lambda DNA molecule is fairly condensed.

DNA, rubber and other so called soft polymers are entropic springs. Imagine the lambda DNA or another polymer molecule as a chain of jointed segments where each segment is unbendable and has a length of one L_p. If $r_{ee} = L_c$ then the segments lie on a straight line, and only this conformation is possible. However, if r_{ee} decreases more conformations are possible as shown in Figure 9. More conformations mean less order and higher entropy. Higher entropy (S) means lower free energy (G) since G = H – TS (H is enthalpy and T is temperature). To increase the end-to-end distance by a applying a force and pulling the ends apart costs energy due to the entropy loss. The polymer is elastic due to entropy loss when stretching it, and thus an entropic spring.

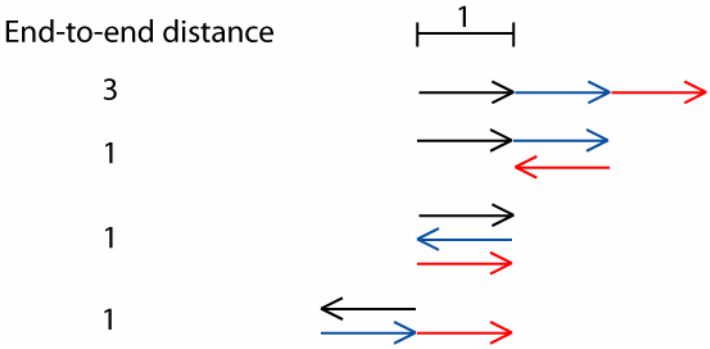

Figure 9. Conformations of an entropic spring. When r_{ee} is 3, the number of conformations possible is one, but when r_{ee} is 1 more conformations are possible. In the figure only positive r_{ee} are considered. More conformations mean higher entropy.

The force (F) as a function of extension or end-to-end distance (r_{ee}), of DNA have been modeled by the standard Worm Like Chain model (WLC) (Marko and Siggia, 1995), (1).

$$F = \frac{k_B T}{L_p}\left(\frac{1}{4(1 - r_{ee}/L_c)^2} - \frac{1}{4} + \frac{r_{ee}}{L_c}\right) \qquad (1)$$

Figure 10 shows force versus extension (r_{ee}) plot of the WLC formula and parameters resembling those of phage lambda DNA at biological conditions. At low extension the force is very small and only slightly increases when the r_{ee} increases. However, when r_{ee} gets close to L_c the force increases dramatically.

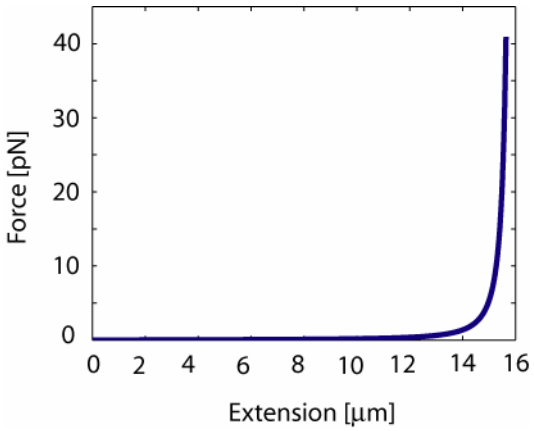

Figure 10. WLC, force vs. extension curve. The curve was plotted using values of L_p = 50 nm and L_c = 16000 nm.

The WLC holds for forces below 10 pN only, whereas the Extensible Worm Like Chain EWLC, inspired by (Odjik, 1995), also works for higher forces up to 50 pN, equation (2). Equation 2 contains an elastic modulus, K, which is mainly determined by the elastic behavior at higher forces up to 50 pN (Wang et al., 1997).

$$F = \frac{k_B T}{L_p}\left(\frac{1}{4(1 - r_{ee}/L_c + F/K)^2} - \frac{1}{4} + \frac{r_{ee}}{L_c} - \frac{F}{K}\right) \qquad (2)$$

In the results section and papers, the WLC and EWLC formulas have been fitted and compared to experimental data from stretching DNA molecules.

The force-extension curve of DNA has a plateau at 65 pN, which is evident in some of the curves shown in the results section. The plateau is not described by any of the WLC equations.

3.3 Thermodynamics

In this thesis, the thermodynamics of interest is those of stretching nucleic acid polymers and the unfolding of RNA pseudoknots by force. The system consist of a single molecule, e.g. a lambda DNA molecule or an RNA pseudoknot, with beads attached in each end, and surrounded by a solvent. The beads are used to apply a force (F) to the molecule, as shown in Figure 14 and Figure 24. The work done by the force equals force times distance, FdX, where X is the end to end distance of the pseudoknot. The first law of thermodynamics states that the change in internal energy of a system equals the sum of heat and work inputs, dU=dq + dw. The equation for the change in internal energy of the system for a reversible process is (using q=TdS):

$$dU=TdS-PdV+FdX.$$

For chemical reactions Gibb's free energy (G) rather than U is commonly used to describe the state of a system. The definition of Gibb's free energy is G=U+PV-TS (or G=H-TS, when using the enthalpy H=U+PV). The change in Gibb's free energy, dG, for a reversible reaction is:

$$dG=-SdT+VdP+FdX.$$

Assuming constant temperature and pressure, the change in Gibbs free energy (ΔG) equals the mechanical work for a reversible process, see (Tinoco, 2004). For the reversible stretching of a DNA molecule under constant temperature and pressure the change in free energy equals FdX, e.g. the area under the force vs. extension curve in Figure 10. At constant temperature and pressure, G is a function of X. In addition, the change in Gibb's free energy can also be defined as a function of F (Tinoco, 2004):

$$dG=-SdT+VdP+XdF.$$

Both definitions are useful, depending on the situation.

At room temperature and salt conditions relevant for biological systems, the double stranded DNA (dsDNA) is condensed and behaves elastically due to entropy. For the single stranded RNA (ssRNA) non-entropic contributions play a significant role and structured sections form. The ssRNA forms double stranded helixes, where the RNA strand forms bonds to itself. The bonds are hydrogen bonds, formed between pairs of complementary nucleotides and hence are denoted base pairs. Stacking interactions between the hydrophobic bases of neighboring base pairs in the helixes are also important. Other examples of interactions in RNA structure include coordinated Mg^{2+} ions, and interactions between double stranded helix and a third section of the strand. Formation of structures decrease the number of possible conformations and therefore costs entropy. In the definition of G, there is a negative sign on the entropic part, and which form, structure or non-structure, that has the lowest energy (G, G=H-TS, lowest energy means most stable) depends on a competition between negative enthalpic contributions from the formation of bonds and increase of entropy from formation of non-structured single strand.

Above approximately 70°C, double stranded nucleic acids denature and RNA structures do not form. In the equation for G, this is reflected by the T in the entropic part. The higher the temperature, the more entropy dominates the free energy. For nucleic acids, the non-structured single strand form is more disordered than the double strand form and structures and therefore single strand has the highest entropy. Above approximately 70 °C, this form has the lowest free energy.

The unfolding of an RNA pseudoknot or the denaturation of dsDNA can be defined as two-state processes. The two states are folded or unfolded and double stranded or single stranded, respectively. At a certain temperature the free energy of the folded pseudoknot equals the free energy of the unfolded pseudoknot and hence $\Delta G = G_{unfolded} - G_{folded} = 0$. This temperature is the melting temperature, T_m.

Now, consider the unfolding of an RNA pseudoknot by the application of force in a pulling experiment at 25 °C. Assuming no partial unfolded states, the process has two states, the folded state and the unfolded state. How does force affect the unfolding of the pseudoknot? It seems reasonable that pulling on each side of the pseudoknot favors the unfolded state. One can define a melting force, F_m, where $\Delta G = G_{unfolded} - G_{folded} = 0$ in analogy to the melting temperature (Tinoco, 2004). The influence of force on the free energy of unfolding an RNA pseudoknot is depicted in Figure 12. For a pseudoknot at F_m, the likelihood of the folded state equals the likelihood of the unfolded state.

To compare ΔG at zero force (F_0) to ΔG at a non-zero force, e.g. F_m a thermodynamic cycle joining the reactions at the two forces is useful, see Figure 11. Using the definitions of dG as function of F or X, respectively, and assuming constant temperature and pressure, one can write the following equations for ΔG's in the cycle in Figure 11:

$$\Delta G_I = G_{F_m,\,folded} - G_{F_0,\,folded} = \int_{F_0}^{F_m} X(F)_{folded}\, dF$$

$$\Delta G_{II} = G_{F_m,unfolded} - G_{F_m,\,folded} = \int_{X_{folded}}^{X_{unfolded}} F_m\, dX$$

$$\Delta G_{III} = G_{F_0,unfolded} - G_{F_m,unfolded} = \int_{F_m}^{F_0} X(F)_{unfolded}\, dF$$

$$\Delta G = \Delta G_I + \Delta G_{II} + \Delta G_{III}$$

It seems reasonable to assume that the folded structure is non-elastic in comparison with unfolded single strand. One can then assume that the extension of the folded structure $X(F)_{folded}$ does not change from F_0 to F_m and then $\Delta G_I=0$. For the unfolded single strand, one can use the WLC equation to as a function for $X(F)_{unfolded}$, and hence ΔG_{III} is estimated by integration of the WLC equation and using a proper persistence length of single stranded RNA. In other words ΔG_{III} is minus the work of stretching the single strand from extension of the folded pseudoknot to the extension of the single strand at F_m. Finally, ΔG_{II} is estimated experimentally as $F_m \times (X_{unfolded}\text{-}X_{folded})$ in an experiment where the force is held constant at F_m, and the change in extension of the molecule is measured. In summary, the change in free energy at zero force equals the work of unfolding at F_m minus the work of stretching the single strand to its extension at F_m:

$$\Delta G^{\circ} = F_m \times \left(X_{unfolded} - X_{folded}\right) - \int_{F_m}^{F_0} X(F)_{unfolded}\, dF$$

Note that the change in free energy of unfolding is always higher at F>0 than at F=0, because of the work needed to stretch the single strand.

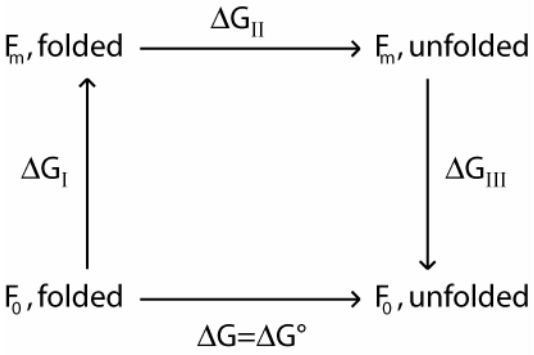

Figure 11. Thermodynamic cycle joining unfolding at two different forces.

Until now in this section, the reversible process has been considered. However, many natural processes are not reversible. As will be shown later, the unfolding of RNA pseudoknots in this work were irreversible processes. This was evident from the hysteresis in the unfolding and refolding curves. Unfolding was at a higher force than refolding and force extension curves for the two reactions did not fit on top of each other. For irreversible processes, part of the work is dissipated. A reversible unfolding might be obtained experimentally with a lower loading rate (pN/s).

Single molecule experiments offer an opportunity to estimate the change in Gibb's free energy for the reversible process (ΔG_{rev}) by analyzing the irreversible process. Crooks' and Jarzynski's methods (Crooks, 1999; Jarzynski, 1997) states how to calculate the change in ΔG_{rev}, from a distribution of irreversible single molecule processes. Even though the process is irreversible, it is interesting to know ΔG for the reversible process, because for a given set of conditions (force, solvent and temperature) we expect the same ΔG_{rev}, even though the processes of unfolding might be different. In other words, the RNA pseudoknot can unfold in different ways, but the energy difference between the folded and the unfolded states is constant. Jarzynski's method was applied to RNA structure unfolding for the first time by Jan Liphardt (Liphardt et al., 2002).

In paper IV of the appendix thesis, Lene Oddershede and Nader Reihani estimated ΔG_{rev} from our experimental data using Crooks' and Jarzynski's methods. I'll show the results of that in chapter 5.

A common method of estimating ΔG_{rev} for nucleic acid structures is analyzing UV absorption profiles from thermal melting experiments; however we did not obtain such data in this work. Theoretical models of the RNA structure can also be used to calculate an estimate of $\Delta G_{rev,}$ examples of such models include *mfold* (Zuker, 2003) and *pknotsRG* (Reeder and Giegerich, 2004). The models are based on data from calorimetric measurements and UV absorption profiles from thermal melting of

oligonucleotides. In chapter 5 I will show estimates of ΔG_{rev} of unfolding RNA pseudoknots obtained by the use of *pknotsRG.*

3.4 Kinetics

In this section, the kinetics of RNA pseudoknot unfolding in the presence of a force is considered. In a simple kinetic model of the unfolding of an RNA pseudoknot in the presence of a force, there are two states: a folded state, and an unfolded state. It is assumed that the unfolding process happens in a single step with no partially unfolded intermediate states. In the process of unfolding, the pseudoknot passes through a transition state as drawn in Figure 12. The reaction rate depends on the distance to the transition state. At temperatures (T) T>0 K the molecules exhibits thermal fluctuations, and the energy of a single molecule will fluctuate. By chance at some point in time thermal fluctuations will bring the molecule to the transition state and the molecule reacts.

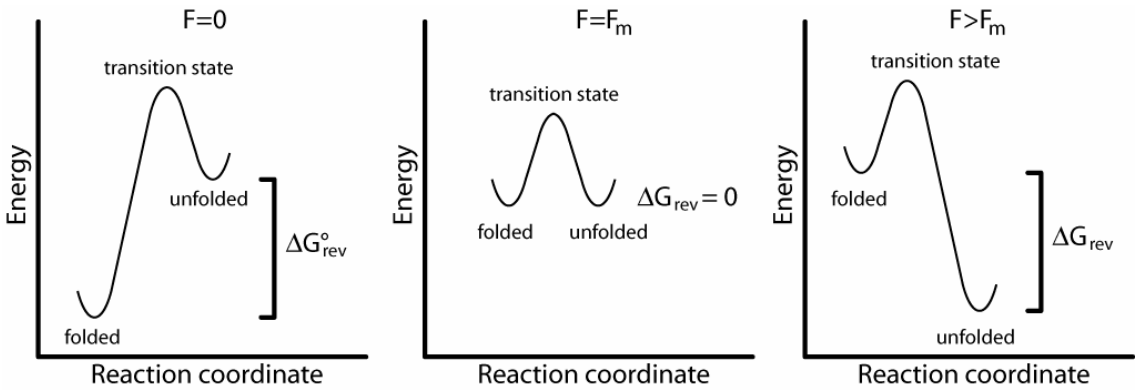

Figure 12. Energy diagram for two-state reaction.

In an optical tweezers experiment (Liphardt et al., 2001), a single RNA hairpin was held at constant force while the change in extension of the molecule was measured. The RNA was observed to hop back and forth between the folded hairpin state and unfolded single strand state. Thermal energy drives the hopping between the two states. This situation is shown in the middle panel of Figure 12.

The rate constant, *k*, often depends on temperature exponentially, as described by the empirical equation proposed by Arrhenius in 1889:

$$k(T) = k_0 e^{E_a / k_B T}$$

The equation can by adopted to describe the force dependence of the rate constant *k(F)* (Tinoco, 2004). It seems reasonable that force favors the unfolded state and if the effect is exponential, one get an Arrhenius-like equation:

$$k(F) = k_0 e^{FX^{\ddagger}/k_B T}$$

Here *k(F)* is the rate constant at a force *F*, and $X^{\ddagger}$ is the distance to the transition state along the reaction coordinate. In the kind of experiment considered here, e.g. the pulling experiment on single RNA pseudoknots, the reaction coordinate and the extension (X) of the molecule is measured on the same axis. RNA structures which have a short $X^{\ddagger}$ during unfolding are denoted 'brittle' where as structures with longer $X^{\ddagger}$ are 'soft'. An analogy to the 'brittle' structure is glass. If you deform a piece of glass just a little, it will break, whereas a softer material allows extensive deformation without breaking. In complex RNA structures, double strand helixes (hairpins) have been shown to be relative soft with $X^{\ddagger}$ = 5-10 nm, whereas a Mg^{++} ion joining two RNA domains are brittle parts of the complex structure, $X^{\ddagger} \sim 1$ nm (Onoa and Tinoco, 2004).

To extract *k(F)* and $X^{\ddagger}$ from an experiment as the one performed in this work, the Arrhenius-like equation has to be modified before it is applied to the experimental data (Tinoco, 2004). Consider the unfolding of a single molecule as a stochastic event. For a given set of conditions (force, temperature and solvent) the pseudoknot has a distribution of life-times. The probability (P) that the pseudoknot has not unfolded decrease by time. In the actual experiment, the force needs to be increased to a force close to F_m or higher in order to decrease P significantly. The change in P is:

$$dP = -k(F)Pdt$$

Solving this equation for P gives:

$$P = e^{-k(F)t}$$

It follows that at constant force the probability that the unfolding of the single pseudoknot has not occurred decrease exponentially.

In the unfolding experiments of this work the force is not constant. We have a constant loading rate (r) and it follows that the force ($F = r \times t$) increase with time (t). Then the Arrhenius-like equation looks like this:

$$k(F) = k_0 e^{rtX^{\ddagger}/k_B T}$$

and substitution k(F) in the equation for dP with this expression gives:

$$dP = -k_0 e^{rtX^{\ddagger}/k_B T} Pdt$$

Integration of this equation gives:

$$r \ln P = -\left[k_0 k_B T / X^{\ddagger}\right]\left[e^{X^{\ddagger}F/k_B T} - 1\right]$$

In experiments with constant loading rate (r), P is estimated as a function of force from the distribution of unfolding forces. For each force, P is a fraction of the total number of

unfoldings, and represents the pseudoknots which have not unfolded at the particular force or any lower force. In the result section the equation above is fitted, with k_0 and $X^{\ddagger}$ as fitting parameters, to a plot of our experimental data for P as a function of F.

The assumption of no intermediate states for the unfolding of an RNA structure is an approximation and actually intermediate states is evident in our data for the unfolding of pseudoknots (see results section). For the unfolding of hairpins, the process was found to be all or none in optical tweezers pulling experiments (Liphardt et al., 2001). The detection of intermediate steps might be limited by the resolution of the experiment and for instance the timescale of single base pair unpairing is expected to be shorter than the resolution in this kind of experiments (Manosas et al., 2007; Wen et al., 2007). However it is still meaningfull to consider the single step reaction for the matter of the concepts involved. Just keep in mind that many fast steps might underlie the single step observed.

When several steps underlie the reaction, there is not just one transition state, but several barriers which is crossed on the path between the two states. Even different paths through the landscape of barriers might be possible. This was illustrated by single molecule unfoldings of the complex structure of the *T. thermophila* ribozyme (Onoa et al., 2003). In the thermodynamics section we saw that an externally applied force changes the relative position (ΔG) of the two states, folded and unfolded. Force changes the energy landscape. Barriers might become smaller or larger at different forces and another barrier may become limiting for the reaction (Merkel et al., 1999).

Chapter 4.

Materials and Methods

4.1 Overview of Materials and Methods

This section is devoted to a detailed description of experimental procedures and materials used in the experiments described in the results section. The experiments are divided into three groups:

1. Stretching single DNA molecules. Single molecule experiment using optical tweezers.
2. Measurement of frameshifting stimulated by IBV derived RNA pseudoknots. Ensemble experiment *in vivo* in *E. coli*.
3. Mechanical unfolding of RNA pseudoknots. Single molecule experiment using optical tweezers.

First, the construction of plasmids (DNA molecules), which serve as the basis for the synthesis of most of the RNA and DNA molecules used in the single molecule experiments, is described. The plasmid names are pTH400, pTH401, pTH421, pTH413 and pTH419. Plasmids pTH400, pTH401, pTH421 are also used in the *in vivo* frameshift assays, which are described after plasmid construction. Then the preparation of samples for the single molecules experiments is described. Finally, the actual single molecule experiments are considered. Materials and methods as well as the treatment of data are described.

4.2 Construction of Plasmids

All enzymes used in the plasmid preparations were from New England Biolabs. The molecular cloning methods were as described in (Sambrook et al., 1989) except if otherwise stated.

4.2.1 Plasmids Encoding a Frameshift Site, Slippery Sequence and Pseudoknot: pTH400, pTH401 and pTH421

pTH400, pTH401 and pTH421 were derived from pOFX302 (Rettberg et al., 1999). These plasmids encode a gene fusion reporter system consisting of a Ptac promoter, bacteriophage T7 gene10 and *lacZ*. pOFX302 was digested with restriction endonucleases HindIII and ApaI which both have unique sites in the plasmid situated in the region between gene10 and *lacZ*. Synthetic DNA oligomeres where purchased (TAG Copenhagen), which encoded a slippery sequence and a pseudoknot. For the control, pTH421, no pseudoknot was encoded in the oligomeres.
Complimentary DNA oligomeres were annealed and inserted between the restriction sites in the plasmid. Oligomeres TH402, TH403 and TH406 (Table 1) were phosphorylated with T4 polynucleotide kinase prior to annealing. Mixtures of annealed oligomeres and plasmid digested with Hind III and ApaI were treated with T4 DNA

ligase and used in transformation of NF1830 (**Table 2**). Plasmids were purified from transformants (Biorad miniprep) and the nucleotide sequences were verified by DNA sequencing (Big Dye, Perkin Elmer) using primer NEB#1212 or TH413 (Table 1).

4.2.2 Plasmids used as templates in PCR amplifications of DNA fragments of 2961 bp and 3256 bp: pTH413 and pTH419

DNA fragments from a digestion of bacteriophage λ DNA with restriction endonuclease HindIII were inserted in the HindIII site of pOFX302. pOFX302 was digested with HindIII, dephosphorylated with calf intestine phosphorylase and gel purified. The linearized and purified plasmid was then mixed with HindIII digested λ DNA. The mixture was treated with T4 DNA ligase and used in transformation of NF1830 (**Table 2**).
Plasmids were purified from several individual transformants (Biorad miniprep) and the identity was checked by agarose gel electrophoresis after digestion with HindIII. Two plasmids were chosen. One showed bands of approximately 8000 bp and 3000 bp was named pTH413 and the other showed bands of approximately 8000 bp and 3200 bp was named pTH419. Plasmids pTH413 and pTH419 were used as templates in PCRs (see 4.4.2) in the preparation of samples for single molecule experiments.

4.3 Frameshift Frequency *in vivo*

4.3.1 Frameshift Assay

The frequencies of ribosomal frameshifting in pTH400, pTH401 and pTH421 constructs were estimated in pulse labeling experiments. The strains used in these assays were derived by transformation of strain MAS90 (**Table 2**) with pTH400, pTH401 or pTH421. Cultures were grown in MOPS minimal media at 37°C for 8-10 generations in the log phase (Rettberg et al., 1999). Expression of the hybrid genes was induced by addition of Isopropyl beta-D-Thiogalactopyranoside (IPTG). IPTG was added to 1 mM final concentration when the cultures reached an optical density of 0.2-0.8 measured at 440 nm.
The time of induction defines t=0. At t=15 min 10 μCi ^{35}S methionine were added to 1 ml culture. After 20 s, 100 μg methionine was added per ml culture, which is approximately 10^5 times molar excess. At t=2 min the culture was moved to 0°C.
The cells were harvested by centrifugation. After removal of the supernatant the pellet was resuspended in 30 μl SDS sample buffer and boiled for 2 min. Half the sample volume was loaded onto an 8.75 or 10 % SDS gel. After gel electrophoresis, the gel was dried and exposed to a Phosphor imager screen (Molecular Dynamics). ImageQuant software (Molecular Dynamics) was used to evaluate protein amounts in the bands. Counts were normalized to the number of methionine residues in the product. The frameshift frequency was calculated as the ratio frameshift product to the sum of frameshift product and non-frameshift product.

4.3.2 Protein Stability in Frameshift Assay

The stability of the proteins was examined by analyzing culture samples taken at different time points after the labeling was stopped with excess unlabelled methionine. 5

ml culture was induced and labeled as described above. 1 ml culture were withdrawn at t=2 min, t=5 min, t=10 min and t=20 min and treated as described for the samples above.

4.4 Preparation of the Samples for Single Molecule Experiments

All enzymes and reaction buffers used in the preparations were from New England Biolabs and molecular cloning methods were as described in (Sambrook et al., 1989) except if otherwise stated.

4.4.1 RNA and Handles

RNA was synthesized in vitro by T7 RNA polymerase. A DNA template for the RNA synthesis was produced by PCR. Plasmids pTH400, pTH401 or pTH421 served as template in the PCRs. Primers were TH412 and TH414. The 5' end of TH414 encodes the T7 promoter. Run-off RNA synthesis are expected to produce 939 nt, 942 nt or 876 nt strands.
Upstream and downstream DNA handles were synthesized in a two step reaction. Upstream and downstream refer to the 5' and 3' regions of the RNA, respectively, where the handle DNAs have complimentarity. The primers for the upstream handle were TH416 and TH407, whereas for the downstream handle they were TH415 and TH408. The first step was an asymmetric PCR reaction. Asymmetric in the sense, that the concentration of one of the primers was ten times reduced. In the first rounds the double stranded product increases exponentially as in a regular PCR, but at some point all of the low contration primer is used and the reaction continues linearly producing a single strand fragment. In the second step the first step reaction was mixed with an equal volume of fresh reaction mixture containing only one primer, TH407 or TH408. Otherwise, the reactions were done at standard PCR conditions using SUPER TAQ polymerase and reaction buffer from HT Biotechnology, 200 µM dNTPs, 10 pg/µl template DNA, 500 fmol/µl of TH407 or TH408 and 50 fmol/µl of TH416 or TH415, respectively.
The downstream handle DNA had a digoxygenin group on its 5' nucleotide, since primer TH408 was synthesized with a digoxygenin on the 5' terminal nucleotide. The upstream handle was labeled with biotin in its 3' end enzymatically. For this terminal-deoxynucleotide-transferase and biotin-N4-CTP were used as recommended by the manufacturer (Pierce).
Handles were annealed to RNA by mixing approximately equal amounts of the nucleotide species in buffer R (10 mM Tris-HCl pH 7.5, 250 mM NaCl, 10 mM Mg_2Cl) or in 10 mM sodium phosphate pH 6.0, 250 mM NaCl, 10 mM Mg_2Cl. The mixture was heated to 65 °C for 8 min and allowed to cool down to room temperature for >30 min. Annealed RNA and handles were stored at -70°C until usage.
To bind the handle/RNA to beads, appropriate dilutions of the handle/RNA mixture and 2.1 µm streptavidin coated polystyrene beads (Bangs) were mixed and incubated for 1 hour at room temperature while gently mixing. The criteria for the dilutions was that in the microscope sample chamber no more than approximately 4 out of 5 beads would form a tether to the 2.88 µm antidigoxygenin coated bead held in the micropipette.
After binding the RNA to the 2.1 µm beads the mixture was diluted in a dilution of 2.88 µm anti-digoxygenin coated beads (prepared as described below) and transferred to the microscope sample chamber. The large extent of dilution ensured that the beads not

used for the experiment would not interfere, but still it was possible to find enough beads in the chamber for several experiments. Dilutions were in buffer R which had been filtered trough a syringe filter of pore size 0.2 μm (Millipore). The chamber was flushed with 5-10 times its volume of the sample dilution prior to the experiment. Experiments were performed at room temperature, 22 °C.

4.4.2 Double Stranded DNA Molecules for Single Molecule Experiments

4.4.2.1 Phage λ genomic DNA

The 48502 bp phage λ genomic DNA (λ DNA) was labeled with biotin in each end. The linearized λ genome has 12 nt single stranded cohesive ends. The 5' ends overhang the 3' ends. Labeling was accomplished by annealing of 3' biotin modified DNA oligomeres complementary to the cohesive ends. First, phage λ genomic DNA (New England Biolabs) was dephosphorylated with calf intestine phosphorylase and DNA oligomeres TH423 and TH424 was phosphorylated with T4 polynucleotide kinase. In ligation buffer, the dephosphorylated λ DNA was mixed with a 10^3 excess of phosphorylated TH423, heated to 75 °C. Then the temperature was decreased to 10-20 °C over more than 10 hours. T4 ligase was added and a ligation reaction was performed at 16 °C.
Excess TH423 was washed away using TE buffer (10mM Tris HCl, 1.0 mM EDTA, pH 8.0) and a micron-100 spin filter (Millipore). Then TH424 was added followed by a second round of annealing, ligation and purification using a spin filter. An aliquot of the labeled λ DNA was digested with BstE II and analyzed by agarose gel electrophoresis. The concentration in the dilution of labeled DNA was judged from the intensity of the ethidium bromide stained bands in the gel.

4.4.2.2 Shorter DNA fragments

DNA fragments (942 bp, 2961 bp and 3256 bp) with biotin in one end and digoxygenin in the other were synthesized in PCR reactions using 5' modified primers. For the forward primer, TH420, the modification was biotin, whereas for the reverse primer, TH408, it was digoxygenin (Table 1). Plasmids pTH401, pTH413 or pTH419 was used as template. The results were DNA fragments of predicted sizes 942 bp, 2961 bp and 3256 bp, respectively. The PCR were done using SUPER TAQ polymerase and reaction buffer from HT Biotechnology, 200 μM dNTPs, 10 pg/μl template DNA, 500 fmol/μl of primers TH420 and TH408.
An aliquot of the labeled DNA fragments was analyzed with agarose gel electrophoresis. The concentration in the dilutions of labeled DNA was judged from the intensity of the ethidium bromide stained bands in the gels. For the 942 bp and 3256 bp fragments the concentrations in the stock solution were ~10^{10} and ~10^9 molecules/μl, respectively.

4.4.2.3 Attachment of DNA fragments to beads

For the attachment of DNA fragments to 2.1 μm streptavidin coated polystyrene beads (Spherotech), 2 μl beads (0.5 w/v %) were mixed with 2 μl of a 0.5×10^3 or 10^3 dilution in TE of the 942 bp fragments or with 2 μl of a 10^1 dilution in TE of the 3256 bp fragments in 46 μl of buffer to final concentrations of 10 mM Tris HCl pH 7.5, 250mM

NaCl, 10 mM $MgCl_2$, 0.1 % BSA 0.01 mg/ml Herring Sperm DNA (Sigma D-7290). After 30 min with gentle mixing, the mixture was centrifuged at 7000×g for 5 min, the pellet was washed two times with buffer C (10 mM Tris HCl pH 7.5, 250mM NaCl, 10 mM $MgCl_2$, 0.1 % BSA 0.01 mg/ml Herring Sperm DNA (Sigma D-7290)). The washed pelleted beads were resuspended in 50 µl buffer C supplemented with 0.02 % (w/v) NaN_3, and stored at 4 °C until use.

4.4.2.4 Sample for single molecule experiment

To prepare a sample for single molecule experiment, the 2.1 µm bead mixtures were diluted in a dilution of 2.88 µm anti-digoxygenin coated beads (prepared as described below) and transferred to the sample chamber for the microscope. The extent of dilution ensured that the beads not used for the experiment would not interfere, but still it was possible to find enough beads in the chamber for several experiments. Dilutions were in buffer C which had been filtered trough a syringe filter of pore size 0.2 µm (Millipore). The chamber was flushed with 5-10 times its volume of the sample dilution prior to the experiment. Experiments were performed at room temperature, 22 °C.

4.4.3 Binding and Cross-linking of Antidigoxygenin to 2.88 µm Beads

To bind antidigoxygenin to beads, 200 µl of 0.5 % (w/v) 2.88 µm protein G coated polystyrene beads (Spherotec) was mixed with 730 µl PBS pH 7.3, 20 µl 200 µg/ml antidigoxygenin (Pierce) and 50 µl 5 M NaCl. The mixture was incubated at room temperature and constant mixing by rotation of the sample tube. The beads were pelleted by centrifugation at 7000×g for 5 min. The pellet was washed in a buffer of PBS pH 7.3, 0.5 % Tween20 (Sigma) and 0.5 M NaCl by three cycles of resuspension and centrifugation. Then the beads were resuspended in 1 ml buffer of 50 mM Na_2HPO_4 pH 8.2 and 100 mM NaCl.
Digoxygenin and protein G bonds were stabilized by cross-linking (formation of covalent bonds) 50 mg of the cross linker (DMP, dimethylpimelinediimidate dihydrochloride) was dissolved in 1 ml 50 mM Na_2HPO_4 pH 8.2, 100 mM NaCl. 100 µl of the DMP solution was added to the resuspended beads and incubated with rotation for 1 hour. The beads were pelleted and resuspended in 1 ml 1 M NaCl. Then the beads were washed two times, first in 100 mM glycine pH 2.8 and secondly in PBS pH 7.3. Finally, the beads were resuspended in PBS pH 7.3, 0.02 % NaN_3 and stored at 4 °C until use.

4.4.4 Binding of ^{32}P labeled DNA to Beads

Experiments were performed to get a measurement of DNA molecules bound to the beads after incubation of beads in a mixture containing the DNA molecules. The DNA molecules used to bind to the beads resemble the 942 bp molecules described above, except here they were isotope labeled with ^{32}P. They were synthesized by PCR using pTH401 as template and primers TH420 (5' biotin modification) and TH408 (5' digoxygenin modification) at the conditions described above except 0.27 µCi α-^{32}P-CTP (1500 Ci/mmol) was added to 20 µl reaction volume. After PCR, DNA was precipitated with ethanol and gel purified.
Using a scintillation counter, the isotope activity in an aliquot of the purified DNA was counted and the corresponding DNA concentration calculated. Three dilutions of the

DNA fragments in TE buffer were made to final DNA concentrations of 10^9, 10^8 and 10^7 molecules/µl. 2 µl of a suspension of $5x10^5$ beads and 2 µl of one of the DNA dilutions (see Table 4, chapter 5) were added to a buffer to a final volume of 50 µl and final concentrations of 10 mM Tris HCl pH 7.5, 250mM NaCl, 10 mM $MgCl_2$, 0.1 % BSA 0.1 mg/ml Herring Sperm DNA (Sigma D-7290).
The mixtures were incubated for 30 min with gentle mixing. Then the beads were pelleted by centrifugation at 7000×g for 5 min, the supernatant removed and washed two times, each time by resuspension in 50 µl buffer B (10 mM Tris HCl pH 7.5, 250mM NaCl, 10 mM $MgCl_2$, 0.1 % BSA 0.1 mg/ml Herring Sperm DNA (Sigma D-7290)) followed by centrifugation and removal of the supernatant. Finally, the beads were resuspended in 50 µl buffer B and the isotope activity was measured. Also, the isotope activity in the supernatants was measured.
The amounts of DNA bound to the beads were estimated from the isotope activities (Table 4, chapter 5). The antidig beads used in this experiment were prepared essentially as described in 'Binding and Cross-linking of Antidigoxygenin to 2.88 µm Beads'. However, antidigoxygenin was not cross-linked and the antidigoxygenin amounts used were for #1 and #4: 4 µl, for #2 and #5: 20 µl, and for #3 and #6: 100 µl. The 2.3 µm and 0.95 µm streptavidin coated beads were from Bangs.

Name	Sequence	Remarks
NEB#1212	cagcactgacccttttg	Sequencing of inserts between HindIII-ApaI. NEB #1212 complementary to pOFX302 approximately 40bp 3' of the ApaI site.
TH401	agctttttaaagcagtaagcgcgcgcacgagc gtcggtgcgcgcgc	Part of insert for pTH400. IBV derived pseudoknot.
TH402	agctagtggatgtgatcctgatgttgtaaagc gacgcttgggcc	Part of insert for pTH400 and pTH401. IBV derived pseudoknot.
TH403	tccactagctgcgcgcgcaccgacgctcgt gcgcgcgcttactgctttaaaa	Part of insert for pTH400. IBV derived pseudoknot.
TH404	caagcgtcgctttacaacatcaggatcaca	Part of insert for pTH400 and pTH401. IBV derived pseudoknot.
TH405	agctttttaaagcagtaagcgcgcgcacgg agcgtcgcgtgcgcgcgca	Part of insert for pTH401. IBV derived pseudoknot.
TH406	tccactagcttgcgcgcgcacgcgacgctc cgtgcgcgcgcttactgctttaaaa	Part of insert for pTH401. IBV derived pseudoknot.
TH407	tgaatccgcggtaccagcac	5' handle oligo, which is complementary to pOFX302 just 5' the HindIII site.
TH408	ataattcgcgtctggccttc	3' handle oligo, which is 5' labeled with digoxygenin and complementary to pOFX302 420 bp 3' the Apa1 site.
TH412	ataattcgcgtctggccttc	Reverse primer for PCR of template for T7 transcription. Sequence identical with TH408.
TH413	ctgattgaccctgagaag	Primer for sequencing of inserts between HindIII-ApaI. Complementary to pOFX302, approximately 100bp 5' of the HindIII site.
TH414	taatacgactcactatagggagagtatacct ctcagttgggtg	Forward primer for PCR of template for T7 transcription (T7 promoter embedded). The 5' part of the primer is also complementary to the T7 promoter in the plasmid, but that is probably

		not a problem.
TH415	ctaattcactggccgtcgtt	Primer for asymmetric PCR for downstream handle.
TH416	gtatacctctcagttgggtg	Primer for asymmetric PCR of upstream handle.
TH420	gtatacctctcagttgggtg	Identical to TH416 except it is 5' biotinylated.
TH423	gggcggcgacct	3' biotin
TH424	aggtcgccgccc	3' biotin
TH428	agctttttaaagcagtaagcgcgggcc	Oligo for insert in pOFX302. For control with no pseudoknot, pTH421.
TH429	cgcgcttactgctttaaaa	Oligo for insert in pOFX302. For control with no pseudoknot, pTH421.

Table 1. DNA oligomeres used in this work.

Name	Genotype
MAS90	*E. coli* K-12, *recA1 Δ(pro-lac) thi ara F': lacI^{q1} lacZ::Tn5 proAB^{+}*
NF1830	*E. coli* MC1000 *recA1 F': lacI^{q1} lacZ::Tn5 proAB^{+}*

Table 2. ***Escherichia coli* strains used in this work.**

4.5 Single Molecule Experiment

4.5.1 Sample Chamber

When I started in the lab, the sample chambers in use consisted of two thin glass plates (approximately 0.15 mm thick) and two pieces of double sticky tape as spacers between the glass plates. Sometimes the tape was replaced by vacuum grease and parafilm. The opening, where the ample was applied, could be sealed by hot melted wax. This is a simple and fast to build chamber suitable for many experiments, but as seen in Figure 13 another design was used in the stretching experiments. This new chamber is much sturdier which is needed when using the glass micropipettes, since they are quite frangible. The in-let and out-let could be sealed and easily re-opened to let a new sample in, something which was no possible whit the wax sealed chamber. Micropipettes had not been used in the laboratory before but after a fair amount of trial and error, I succeeded in holding a polystyrene bead at the tip of a micropipette. The first type of micropipette that we used was pulled from glass tubes 1-2 mm in outer diameter using a programmable micropipette puller. The tip was trimmed by melting and breaking under a specialized microscope. With these materials it was possible to make micropipettes which had the desired tip. The tip should have about one micron diameter and had to be relatively clean-cut in order to get a close fit to the bead. We used these pipettes in the beginning of the project, but they had two main drawbacks.

These pipettes was skewed, meaning that the vertical distance from the bottom of the chamber to the tip of the pipette varied a lot after the pipettes had been immobilized by the parafilm layers of the chamber (see Figure 13). The second drawback was that the pipettes often became blocked because debris got stuck somewhere along the path where the pipette was narrowing down from 1 mm to 1 µm. The blocking resulted in a loss of pressure control and hence the pipette could not be used for experiments.
After visiting Lisa Green in Ignacio Tinoco's laboratory, I started pulling my pipettes from the same thin glass tubes as they use (OD= 80 µm and ID=40 µm), see (Wuite et al., 2000). This type of pipettes did not have the problems described above.

A drawing of the sample chamber is shown in Figure 13. The sample chamber was a sandwich of a thin microscope cover glass, two layers of parafilm and thick microscope glass prepared with drilled holes and was mounted in a chamber holder made of aluminum plate ("chamber plate" and "flow tops" in Figure 13). The parafilm layers were cut to create a cell for the sample. Flow-in and flow-out tubes allowed the sample to be flushed in and out of the cell. Micropipettes were made from glass tubes (ID 40 mm, OD 80 mm, KG-33 glass; Garner Glass) using a micropipette puller (Sutter). The micropipettes were coupled to a syringe which was used to control the pressure in the micropipette.

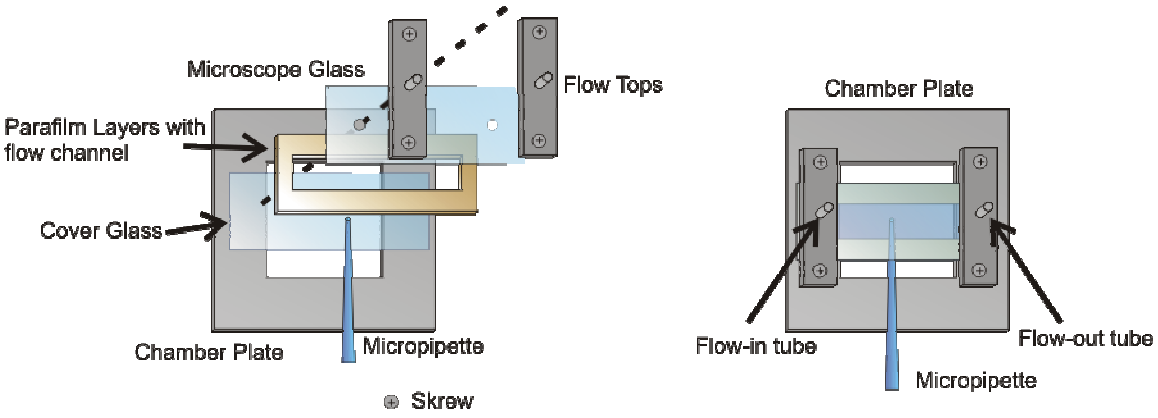

Figure 13. Sample chamber. Schematic drawing of the sample chamber. The chamber and chamber holder were designed and constructed in this work and later used by other students in lab, one of them, Dejan Trpcevski, made this drawing).

The orientations of the micropipette are crucial for the length measurements in the stretch and relax experiments, see 5.2.3. Unfortunately, this issue was realized rather late in this thesis work. The orthogonal geometry results in distorted length measurements due to bending of the micropipette. Using the parallel geometry one should avoid this effect. Accordingly, only for the stretching of our control PK421 RNA and while stretching DNA as described in Paper II (Appendix), the distortion was avoided by using the parallel geometry. However, this issue has no effect on our main conclusions regarding, the relative stability of different pseudoknots.

4.5.2 Equipment

The optical trap equipment is based on a 1064 nm $NdYVO_4$ laser and is implemented in an inverted Leica microscope with a back focal quadrant photodiode detection scheme,

for a full description see (Oddershede et al., 2001). The water immersion objective (Leica, NA=1.2) allowed optical trapping at any depth within the sample. A laser power of 0.8 W, measured at the output of the laser, gave a trap stiffness in the range of 0.1-0.2 pN/nm. A micropipette with a tip diameter of approximately 1 μm was pointing into the sample chamber. Suction could be applied to the pipette to firmly attach a bead to the tip.
The pipette was immobilized with respect to the chamber, which was mounted on a two-dimensional translationable piezoelectric stage (Physik Instrumente) with capacitative feedback control and nanometer position resolution. Data acquisition and control of the stage were performed using custom made Labview programs. Simultaneous control over piezo stage and output from the quadrant photodiode allows for measurements of corresponding values of force and distance.

4.5.3 Procedure for Experiments with RNA

To form a tether between the two beads, first a 2.88 μm bead was trapped in the optical trap, and then the pipette tip was moved near the bead, which was then released and attached to the pipette. Then a 2.1 μm bead was trapped in the optical trap. The beads were positioned about 10 μm apart but in the same depth by adjusting the stage position and microscope focus. A time series of the thermal fluctuation of the bead inside the trap was monitored to calibrate the optical trap. The trap stiffness and a factor to convert the quadrant photodiode signal in Volts into positions in nm were estimated using a Matlab program (Hansen et al., 2006) which takes aliasing and the filtering effect of the quadrant photodiode into account (Berg-Sorensen et al., 2003).
To form a tether between the two beads they had to be moved into close proximity of each other. First the centers of the beads were aligned on an axis parallel to the x-axis of the piezo stage. To achieve that, the bead in the pipette was moved by manual control of the piezo stage's position while watching the images of the beads. The precision of this alignment was probably down to one hundred nanometers.
The next step was to bring the beads in close distance, 50 nm or less, to make the formation of a tether likely within a few minutes. Distortion of the diode signal indicated close proximity of the beads.
When a tether was formed, it was detected when the experimenter tried to move the pipette away. The RNA/DNA duplex tethers was stretched and relaxed in consecutive cycles. In one cycle the pipette was moved 600-800 nm at 100 nm/s and reverse while the quadrant photodiode signal and the stage position were sampled at 5 kHz. In the force range of pseudoknot unfolding the loading rate is nearly constant at about 10 pN/s, since the force extension curve is close to vertical in this range.

4.5.4 Data Treatment and Filtration for the RNA Experiment

The stage signal was smoothed with a sliding window 3000 data points wide, before the time series were averaged in 10 ms non overlapping windows. The force exerted on the bead in the trap and it’s position were calculated using both coordinates of the quadrant photodiode, while the first point of the time series served as origin for the coordinate system. The change in tether length was calculated by subtraction of the movement of the bead in the trap from the stage movement. The presented data represent at least 8, 10 and 9 individual molecules of PK400, PK401 or PK421 RNA.

Traces were pooled and filtered in order to find true traces of single RNA molecule. Two criteria were used in the filter which was applied on the low force part of the traces. For stretch traces the first 250 ms were considered and for relax traces the last 250 ms. The first criterion was flatness of the curve, which was analyzed by fitting a straight line to the data points. Traces for which the slope of the line was within ±50 nm/s passed the filter. The rationale for this critria is; when stretching beads bound to each other from a sample without RNA/DNA the force increase linearly with extension. However, when a single RNA/DNA tether is stretched we expect a constant force of zero pN at low extensions, and hence a curve resembling the WLC-model. The second criterion was the deviation of the bead positions. Again rationale for the critria came from stretching beads bound to each other from a sample without RNA/DNA. For these unintented bonds we observed very small fluctuations of the trapped bead. Whereas when the bond is a single RNA/DNA tether we expect fluctuations when the tether is relaxed. A trace passed the filter if the standard deviation on the bead positions distance to the fitted line was between 3.5 and 7 nm. For the filtering only the signal of one photodiode coordinate was considered, for which the signal was approximately 10 times higher than for the other. This coordinate was almost parallel with the direction of pipette motion.

4.5.5 Procedure for shorter DNAs

For single molecule stretching experiments with 942 bp and 3256 bp DNA fragments, the procedure was as described in 'Procedure for experiments with RNA' except for 3256 bp fragments the pipette was moved 1000-2000 nm instead of 600-800nm. As for the RNA data, the stage signal was smoothed with a sliding window 3000 data points wide, before the time series were averaged in 10 ms non overlapping windows. The force exerted on the bead in the trap and it's position were calculated using both coordinates of the quadrant photodiode, while the first point of the time series served as origin for the coordinate system. The change in tether length was calculated by subtracting the movement of the bead in the trap from the stage movement.

4.5.6 Procedure for λ DNA

Two strategies were attempted for making tethers of biotin labeled λ DNA and 2.3 μm streptavidin coated polystyrene beads (Bangs).
Strategy 1: Samples of equal volumes of a λ DNA solution and a dilution of the bead stock suspension (1 v/w %) were prepared as described in Table 3. λ DNA and beads were diluted in buffer B. Then the sample was transferred to the sample chamber mounted on the microscope. The laser tweezers was used to grab beads which had another bead close by. Then the sample chamber was translated to see if the two beads were attached to each other. Then the one of the beads, which was not in the trap, was attached to a micropipette by suction. Then, to stretch the molecule, the pipette was moved relative to the tweezers in 1 μm steps, using the piezo stage. For each step the pipette was held at constant position for 1s while data from the quadrant photodiode position detector was collected.
Strategy 2: A dilution of 2.3 μm streptavidin coated polystyrene beads was transferred to the sample chamber, and then a bead was grapped by the laser tweezers. A 50 ml syringe, where the piston was removed, served as buffer container. The container was

coupled to the sample chamber by a tube and its elevation was adjustable. This primitive micro fluidic system was used to establish a flow of buffer in the sample chamber resulting in an almost constant ~8 pN drag force on the bead in the trap. The buffer was buffer B containing 10^5 molecules/µl of λ DNA. A sudden increase in drag force to ~14 pN was attributed to the attachment of a λ DNA molecule to the bead in the trap. In a few times the other end of the DNA was attached to a bead held in a micropipette. However, due to the lacking robustness of the primitive micro fluidic system, the tethers were destroyed before the actual stretching experiments could be performed. In this thesis we did not attempt to improve the λ DNA stretching experiment further.

4.5.7 Computer programs (credits)

Several custom made computer programs were used in the optical tweezers experiments. A Labview program for the capture of time series for calibration of the trap was written by Kirstine Berg-Sørensen. The Matlab program for the fits to calibration data is described in (Hansen et al., 2006). The following Labview and Matlab programs were made as part of this Ph.D. project. Labview programs for the actual stretching experiments were written by Nader Reihani, with contributions from Thomas Møller Hansen. The Matlab programs for combination of calibration data and data from stretching experiment, as well as filtering of traces programs, were made by Thomas Møller Hansen.

Chapter 5.

Results

5.1 Overview

The goal of this work was to stretch and mechanically unfold mRNA pseudoknots and relate their mechanical properties to their biological activity: stimulation of ribosomal frameshifting.

The mechanical unfolding studies proved to be a substantial experimental challenge. When the project started we had a suitable optical tweezers setup and methods for calibration and some methods of using the equipment. However, additional materials and methods had to be developed, before we finally were able to succeed in the desired experiment: the mechanical unfolding of RNA pseudoknots. Some, of these technique related results are treated in the Chapter 4, Materials and Methods, only. In this chapter the experiments of stretching DNA, measuring ribosomal frameshifting and stretching RNA are considered.

The RNA molecules used were relatively short with L_c (contour length) below 300 nm and thereby close to the resolution in a light microscope. The first attempts to detect tethers and measure the force and extension relation with these molecules failed. To practice the skills for this kind of experiments with something easier before returning to the RNA, the 50 times longer bacteriophage λ DNA (L_c=16495 nm) replaced the short RNAs. This should make it possible, in the microscope, to easily identify the tethers consisting of a DNA molecule with a bead attached in each end. DNA is chemically more stable than RNA and less prone to degradation by ubiquitous nucleases. After successful formation and stretching experiments with tethers of single λ DNA molecules, the molecule length was stepwise reduced. First, to one of L_c=1107 nm, and second, to one of L_c=320 nm, similar in length to the RNA. Finally, the single molecule stretching experiments were done with pseudoknot encoding RNAs.

5.2 Stretching DNA

5.2.1 Bacteriophage λ DNA

The principle of a stretching experiment with DNA (or RNA) is shown in Figure 14. The λ DNA was attached to polystyrene beads via specific biotin-streptavidin bonds. The molecule was stretched when the pipette was moved, while the force acting on the molecule was measured in the laser trap. The laser trap exerts force on the trapped bead and within certain limits the stiffness of the optical trap is constant. Hence, when the trap stiffness is known, the force exerted on the bead can be calculated from the

displacement of the bead from the trap centre, which was monitored. The position of the bead in the pipette with respect to the bead in the trap was controlled by a piezo electric stage. To stretch the molecule the distance between the beads was increased. The change in the end-to-end distance of the molecule was calculated by subtraction of the displacement of the bead in the trap from the displacement of the pipette.
To form tethers, which is a λ DNA or other polynucleotide molecule with a bead bound in each end, streptavidin coated beads and biotin modified λ DNA were mixed and examined in the microscope. A bead was trapped and when the sample was subsequently moved one could see if the bead was "single" or if it was part of a tether with another bead. 1 % of the beads examined were part of a tether and it took approximately 1 hour to examine 100 beads. Different bead concentrations, λ DNA concentrations, incubation times and mixing methods were tested in an attempt to increase the frequency of tethers, see Table 3. None of the tests gave more than 1 % tethers but some of the treatments seemed to decrease the frequency of tethers. A plausible explanation for the low frequency of tether formation is that both of the biotinylated ends of the DNA bind to the same streptavidin coated bead.

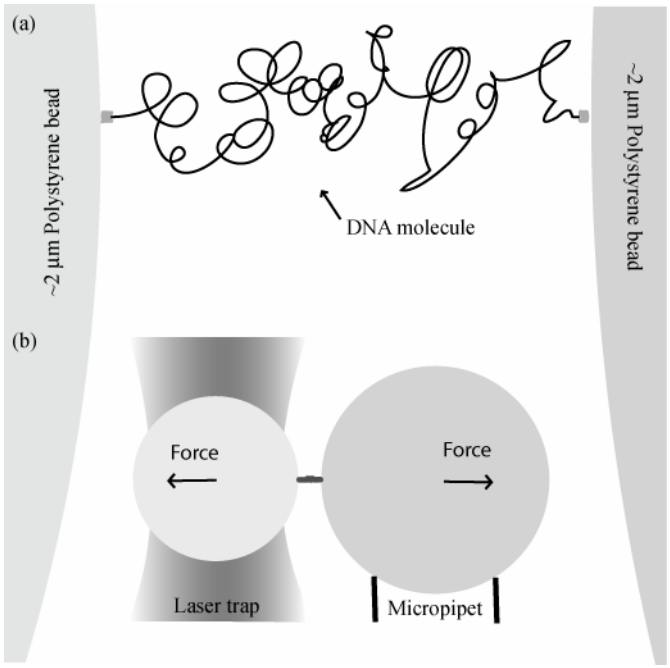

Figure 14. Experimental setup for stretching of single DNA molecules. The two beads are drawn at the same scale. The dimensions of the DNA are not to scale. a) Generally, the DNA is attached to beads with biotin-streptavidin and digoxygenin-antidigoxygenin bonds. For λ DNA both ends was biotinylated and streptavidin beads were used. b) One bead is placed in the force measuring laser trap, while the other bead is attached to a micropipette. The micro pipette was moved with respect to the laser trap in order to stretch and relax the molecule.

Dilution factor for beads	Concentration of DNA [molecules/µl]	Treatment	Result [number of tethers/beads examined]
80	10^6	Mixed by pipetting up and down a few times.	3/200
80	10^7	As above.	1/100
80	10^6	As above and 3 min ultrasound.	0/100
80	10^6	As above and pipetting up and down 100 times.	0/200
80	10^6	Mixed by pipetting up and down a few times and 30 min ultrasound.	0/200
10	10^6	Mixed by pipetting up and down a few times.	1/100
80	10^6	Mixed by pipetting up and down 100 times.	1/100
80	10^6	Mixed by pipetting up and down a few times and examined after 10 hours.	0/200
80	10^6	Mixed by pipetting up and down a few times and examined after 4 days.	0/200
80	10^6	Mixed by gently hitting the tube with a finger 100 times.	0/150

Table 3. Mixtures of beads and λ DNA. Equal volumes beads and λ DNA were mixed and treated as indicated. The number of tethers and beads examined is show for each sample.

A second strategy for tether formation was attempted, which involved a primitive micro fluidic system (see materials and methods). After several trials, the conclusion was that one needs a more robust micro fluidic system, perhaps as the one described in (Wuite et al., 2000).

When a tether was found, it was brought to a micropipette protruding into the chamber. One of the beads was attached to the micropipette by suction, while the other was in the laser trap. Force versus extension data from stretching the DNA is shown in Figure 15. The force is low and almost constant at short extensions while when the extension approaches a certain value (the contour length) the force increases fast. The curve has the general shape, which have been seen previously in stretching experiments with λ DNA (Smith et al., 1996; Wang et al., 1997). However, one would expect a lower force close to zero for the plateau at short extensions. This offset on the force axis might be caused of a calibration error, but we did not investigate this issue further at this point. However, these data convincingly show the ability to form tethers with λ DNA, and to stretch λ DNA, and therefore shorter DNA molecules were used in the next step on the path towards stretching the short RNAs.

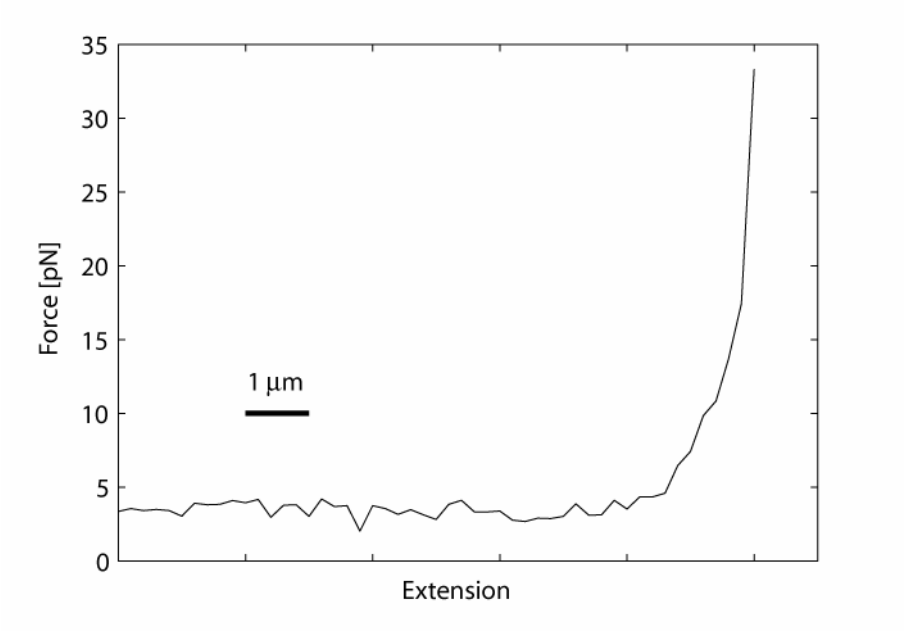

Figure 15. Force-Extension Curve for λ DNA.

5.2.2 Binding of 942 bp (L_c=320 nm) ^{32}P Labeled DNA to Beads

DNA molecules of 3256 bp and 942 bp with a digoxygenin in one end and biotin in the other were synthesized (see materials and methods). The modifications in the end allow for specific attachment to anti-digoxygenin and streptavidin coated beads. To measure the number of molecules binding to the beads a 942 bp DNA molecule was synthesized using α-^{32}P-CTP of known specific activity. The molecules with α-^{32}P-CTP incorporated was allowed to bind to different batches of beads, then the beads was washed and the activity in the fractions of beads and washing buffer were measured (see materials and methods). All batches of beads that allow a specific attachment of a DNA molecule bound a significant number of molecules, varying from a few to more than 1000 (Table 4).

The number of molecules bound was dependent of the DNA concentration in the three dilutions of DNA, which was used in the binding experiments. In the control with no DNA, no molecules were bound as expected. The "2.88 µm no antidig." beads, which do not allow specific binding, bound only few molecules.

The method to be used for tether formation was to bring the bead with DNA molecules bound via biotin-streptavidin close to an antidigoxygenin bead to allow the digoxygenin end of the DNA molecule to bind the second bead. If the number of DNA molecules on the first bead is too high, more than one molecule might bind both beads.

Almost 100 molecules bound to a streptavidin coated 2.3 µm beads using the most concentrated DNA dilution. This corresponds to a mean area of 1.66 x 10^5 nm^2/molecule and is equal to a circle with a radius of 230 nm. This number of DNA molecules on a bead was reasonable for the first attempts to form tethers. For the antidigoxygenin beads, the batch that bound the highest number of DNA molecules was chosen, "2.88 µm antidig. #2".

Beads	DNA: 10^7 μl^{-1}		DNA: 10^8 μl^{-1}		DNA: 10^9 μl^{-1}		no DNA
	% bound	molecules/ bead	% bound	molecules/ bead	% bound	molecules/ bead	molecules/ bead
2.88 µm antidig. #1	28	18	30	116	24; 32	1071; 1307	
2.88 µm antidig. #2	54	16	37	134	36; 38	1613; 1551	
2.88 µm antidig. #3	0; 25	0; 15			16; 14	690; 623	
2.88 µm antidig. #4	17	16	21	94	21; 19	902; 730	0
2.88 µm antidig. #5	20	11	17	66	23; 19	980; 732	
2.88 µm antidig. #6	0; 30	0; 23			7; 10	330; 443	0
2.88 µm no antidig.	5; 14	2; 17			0; 1; 0	2; 33; 3	0
2.3 µm strept. av.	21; 0	19; 0	3; 6	12; 20	2; 2	93; 95	0
0.95 µm strept. av.	2; 7	1; 3	15	62	9; 7	393; 321	0

Table 4. Binding of ^{32}P labeled DNA to beads. DNA was bound to beads and the number of molecules bound was measured as described in materials and methods.

5.2.3 Stretching 3256 bp DNA Molecules (L_c=1107 nm)

A tethers was formed, in which one end of the 3256 bp DNA molecule was attached to a bead in the laser trap while the other end was attached to a bead in a micropipette. The molecule was stretched when the pipette was moved, while the force acting on the molecule was measured in the laser trap (see materials and methods). To relax the molecule the movement of the pipette was reversed. Several cycles of stretching and relaxing were performed for each molecule. Figure 16 shows a curve from stretching the 3256 bp DNA. At low extension, the force is constant and close to zero. At further extension the force increases until a new plateau is reached at ~65 pN. When the stretching continues after the plateau, the force increases fast to over 100 pN. This is a characteristic lapse of a force extension curve of double stranded DNA, and clearly this is evidence of the stretching of a single molecule of the 3256 bp DNA.
The curve is not perfect though, and clearly the curve shows an apparently unphysical behavior after the plateau where the force increases while the extension seem to decrease. This is probably due to an erroneous calibration parameter. Over estimation of the conversion factor translating the photodiode signal in Volts to position in nm would explain, because it might result in a too large value for the beads movement in the trap which is subtracted from stage movement to give the change in molecule extension (see Materials and Methods).

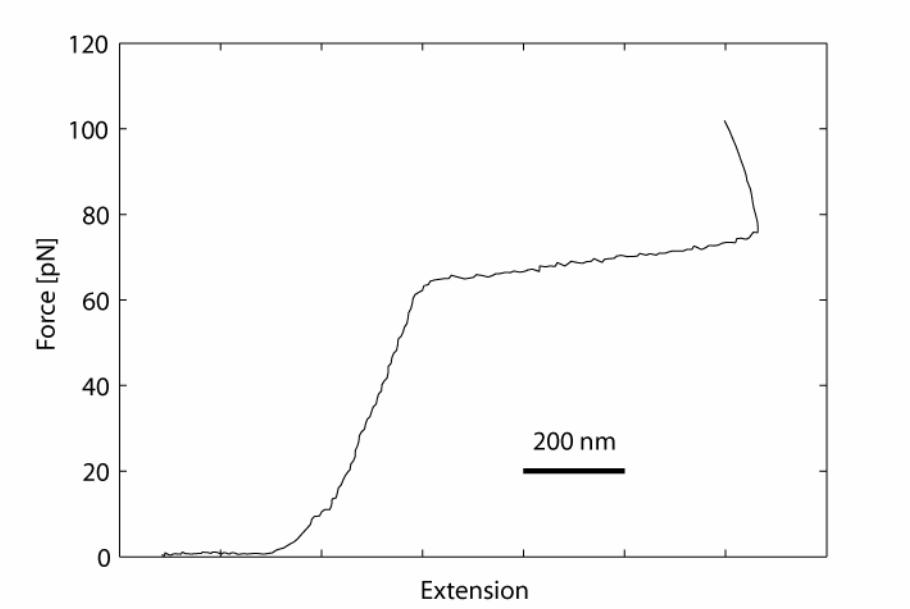

Figure 16. Force-Extension Curve for 3256 bp DNA.

When comparing to the force extension measured by other groups (Pant et al., 2005; Smith et al., 1996; Wang et al., 1997), a less steep curve are seen in Figure 16, when going from zero force to the plateau. Analogues, the plateau is less horizontal in Figure 16 comparing to the plateaus seen for λ DNA. This distortion is due to bending of the micropipette as illustrated in Figure 17. When I turned the micropipette to get the parallel orientation the distortion disappeared. The curve got steeper and the plateau more horizontal. This result is described in more detail in paper II of the appendix. From the data in Paper II (Appendix) the pipette stiffness was estimated to ~0.3 pN/nm. Of course, individual pipettes have varying inner and outer diameters and have differing suspension lengths from their fixed point to the tip, so their flexibility in the orthogonal direction can be expected to vary substantially.

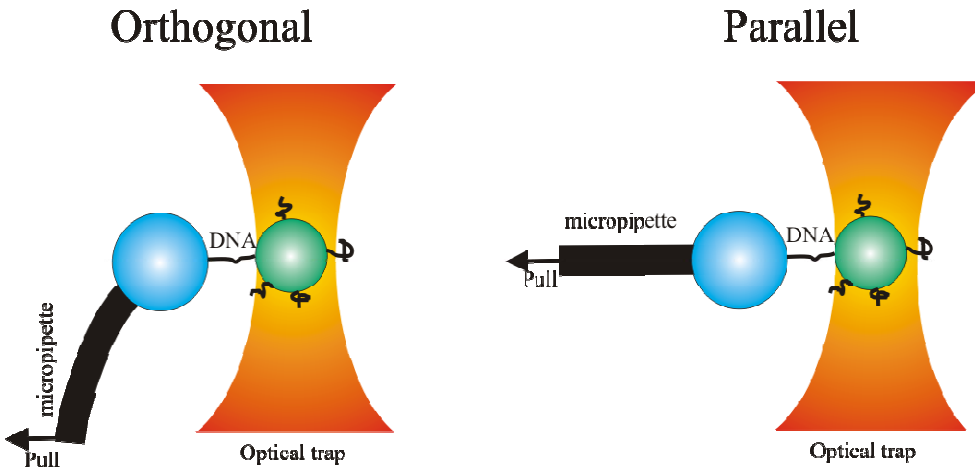

Figure 17. Two geometries for micropipette orientation with respect to pulling direction. The orthogonal geometry was used throughout this work except for the stretching of PK421 RNA and in some parts of Paper II (Appendix), where the parallel geometry was used. The orthogonal geometry results in distorted length measurements due to bending of the micropipette. Using the parallel geometry one should avoid this effect. (Drawing made by Lene Oddershede).

5.2.4 Stretching 942 bp DNA Molecules (L_c=320 nm)

As the last step before turning to stretching experiments with RNA, a DNA molecule with similar length was used to form tethers and perform stretching experiments (see Materials and Methods). The force extension curve for 942 bp DNA in Figure 18 resembles the curves seen with the longer DNA molecules. At low extensions the force is constant and close to zero, but when the extension approaches the contour length of the molecule the force increases fast. To our knowledge, DNA molecules this short, only ~6 times the persistence length for DNA, have not been stretched before.

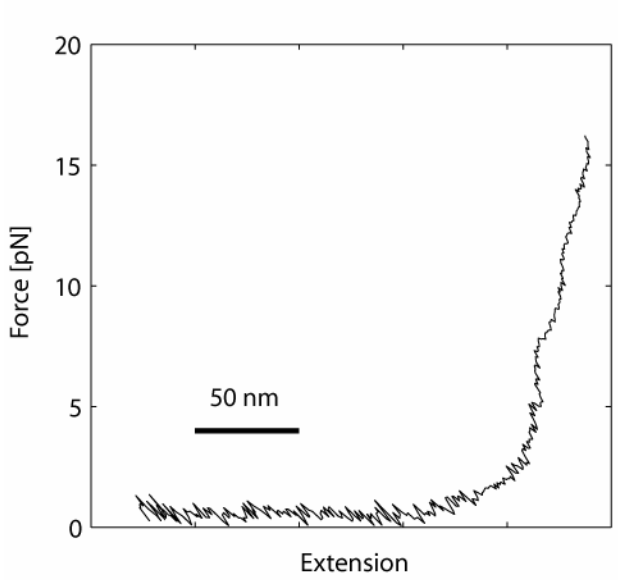

Figure 18. Force-Extension Curve for 942 bp DNA.

In paper III (appendix), the WLC model was fitted to the force-extension curve of these short DNA's, but a reasonable fit can only be made if the persistence length is allowed to be a fitting parameter. If made a fitting parameter, the 'apparent persistence length' is found as 8.7±4 nm, a number which is significantly lower than the physical value (~ 50 nm). This results is not surprising since the WLC model is derived for $L_p << L_c$.

5.3 Frameshifting

5.3.1 Frameshift Sites

In this work an artificial site of programmed ribosomal frameshift resembling that of IBV was investigated. Frameshifting in IBV has been studied extensively by Brierley and co-workers. As a typical -1 frameshift site it includes a slippery sequence and a stimulatory element, which in this case is a 3' pseudoknot (Figure 19). The slippery sequence we used was UUUAAAG rather than UUUAAAC found in IBV, since XXXAAAG is known to be highly "shifty" in *Escherichia coli* (Weiss et al., 1989). The choice of pseudoknot was inspired by the work of Napthine *et al.* (Napthine et al., 1999). They measured frameshift efficiencies in rabbit reticulocyte extracts of a series

of IBV derived pseudoknots with different lengths of stem1 (see Figure 19). Remarkable, frameshift efficiency decreased 7-fold when the length of stem1 was reduced from the wild type length of 11 bp to 10 bp, however when the authors did a structure probing analysis both RNAs formed pseudoknots and appeared indistinguishable in conformation.
Furthermore, their predicted ΔG for stem1 of the wild type IBV and IBV derived pseudoknots with 11 bp and 10 bp stem1 did not correlate with the differences in frameshifting efficiency.
In our experiments, two IBV-like pseudoknots with 11 bp and 10 bp stem1 were compared for frameshift efficiency and mechanical stability in a single molecule experiment. Rather than using the exact same structures as Napthine *et al.* used, the pseudoknots in this work had longer loop2, as in the wild type pseudoknot. This was to make sure that the difference in length of folded and unfolded pseudoknot was above the detection limit of the single molecule experiment. Frameshift efficiency is insensitive to deletions making the loop length shorter than the wild type length of 32 nt as long as the length is above a certain minimal length (Napthine et al., 1999).

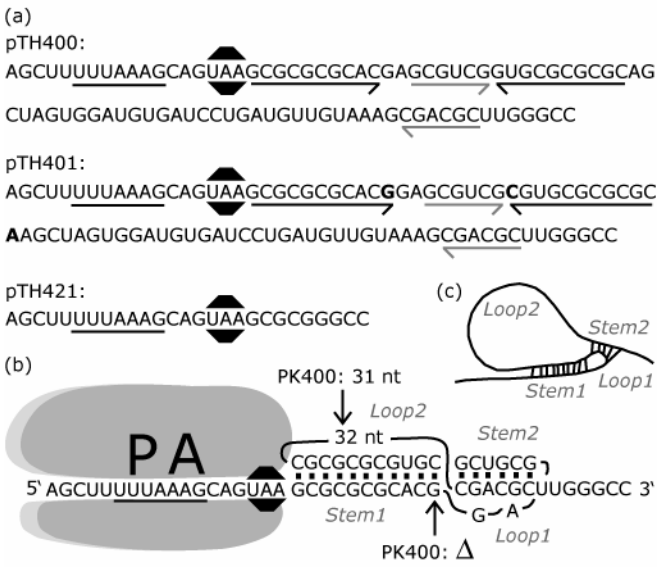

Figure 19. Frameshift Sites. a) Sequences of frameshift sites encoded in plasmids pTH400, pTH401 and pTH421. The slippery sequence is underlined and the stop codon UAA is marked by a black "stop sign". pTH400 and pTH401 encodes the pseudoknots PK400 and PK401. The nucleotides which can form double stranded stems are underlined by arrows; stem1 by black arrows and stem2 by grey arrows. The three nucleotides present only in PK401 are in bold. b) Schematic drawing of an mRNA where the ribosome is positioned with the slippery sequence in it's A- and P-site. The secondary structure of PK401 is indicated with coaxially stacked stems and single stranded loops. Differences to PK400 are indicated by arrows. c) Schematic drawing of pseudoknot.

5.3.2 Two-Fold Difference in Frameshift Frequency when the Pseudoknots are expressed in *E. coli*

Three plasmid constructs were made for measurements of frameshift efficiency. They have the slippery sequence and a 6 nt spacer followed by either a pseudoknot with 11 bp

stem1, a pseudoknot with 10 bp stem1 or no pseudoknot as a control. These elements were inserted in the end of an open reading frame (*orf*) which originates from bacteriophage T7 gene10.
Translation of the *gene10 orf* and the slippery sequence without frameshift will lead to termination at a stop codon in the spacer between slippery sequence and pseudoknot, and release of a 28 kDa termination product. If the ribosome frameshifts -1 at the slippery sequence, then the stop codon is out of frame, and translation continues through the pseudoknot and into a *lacZ orf*. Frameshift and termination at the end of the *lacZ orf* result in a longer 147 kDa frameshift product (Figure 20). The relative amounts of termination and frameshift products were used to estimate the frameshift frequency.

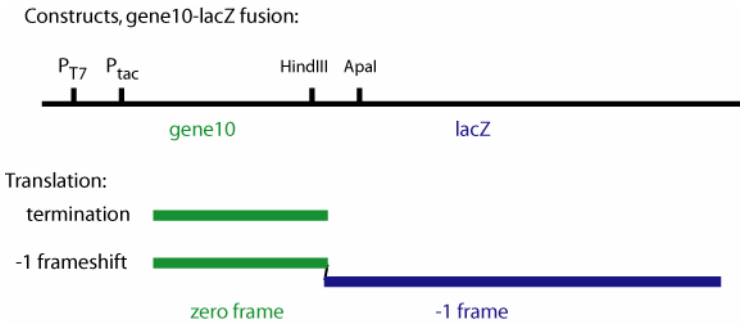

Figure 20. Gene fusions and expression products. At the frameshift site placed between the HindIII and ApaI sites. Ribosomes translating the mRNA without a frameshift terminates at the frameshift site and produce a short protein, whereas frameshifting ribosomes continues translation in the -1 frame and produce a longer protein.

Protein was labeled in pulse chase experiments with cultures of *E. coli* expressing the constructs. Proteins were then separated by gel electrophoresis (Figure 21). Prominent bands corresponding to the termination and frameshift products are identified when lanes of induced cultures are compared with those of uninduced cultures. The presence of the frameshift products in lanes of PK400 and PK401 constructs indicates efficient ribosomal frameshift with either of the pseudoknots encoded in the construct. However, in the control without a pseudoknot only the termination product is visible.
The relative amounts of proteins were estimated to calculate frameshift frequencies. The PK401 construct, which encodes the pseudoknot with an 11 bp stem1, as in the wild type IBV pseudoknot, has the highest frequency of frameshift, 14% ± 1.5 % (mean ± SEM). The pseudoknot with 10bp stem1 leads to two-fold less frameshift. The frequency for the PK400 construct is 5.9% ± 0.40 %. For the PK421 control construct, frameshift frequency is below the detection limit of 1 %.

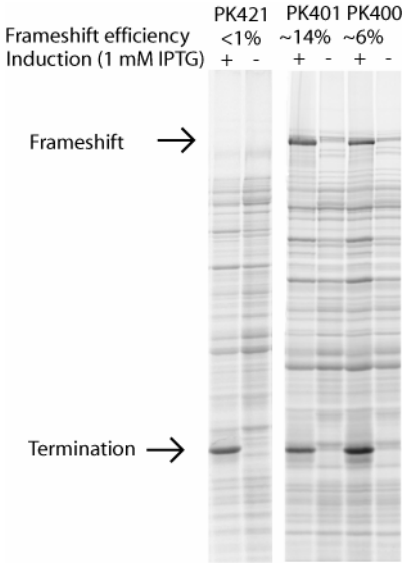

Figure 21. Frameshift Assay. Autoradiogram of SDS-polyacrylamide gel showing proteins labeled by ^{35}S-methionine. Expression from plasmids of genes encoding frameshift sites are induced by the presence of IPTG. For the constructs encoding pseudoknots, PK400 or PK401, induction leads to synthesis of two proteins, indicated by arrows. One protein from ribosomes terminated at the zero frame stop codon which follows the slippery sequence and another protein from ribosomes which frameshifted to the -1 frame. Only the termination product is detected for the construct with no pseudoknot, PK421. The frameshift frequency is given above each lane.

5.3.3 Protein Stability in Frameshift Assay

In the frameshift assay, it is important that the termination and frameshift products are stable. If the products are degraded the estimates of frameshift efficiency will be erroneous. Cultures were labeled with a pulse of ^{35}S-methionine followed by the addition of a chase with 10^5 times molar excess of unlabelled methionine. Samples were withdrawn from the culture 2, 5, 10 and 20 min after the pulse. The samples were analyzed by PAGE (polyacrylamide gel electrophoresis). Figure 22 shows an autoradiogram of the gel. For both plasmids, the protein amounts are the same at all times. It was concluded that the frameshift assays are not corrupted by protein instability.

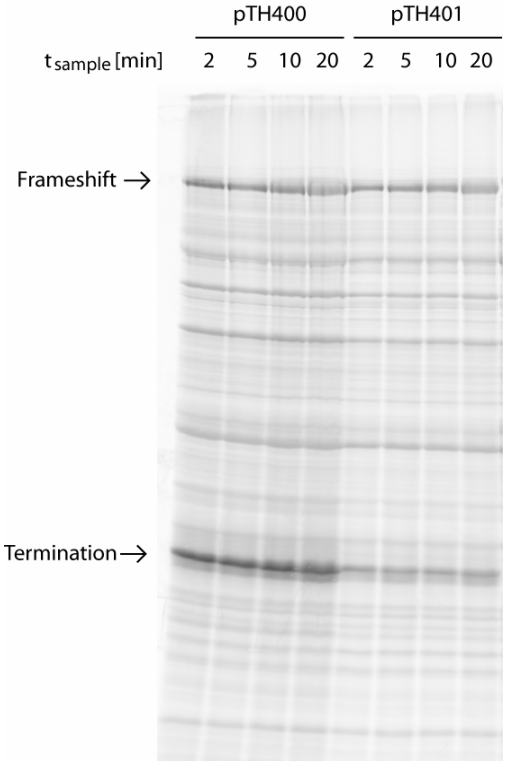

Figure 22. Protein stability in frameshift assay. Autoradiogram of SDS-polyacrylamide gel showing proteins labeled by ^{35}S-methionine. Expression from plasmids of genes encoding frameshift sites are induced by the presence of IPTG. For the constructs encoding pseudoknots, pTH400 or pTH401, induction leads to synthesis of two proteins, a termination product and a frameshift product, see arrows. A pulse of ^{35}S-methionine was given a t_0=0, after a time, t_{sample}, samples were withdrawn.

5.4 Single Molecule Experiment with RNA Pseudoknots

5.4.1 Unfolding of pseudoknots

The pseudoknots were unfolded by exerting a mechanical force on single molecules which encodes the structures. The RNA molecules were attached to micron sized polystyrene beads via DNA handles (Figure 24). Single stranded complimentary DNAs were annealed to the RNA 5' and 3' of the pseudoknot encoding sequence to form RNA/DNA duplexes of about 400 bp. Figure 23, lane 2 show a faint band of RNA without handles (single strand polynucleotides bind the ethidiumbromide stain approx. 10 times less efficient than double stranded). This RNA shifts up in the gel after annealing one of the handles; this can be seen by comparison of lane 3 and 4 with lane 6. After annealing of both handles a prominent band appears representing the complete RNA/DNA duplex, lane 5. The DNA handles were labeled with biotin or digoxygenin in the ends, which allow stable attachment to beads coated with streptavidin or anti-digoxygenin.

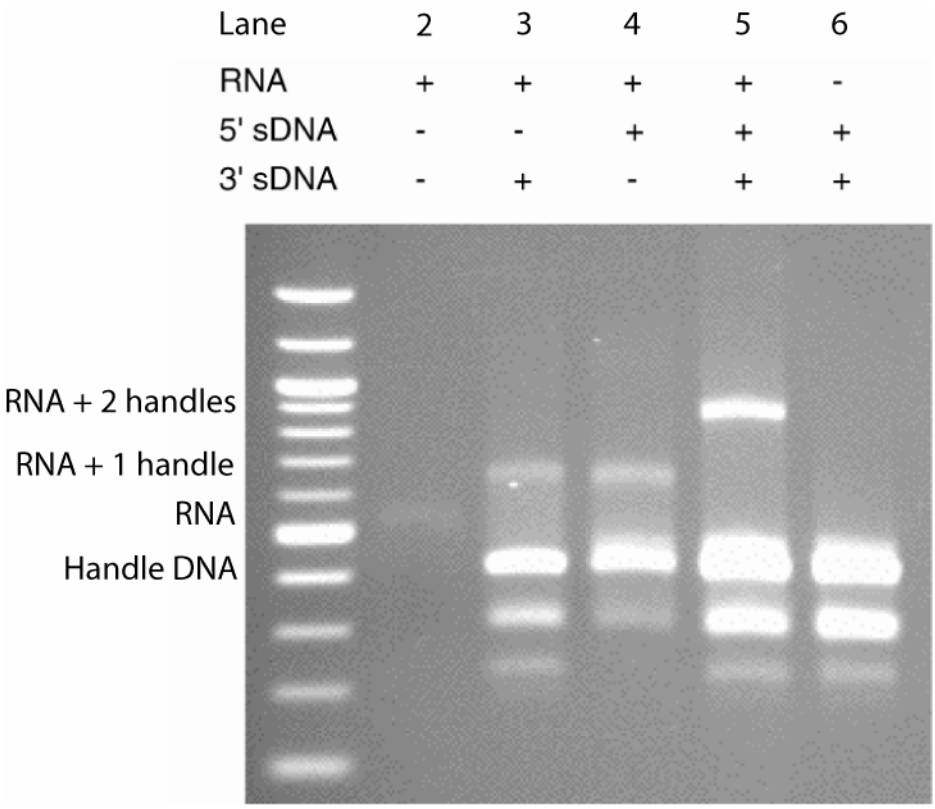

Figure 23. Agarose gel with ethidium bromide stained of RNA and DNA handles. The first lane shows a 100 bp DNA ladder. For the other lanes RNA and DNA handles were mixed as indicated and annealed prior to loading in the gel.

Tethers were formed, in which one end of the RNA/DNA duplex was attached to a bead in an optical trap while the other end was attached to a bead in a micropipette. The optical trap exerts force on the trapped bead and was used to measure force. Within certain limits the stiffness of the optical trap is constant. Hence, when the trap stiffness is known, the force exerted on the bead can be calculated from the displacement of the bead from the trap centre, which was monitored. The position of the bead in the pipette with respect to the bead in the trap was controlled by a piezo electric stage. To stretch the molecule the distance between the beads was increased. The change in the end-to-end distance of the molecule was calculated by subtraction of the displacement of the bead in the trap from the displacement of the pipette. To relax the molecule the movement of the pipette was reversed. Several cycles of stretching and relaxing was performed for each molecule.

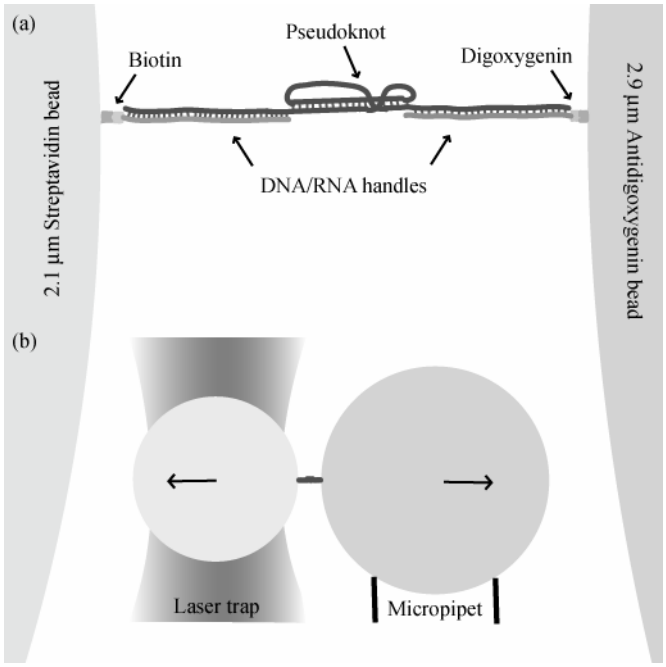

Figure 24. Setup for RNA Single Molecule Experiment. The two beads are drawn at the same scale, as is the total length of the RNA/DNA duplex using its contour length. The dimensions of handles and pseudoknot are not to scale with respect to each other. a) The RNA with complementary DNA handles is attached to beads with biotin-streptavidin and digoxygenin-antidigoxygenin bonds. The RNA/DNA heteroduplexes are 426 base pairs and 415 base pairs and leaves the middle region of the RNA free to form structures. The nucleotide sequences of the middle region are listed in **Figure 19**. B) One bead is placed in the force measuring laser trap, while the other bead is attached to a micropipette. The micro pipette was moved with respect to the laser trap in order to stretch and relax the molecule.

Curves of force and extension from one cycle of stretching and relaxing the PK421 control RNA are shown in Figure 25. The force increases continuously with increasing extension of the molecule and faster at longer extension. In the curves for the PK400 and PK401 RNAs, which encode pseudoknots, a sudden elongation of the molecules is observed in the stretching curve corresponding to unfolding of the pseudoknot. This sudden elongation is referred to as a rip. Surprisingly, the general slope at higher forces of the force extension curves varied substantially, as evident in Figure 25 when comparing PK400 with PK421 and PK401. The variation was also evident when comparing different tethers of the same RNA, PK400 or PK401, held in different micropipettes. The variation in the general slope of the traces is consistent with variations in pipette flexibility. The pipette flexibility leads to distortion of the length measurements when using an orthogonal geometry (see Figure 17).

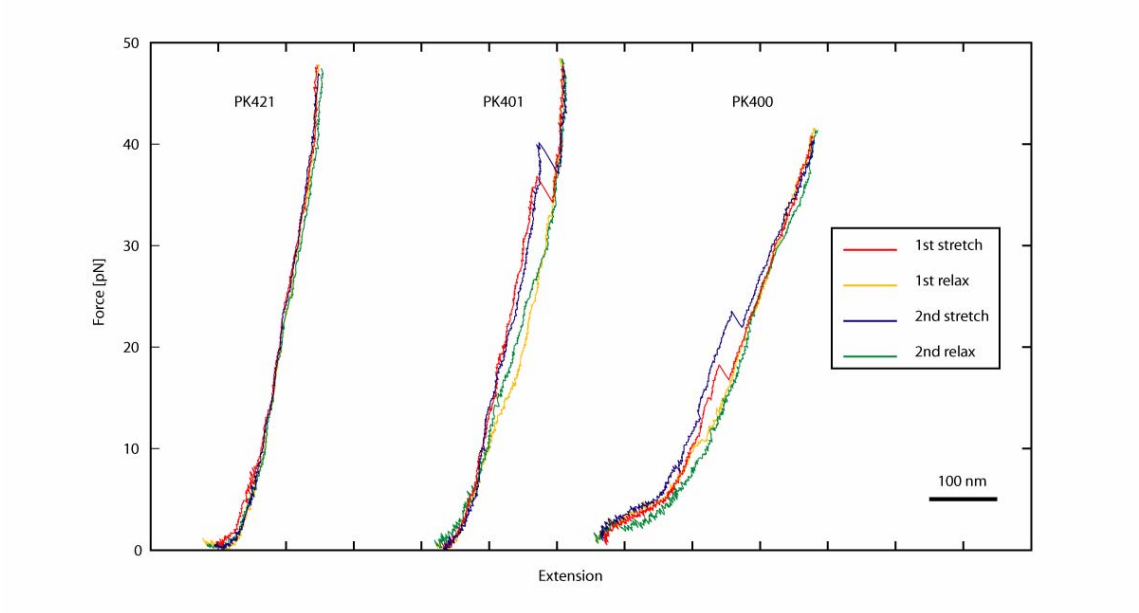

Figure 25. Stretch and Relax Curves of Single Molecules. Force and change in extension were measured in several cycles of stretching and relaxing of single molecules. Here data from two cycles are shown for pseudoknot containing RNA, PK400 and PK401, and for the no pseudoknot control PK421.

5.4.2 Filtering to avoid false positives tethers

One fourth of the PK400 and one half of PK401 stretching curves showed the rip characteristic of a single molecule unfolding event. The tethers not showing rips might be false positives in the sense that the beads are attached, but not by a single RNA/DNA duplex as intended. Such false positives certainly exist since tethers were formed in a control experiment with no RNA/DNA duplex added, however they appeared relative infrequently. The false tethers might be polystyrene hairs on the beads, dirt, or multiple RNA/DNA tethers.

In an attempt to avoid false positive tethers in the data set all traces were subjected to a filter using two criteria on the low force part of the force extension curve. The curve should be relatively horizontal and the distribution of bead positions relatively broad (see 4.5.4 for an exact definition of the criteria). The rationale is that these properties apply to a tether of a single RNA/DNA duplex at low force, but not to many of the unspecific attachments and adhesions of the beads.

After filtering the fraction of traces with a rip for PK400, PK401 and PK421 RNA were 42 %, 63 % and 12 %, respectively. The filter processing substantially increased the fraction of PK400 and PK401 stretch traces showing a rip, especially for the PK400 RNA, while fraction for PK421 slightly decreased. Still, the filter is not perfect, which is illustrated by the fact that one of the false tethers formed in the control experiment with no RNA passed the filter (data not shown).

	PK400 stretch			PK400 relax
	rip	**no rip**	**total**	**total**
no filter [number of traces]	**48**	**134**	**182**	**152**
filter [number of traces]	**32**	**44**	**76**	**73**
no filter [fraction]	**0.26**	**0.74**	**1.00**	
filter [fraction]	**0.42**	**0.58**	**1.00**	
	PK401 stretch			PK401 relax
	rip	**no rip**	**total**	**total**
no filter [number of traces]	**116**	**110**	**226**	**180**
filter [number of traces]	**100**	**59**	**159**	**135**
no filter [fraction]	**0.51**	**0.49**	**1.00**	
filter [fraction]	**0.63**	**0.37**	**1.00**	
	PK421 stretch			PK421 relax
	rip	**no rip**	**total**	**total**
no filter [number of traces]	**11**	**65**	**76**	**46**
filter [number of traces]	**8**	**59**	**67**	**42**
no filter [fraction]	**0.14**	**0.86**	**1.00**	
filter [fraction]	**0.12**	**0.88**	**1.00**	

Table 5. Filtering of traces using two criteria (see text).

Three other criteria for the filter were also tested, but not used in the final filtering. The first of those was that the trace should contain forces above 40 pN in order to be considered. We chose not to use this criteria, since even one of the desired single molecule traces could have a maximal force below 40 pN e.g. if tether broke or that we by chance didn't pull it far enough to get such a force. The second of those was a stricter criterion for the flatness of the low force part of the curve. The third criterion was that the rip length should be greater than 10 nm. An important point from testing those different criteria was that adding these criteria reduced the number of traces to be considered, but it did not change the average rip force significantly. Also it did not change our main the conclusion, namely that PK401 unfold at a significantly higher force than PK400.

5.4.3 Differences in Unfolding and Refolding Traces

With the resolution used in this work the pseudoknots seem preferably to unfold in one step, since only one rip is observed in the majority of the stretch curves. However, when the datasets were examined before averagering the data points, 4 of 100 traces from PK401 showed an intermediate state. For these four traces it is noteworthy, that the first unfolding part is longer than the second in all data sets. This suggests that stem2 melts prior to stem1. None of the 32 PK400 traces showed an intermediate state.
The relax curves in Figure 25 show gradual convergence to the stretch curve while the force decreases. However, the relax curves differ substantially qualitatively. For both of the pseudoknots the relax traces were grouped into five categories, depending on how the relax curve fitted with the corresponding stretching curve:

I) One clear refolding transition.
II) One smaller refolding event plus a gradual refolding.
III) Two clear refolding events.
IV) One gradual and slow refolding (as in Figure 25).

V) None of the others.

For the PK400, 22 refolding traces were analyzed, whereas for PK401, 73 refolding traces were analyzed. The distribution is shown in Table 6.

	I) One clear refolding transition	II) One smaller refolding event plus a gradual refolding	III) Two clear refolding events	IV) One gradual and slow refolding	V) None of the others
PK400	**5.7%**	**26%**	**8.0%**	**39%**	**22%**
PK401	**25%**	**20%**	**18%**	**28%**	**8.9%**

Table 6. Refolding trace categories.

5.4.4 Unfolding and Refolding Forces

The distribution of rip forces, at which the structure unfolds, is shown in Figure 26a. The mean forces were 31±1.9 pN for the PK400 and 39±1.5 pN (mean ± SEM) for the PK401 pseudoknot. These values are significantly different (student t-test, H_0: The two distributions have the same mean, $p<0.005$). The PK401 pseudoknot, which stimulates the highest level of frameshifting, unfolds at the largest forces. Hence, for the two pseudoknots these properties correlate, which is consistent with the '9 Å model' and the pausing model of -1 ribosomal frameshift.

The variation in unfolding forces is expected to reflect the stochastic nature of a thermally facilitated process. Surprisingly, the unfolding forces are relatively broadly distributed. The standard deviations of 10 and 15 pN are 20-30 fold greater than found in similar experiments of unfolding other RNA structures (Li et al., 2006; Liphardt et al., 2001). Whether the broad distribution is due only to the nature of RNA pseudoknots or it is simply due to a higher experimental error in our setup is an open question.

Clearly, the III) category shows that in a substantial fraction of the refolding traces, there are two distinguishable events. For PK401 these two distinguishable events happen at 9.4±4 pN and 19±4 pN (mean±SD), respectively. One might speculate that this originates from the refolding e.g. of the stem1 followed by a refolding of stem2. The refolding data from PK400 was too sparse to allow a similar analysis.

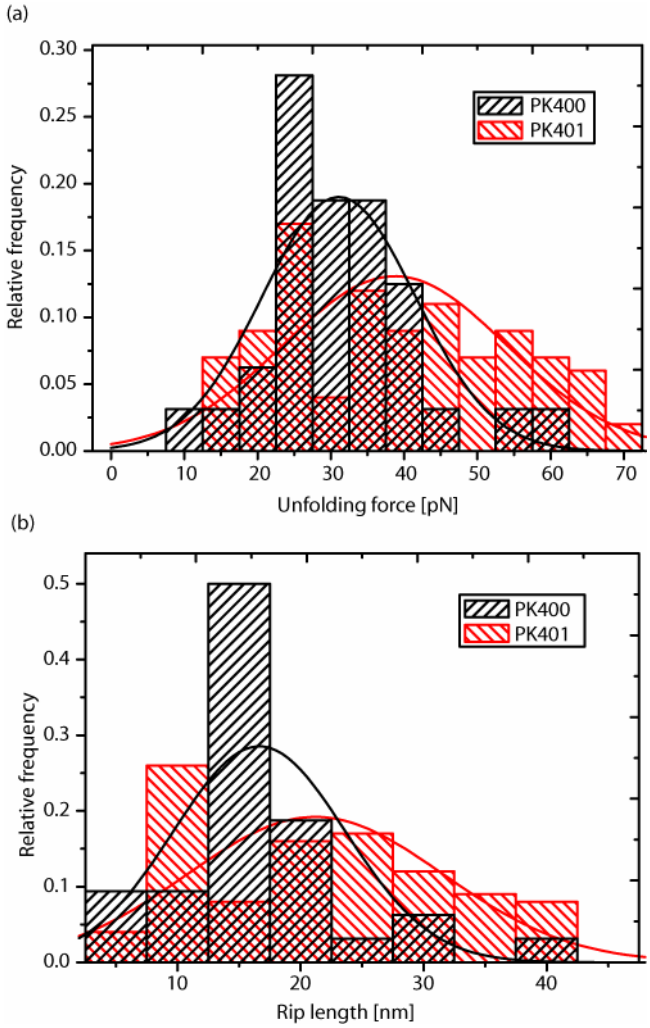

Figure 26. Histograms of Unfolding Forces and Rip Lengths. The distributions of unfolding forces (a) and rip lengths (b) are shown in histograms. The values were estimated from individual stretching curves of PK400 and PK401 RNA's. Also Gaussian curves are drawn based on the calculated mean and standard deviation of the data sets.

5.4.5 Rip Lengths

Figure 26 shows the distribution of rip lengths. The mean rip length were 17±1.2 nm for the PK400 and 21±1.0 nm for the PK401 pseudoknot. These lengths are significantly different (student t-test, H_0: The two distributions have the same mean, $p<0.005$). A theoretical estimate of the rip length was calculated from the EWLC formula (Marko and Siggia, 1995; Odjik, 1995) setting the persistence length of ssRNA (single stranded RNA) to 1 nm, the contour length to 0.59 nm/nt (Tinoco, 2004) and the stretch modulus *K* to 1 nN. The pseudoknots were approximated by a continuous helix of 16 and 17 bp with a rise of 0.28 nm/bp as in the canonical RNA A-helix (Holbrook and Kim, 1997). The pseudoknots and duplex handles were treated as non-elastic. The results are predicted rip lengths of 27.8 and 30.1 nm, which are, respectively, a half and a third longer than the measured values. The rip length data is summarized in Table 7.
The slope of a rip and of the noise seen throughout the curves is due to the properties of the optical trap. When the pseudoknot unfolds the bead in the trap moves to adjust to the increase in length of the RNA. In the trap, force is measured from the distance of bead

moved from the centre of the trap. Force and distance are thus coupled by the spring constant which describes the trap stiffness. The slope of the rip and the noise are equal to the value of the spring constant. The predicted rip length does not change significantly even when the drop in force after the rip is included in the calculations.
The discrepancy between the actual and the predicted rip lengths is consistent with the distortive effect of the flexibility of the micropipettes when used in the orthogonal geometry (see Figure 17). Hence, a force drop of 1-2 pN after rip would result in a pipette movement of 3-6 nm using 0.3 pN/nm for the pipette stiffness.

5.4.6 Thermodynamics

The total work of unfolding the pseudoknot was estimated from the experimental data as the area underneath the force-extension curve during unfolding. The work is 317 ± 48 kJ/mol for PK400 and 501 ± 36 kJ/mol for PK401. Due to the distortive effect of the micropipette flexibility, when used in the orthogonal geometry (see 5.2.3), these numbers are probably overestimated. The total work includes the irreversible and reversible parts of the work of unfolding the pseudoknot as well as the work of stretching the ssRNA of the unfolded pseudoknot to its extension at the unfolding force.
Estimates of the change in free energy of unfolding the structures was calculated from the nucleotide sequence of the pseudoknots by the *pknotsRG* algorithm (http://bibiserv.techfak.uni-bielefeld.de/pknotsrg/, (Reeder and Giegerich, 2004), and were 151 kJ/mol for PK400 and 165 kJ/mol for PK401 at 37 °C and 1 M Na^+.
A theoretical estimate of the work of stretching the ssRNA of the unfolded pseudoknot from zero to it's extension at the unfolding force was calculated by integration of the EWLC formula (Marko and Siggia, 1995; Odjik, 1995) with respect to extension (Tinoco, 2004)and was 111 kJ/mol for PK400 and 127 kJ/mol for PK401. The thermodynamics data is summarized in Table 7.
The energy estimates are consistent with a significant irreversible work of unfolding at the experimental conditions (20 °C, 10 mM Tris-HCl pH 7.5, 250 mM NaCl, 10 mM Mg_2Cl). The loading rate was approximately 10 pN/s. Using a slower loading rate should decrease the irreversible part of the work, but is difficult in practise due to low frequency drift of the equipment..

RNA	ΔG^0_{theory} kJ/mol	$W_{str,theory}$ kJ/mol	$\Delta G_{total,theory}$ kJ/mol	R_{theory} nm	R_{exp} nm	W_{total} kJ/mol	$\Delta G_{Jarzynski}$ kJ/mol	ΔG_{Crooks} kJ/mol
PK400	151	111	262	27.8	17±1.2	317±48	77.6	------
PK401	165	127	292	30.1	21±1.0	501 ± 36	94	104

Table 7. Experimental and calculated thermodynamics parameters for mechanical unfolding of the two RNA pseudoknots. ΔG^0_{theory} is the standard Gibbs free energy of unfolding the pseudoknot at 37 C in 1M Na+ obtained from the *pknotsRG* algorithm http://bibiserv.techfak.uni-bielefeld.de/pknotsrg/. $W_{str,theory}$ is the calculated work it takes to stretch the RNA tether from zero to the unfolding force using equation 1. $\Delta G_{total,theory} = \Delta G^0_{theory} + W_{str,theory}$. R_{theory} is the calculated change in length of the RNA tether during the unfolding process, R_{exp} is the similar value experimentally measured. W_{total} is the area underneath the F-x curve during unfolding. $\Delta G_{Jarzynski}$ and ΔG_{Crooks} are the Gibbs free energies found by Jarzynski's and Crooks methods, respectively.

In paper IV, Lene Oddershede and Nader Reihani calculated the reversible work of unfolding the pseudoknots from the total work (irreversible + reversible) by the methods of Jarzynski and of Crooks (Crooks, 1999; Jarzynski, 1997), see Table 7. These estimates are significantly lower than the ones obtained by the *pknotsRG* algorithm. Jarzynski and Crooks assume a two-state process and we do observe more than two states in some traces (intermediate states, see 5.4.3). Hence, it is not trivial whether these methods apply. But since, at present, no theory exists which take intermediate states into account, Jarzynski and Crooks methods were employed.

5.4.7 Kinetics

Kinetic parameters were extracted the from repetitive unfolding of a single molecules at constant loading rate, r, as described in (Evans and Ritchie, 1997; Tinoco, 2004). The probability, P, that the unfolding reaction has not occurred at a particular force, F, was calculated from the distribution of unfolding forces. Figure 27 shows plots of (r ln(1/P)) versus F and fits to the derived in section 3.4: $(r \times \ln(1/P)) = \ln[k(0)/b][\exp(bF)-1]$, where k(0) is the apparent rate constant at zero force and $b = X^{\ddagger}/k_BT$. $X^{\ddagger}$ is the distance to the transition state. The low and apparently similar values $X^{\ddagger} = 0.18 \pm 0.06$ nm for PK400 and $X^{\ddagger} = 0.19 \pm 0.01$ nm for PK401 show that both pseudoknots are "brittle" structures. They resist mechanical deformation but once they are deformed they fracture. $k(0) = 0.16 \pm 0.08$ s^{-1} for PK400 and $k(0)= 0.074 \pm 0.007$ s^{-1} for PK401, but this difference is not statistically significant. The rate constant of unfolding depend on force in an Arrhenius like expression, $k(F) = k(0) \times \exp(FX^{\ddagger}/k_BT)$. At a constant force of 20 pN the lifetime is 4 s, using $X^{\ddagger} = 0.2$ nm and $k(0) = 0.1$ s^{-1}.

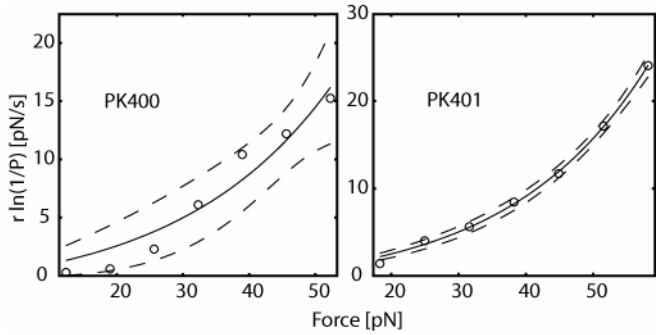

Figure 27. Fits to a Kinetic Equation. The kinetic equation is explained in the text. The graphs show experimental values (circles), expected values (line, last equation in section 3.4) as well as 95 % confidence intervals (dashed line).

Chapter 6.

Discussion

In this work two pseudoknots have been compared by single molecule stretching experiments and by a ribosomal frameshift assay in living cells. The two pseudoknots were constructed in such a way that they differ minimally in structure but, from previous observations (Napthine et al., 1999) were expected to show significant variation in their ability to cause frameshifting at a slippery sequence. The two structures differ by three nucleotides which cause the length of their stem1 to be able to form 10 and 11 bp, respectively (Figure 19). As predicted, the pseudoknots efficiently stimulated frameshift *in vivo* with a two fold difference in frequency (Figure 21).

In an attempt to mimic the action of a translating ribosome we chose to perform stretching experiments, on single RNA molecules containing our two different pseudoknots. The difference in unfolding forces correlates positively to the difference in frameshift frequencies for the two pseudoknots investigated. This is consistent with the '9 Å model' of frameshift stimulation which builds on the possible resistance of the pseudoknot to unfold at its entrance into the mRNA channel of the ribosome. The pseudoknot therefore blocks the channel and forces the ribosome to slip one base downstream at the accommodation step. A step that in the normal translational cycle causes a 9 Å allosteric induced movement in the ribosome upon GTP hydrolysis at the incoming ternary complex Figure 3.

The single molecule stretching experiments reveal physical properties unaccounted for by equilibrium calculations of ΔG and ΔG estimated from thermal melting ensemble measurements. The mean work needed for unfolding of the two pseudoknots was significantly larger than the work calculated for the reversible unfolding. This is consistent with the irreversible nature of the unfolding process in the experiments. I expect the mechanical unfolding of the pseudoknot by the ribosome to follow yet another path, since the direction and magnitude of the forces applied by the ribosome is different from those in the optical tweezers experiment or in thermal melting. However it seems reasonable, that the pseudoknot which is most stable in the experiment is also most stable with regards to unfolding by a ribosome.

Interestingly, the work of unfolding the pseudoknots by stretching was much greater than the energy released by hydrolysis of GTP in the accommodation step (~35 kJ/mole ~60 pN nm). Thus, we expect that unfolding of the pseudoknot is an energetic barrier to the movement of the ribosome.

In comparison to a stem-loop structure, the pseudoknot has lost its rotational freedom in the stem1 helix due to the "locking" via base pairing in stem2. This locking could cause a need for more bp to be broken simultaneously, probably in stem2, before the structure resolves. In accordance, stem loop structures have previously been shown not to be a

hindrance for ribosome movement *in vivo* (Sorensen et al., 1989) and unable to stimulate frameshifting in IBV (Somogyi et al., 1993).

It is noteworthy, that the pseudoknots preferably unfold in one step and not in two steps, one for each stem. For those four PK401 traces, that did show an intermediate state, consistently in all data sets the first unfolding part is longer than the second, suggesting that stem2 goes first and then stem1. The relax curves differ substantially and could be sorted into five categories based on their qualitative appearance. These qualitative differences might represent different paths in the energy landscape when going from the unfolded to the folded state.

I the kinetic analysis, the difference between the two pseudoknots could not be attributed to a single kinetic parameter, k (0) or $X^{\ddagger}$ due to the statistics of the data set, the analysis revealed that pseudoknots are "brittle" structures with $X^{\ddagger}$ values close to 0.2 nm. Previously, secondary structures such as stem loops were shown to be compliant with $X^{\ddagger}$ values of 5-10 nm, whereas tertiary structures were "brittle" with $X^{\ddagger}$ values close to 1 nm (Liphardt et al., 2001; Onoa et al., 2003). It seems that for this aspect, the pseudoknots resemble tertiary structure more than the related stem-loop secondary structures. The 'brittleness' might be important for the stimulation of frameshift.

One might assume the rate constant depend on force in an Arrhenius like expression, $k(F) = k(0) \exp(FX^{\ddagger}/k_BT)$. At a constant force of 20 pN the mean lifetime is 4 s, using $X^{\ddagger} = 0.2$ nm and $k(0) = 0.1\ s^{-1}$. The ratio of the two pseudoknots lifetimes is independent of force, provided that the $X^{\ddagger}$ values are equal. Although the two fold difference in k(0) between the two structures were not found to be significant, it could indicate a two fold difference in their mean lifetime. This could support the pausing hypothesis of ribosomal frameshifting where the time spent on the slippery sequence, caused by pausing at the pseudoknot, is important to explain the increase in the probability of frameshifting accordingly (Rice et al., 1985). However, future experiments yielding data from more than two different structures are needed to build a firm correlation.

From the stretching experiments it seems that there is a large difference in the mechanical strength of the pseudoknots, and it therefore seems most likely that the work needed to unfold such a structure causes the difference in stimulatory effects on frameshifting. It is worthwhile to unfold more pseudoknots and measure their ability to stimulate frameshifting in order build a sound correlation.

For future experiments it is worth doing an effort to reduce the variation in the measurements since it seems large compared to the measured values. This experimental variation is seen in data in several ways: 1) there is a significant variation in the general slope of the traces (Figure 25). I expect the slope within one kind tether to be same in all experiments. 2) Within one kind of tether and at a particular force, the rip length should be the same for a complete unfolding of the pseudoknot. To evaluate the variation in rip lengths (Figure 26), it might be necessary to normalize the data to a particular force. Such normalization is non-trivial since the lack of a model describing the force-extension relationships of the tethers. 3) In order to analyze the data we had to

normalize the data so to make the first point in the trace correspond to zero force and zero extension (see 4.5.4). With a calibration of the trap which describes the trap precisely during the actual stretch experiments, such a harsh treatment of the data should be unnecessary.

As mentioned above it would be worthwhile to unfold more pseudoknots and measure their ability to stimulate frameshifting in order build a sound correlation. To address this point one could make more mutant derivatives of the IBV pseudoknot. This might give a variety of frameshift efficiencies and corresponding mechanical stabilities and help prove or disprove the positive correlation between frameshift stimulation and mechanical stability found in this thesis. The data set should be supplemented by data for the 3D-structures in order to understand the relations of structure, mechanical stability and ability to stimulate frameshifting.

To address the observed correlation in a broader sense, pseudoknots from other viruses should be tested. There exist two classes of pseudoknots basis on structure (Giedroc et al., 2000) and it would be informative to study pseudoknots from both classes. Other structures which act as downstream stimulators in programmed ribosomal frameshifting includes three-way junctions, kissing-loops and hairpins (Baranov et al., 2006; Larsen et al., 1997). If these structures are added to the data set it will be interesting to look for common and non-common properties in order to better understand the mechanism of frameshift stimulation.

Another future approach to the studies of protein synthesis and ribosomal frame maintenance is to do optical tweezers experiments with single ribosomes directly in the sample chamber (Vanzi et al., 2005).

References

Atkins, J.F., P.V. Baranov, O. Fayet, A.J. Herr, M.T. Howard, I.P. Ivanov, S. Matsufuji, W.A. Miller, B. Moore, M.F. Prere, N.M. Wills, J. Zhou, and R.F. Gesteland. 2001. Overriding standard decoding: implications of recoding for ribosome function and enrichment of gene expression. *Cold Spring Harb Symp Quant Biol* 66:217-232.

Atkins, J.F., D. Elseviers, and L. Gorini. 1972. Low activity of -galactosidase in frameshift mutants of Escherichia coli. *Proc Natl Acad Sci U S A* 69(5):1192-1195.

Baranov, P.V., O. Fayet, R.W. Hendrix, and J.F. Atkins. 2006. Recoding in bacteriophages and bacterial IS elements. *Trends Genet* 22(3):174-181.

Baranov, P.V., R.F. Gesteland, and J.F. Atkins. 2004. P-site tRNA is a crucial initiator of ribosomal frameshifting. *Rna* 10(2):221-230.

Baranov, P.V., O.L. Gurvich, A.W. Hammer, R.F. Gesteland, and J.F. Atkins. 2003. Recode 2003. *Nucleic Acids Res* 31(1):87-89.

Berg-Sorensen, K., L. Oddershede, E.L. Florin, and H. Flyvbjerg. 2003. Unintended filtering in a typical photodiode detection system for optical tweezers. *Journal of Applied Physics* 93(6):3167-3176.

Crooks, G.E. 1999. Entropy production fluctuation theorem and the nonequilibrium work relation for free energy differences. *Phys. Rev. E* 60:2721-2726.

Evans, E., and K. Ritchie. 1997. Dynamic strength of molecular adhesion bonds. *Biophys J* 72(4):1541-1555.

Farabaugh, P.J. 1996. Programmed translational frameshifting. *Microbiol Rev* 60(1):103-134.

Gesteland, R.F., and J.F. Atkins. 1996. Recoding: dynamic reprogramming of translation. *Annu Rev Biochem* 65:741-768.

Giedroc, D.P., C.A. Theimer, and P.L. Nixon. 2000. Structure, stability and function of RNA pseudoknots involved in stimulating ribosomal frameshifting. *J Mol Biol* 298(2):167-185.

Hansen, P., I. Tolic-Norrelykke, H. Flyvbjerg, and K. Berg-Sorensen. 2006. Tweezercalib 2.0: Faster version of a MatLab package for precision calibration of optical tweezers. *Comput. Phys. Commun.* 174:518-520.

Holbrook, S.R., and S.H. Kim. 1997. RNA crystallography. *Biopolymers* 44(1):3-21.

Jacks, T., H.D. Madhani, F.R. Masiarz, and H.E. Varmus. 1988. Signals for ribosomal frameshifting in the Rous sarcoma virus gag-pol region. *Cell* 55(3):447-458.

Jarzynski, C. 1997. Nonequilibrium Equality for Free Energy Differences. *Phys. Rev. Lett.* 78:2690-2693.

Kontos, H., S. Napthine, and I. Brierley. 2001. Ribosomal pausing at a frameshifter RNA pseudoknot is sensitive to reading phase but shows little correlation with frameshift efficiency. *Mol Cell Biol* 21(24):8657-8670.

Kurland, C.G. 1979. Translational accuracy and the fitness of bacteria. *In* Nonsense Mutations and tRNA Suppressors. Celis JE, Smith JD, editors. Academic Press., London. 98-108.

Larsen, B., R.F. Gesteland, and J.F. Atkins. 1997. Structural probing and mutagenic analysis of the stem-loop required for Escherichia coli dnaX ribosomal frameshifting: programmed efficiency of 50%. *J Mol Biol* 271(1):47-60.

Larsen, B., N.M. Wills, R.F. Gesteland, and J.F. Atkins. 1994. rRNA-mRNA base pairing stimulates a programmed -1 ribosomal frameshift. *J Bacteriol* 176(22):6842-6851.

Li, P.T., D. Collin, S.B. Smith, C. Bustamante, and I. Tinoco, Jr. 2006. Probing the mechanical folding kinetics of TAR RNA by hopping, force-jump, and force-ramp methods. *Biophys J* 90(1):250-260.

Liphardt, J., S. Dumont, S.B. Smith, I. Tinoco, Jr., and C. Bustamante. 2002. Equilibrium information from nonequilibrium measurements in an experimental test of Jarzynski's equality. *Science* 296(5574):1832-1835.

Liphardt, J., B. Onoa, S.B. Smith, I.J. Tinoco, and C. Bustamante. 2001. Reversible unfolding of single RNA molecules by mechanical force. *Science* 292(5517):733-737.

Manosas, M., J.D. Wen, P. Li, S. Smith, C. Bustamante, I. Tinoco Jr, and F. Ritort. 2007. Force unfolding kinetics of RNA using optical tweezers. II. Modeling experiments. *Biophys J*.

Marko, J.F., and E.D. Siggia. 1995. Stretching DNA. *Macromolecules* 28(26):8759-8770.

Merkel, R., P. Nassoy, A. Leung, K. Ritchie, and E. Evans. 1999. Energy landscapes of receptor-ligand bonds explored with dynamic force spectroscopy. *Nature* 397(6714):50-53.

Namy, O., S.J. Moran, D.I. Stuart, R.J. Gilbert, and I. Brierley. 2006. A mechanical explanation of RNA pseudoknot function in programmed ribosomal frameshifting. *Nature* 441(7090):244-247.

Napthine, S., J. Liphardt, A. Bloys, S. Routledge, and I. Brierley. 1999. The role of RNA pseudoknot stem 1 length in the promotion of efficient -1 ribosomal frameshifting. *J Mol Biol* 288(3):305-320.

Oddershede, L., S. Grego, S.F. Nørrelykke, and K. Berg-Sorensen. 2001. Probing Biological Surfaces. *Probe Microscopy* 2:129-137.

Odjik, T. 1995. Stiff chains and filaments under tension. *Macromolecules* 28:7016-7018.

Onoa, B., S. Dumont, J. Liphardt, S.B. Smith, I. Tinoco, Jr., and C. Bustamante. 2003. Identifying kinetic barriers to mechanical unfolding of the T. thermophila ribozyme. *Science* 299(5614):1892-1895.

Onoa, B., and I. Tinoco, Jr. 2004. RNA folding and unfolding. *Curr Opin Struct Biol* 14(3):374-379.

Pant, K., R.L. Karpel, I. Rouzina, and M.C. Williams. 2005. Salt dependent binding of T4 gene 32 protein to single and double-stranded DNA: single molecule force spectroscopy measurements. *J Mol Biol* 349(2):317-330.

Plant, E.P., and J.D. Dinman. 2005. Torsional restraint: a new twist on frameshifting pseudoknots. *Nucleic Acids Res* 33(6):1825-1833.

Plant, E.P., K.L. Jacobs, J.W. Harger, A. Meskauskas, J.L. Jacobs, J.L. Baxter, A.N. Petrov, and J.D. Dinman. 2003. The 9-A solution: how mRNA pseudoknots promote efficient programmed -1 ribosomal frameshifting. *Rna* 9(2):168-174.

Reeder, J., and R. Giegerich. 2004. Design, implementation and evaluation of a practical pseudoknot folding algorithm based on thermodynamics. *BMC Bioinformatics* 5:104.

Rettberg, C.C., M.F. Prere, R.F. Gesteland, J.F. Atkins, and O. Fayet. 1999. A three-way junction and constituent stem-loops as the stimulator for programmed -1

frameshifting in bacterial insertion sequence IS911. *J Mol Biol* 286(5):1365-1378.
Rice, N.R., R.M. Stephens, A. Burny, and R.V. Gilden. 1985. The gag and pol genes of bovine leukemia virus: nucleotide sequence and analysis. *Virology* 142(2):357-377.
Rohrbach, A. 2005. Stiffness of Optical Traps: Quantitative Agreement between Experiment and Electromagnetic Theory. *Phys. Rev. Lett.* 95:168102.
Sambrook, J., E.F. Fritsch, and T. Maniatis. 1989. Molecular Cloning: A Laboratory Manual. Cold Spring Harbor Laboratory Press, NY.
Smith, S.B., Y. Cui, and C. Bustamante. 1996. Overstretching B-DNA: the elastic response of individual double-stranded and single-stranded DNA molecules. *Science* 271(5250):795-799.
Somogyi, P., A.J. Jenner, I. Brierley, and S.C. Inglis. 1993. Ribosomal pausing during translation of an RNA pseudoknot. *Mol Cell Biol* 13(11):6931-6940.
Sorensen, M.A., C.G. Kurland, and S. Pedersen. 1989. Codon usage determines translation rate in Escherichia coli. *J Mol Biol* 207(2):365-377.
Svoboda, K., and S.M. Block. 1994. Biological applications of optical forces. *Annu Rev Biophys Biomol Struct* 23:247-285.
ten Dam, E., I. Brierley, S. Inglis, and C. Pleij. 1994. Identification and analysis of the pseudoknot-containing gag-pro ribosomal frameshift signal of simian retrovirus-1. *Nucleic Acids Res* 22(12):2304-2310.
Tinoco, I., Jr. 2004. Force as a useful variable in reactions: unfolding RNA. *Annu Rev Biophys Biomol Struct* 33:363-385.
Tu, C., T.H. Tzeng, and J.A. Bruenn. 1992. Ribosomal movement impeded at a pseudoknot required for frameshifting. *Proc Natl Acad Sci U S A* 89(18):8636-8640.
Vanzi, F., Y. Takagi, H. Shuman, B.S. Cooperman, and Y.E. Goldman. 2005. Mechanical studies of single ribosome/mRNA complexes. *Biophys J* 89(3):1909-1919.
Wang, M.D., H. Yin, R. Landick, J. Gelles, and S.M. Block. 1997. Stretching DNA with optical tweezers. *Biophys J* 72(3):1335-1346.
Weiss, R.B., D.M. Dunn, A.E. Dahlberg, J.F. Atkins, and R.F. Gesteland. 1988. Reading frame switch caused by base-pair formation between the 3' end of 16S rRNA and the mRNA during elongation of protein synthesis in Escherichia coli. *Embo J* 7(5):1503-1507.
Weiss, R.B., D.M. Dunn, M. Shuh, J.F. Atkins, and R.F. Gesteland. 1989. E. coli ribosomes re-phase on retroviral frameshift signals at rates ranging from 2 to 50 percent. *New Biol* 1(2):159-169.
Wen, J.D., M. Manosas, P. Li, S. Smith, C. Bustamante, F. Ritort, and I. Tinoco Jr. 2007. Force unfolding kinetics of RNA using optical tweezers. I. Effects of experimental variables on measured results. *Biophys J*.
Wuite, G.J., R.J. Davenport, A. Rappaport, and C. Bustamante. 2000. An integrated laser trap/flow control video microscope for the study of single biomolecules. *Biophys J* 79(2):1155-1167.
Zuker, M. 2003. Mfold web server for nucleic acid folding and hybridization prediction. *Nucleic Acids Res* 31(13):3406-3415.

Appendix

Paper I:

Maintenance of the correct open reading frame by the ribosome, Hansen TM, Baranov PV, Ivanov IP, Gesteland RF and Atkins JF, EMBO Rep. :499-504 (2003).

Paper II:

T.M. Hansen, N. Reihani, and L. Oddershede: "Combining optical tweezers and micropipettes for DNA stretching: Elasticity of micropipette crucial", NATO Springer proceedings (2005).

Paper III:

Stretching short DNA tethers using optical tweezers N. Reihani, L. Bosanac, T.M. Hansen, and L. Oddershede, SPIE proceedings, vol. 6326 p.21-28 (2006).

Paper IV:

Correlation between mechanical strengt of RNA pseudoknots and ribosomal frameshifting, T.M. Hansen, S.N.S. Reihani, L. Oddershede, and M. Sørensen, PNAS, vol.104, p.5830-5835 (2007).

EMBO reports

scientific report

Maintenance of the correct open reading frame by the ribosome

Thomas M. Hansen†, Pavel V. Baranov*, Ivaylo P. Ivanov, Raymond F. Gesteland & John F. Atkins+*

Department of Human Genetics,University of Utah, Salt Lake City, Utah, USA

During translation, a string of non-overlapping triplet codons in messenger RNA is decoded into protein. The ability of a ribosome to decode mRNA without shifting between reading frames is a strict requirement for accurate protein biosynthesis. Despite enormous progress in understanding the mechanism of transfer RNA selection, the mechanism by which the correct reading frame is maintained remains unclear. In this report, evidence is presented that supports the idea that the translational frame is controlled mainly by the stability of codon–anticodon interactions at the P site. The relative instability of such interactions may lead to dissociation of the P-site tRNA from its codon, and formation of a complex with an overlapping codon, the process known as P-site tRNA slippage. We propose that this process is central to all known cases of +1 ribosomal frameshifting, including that required for the decoding of the yeast transposable element Ty*3*. An earlier model for the decoding of this element proposed 'out-of-frame' binding of A-site tRNA without preceding P-site tRNA slippage.

EMBO reports **4**, 499–504 (2003)

doi:10.1038/sj.embor.embor825

INTRODUCTION

A crucial rule of protein synthesis is the triplet character of genetic decoding. How the translational machinery maintains the proper reading frame is a question of primary importance. A small number of genes, the translation of which requires a switch between open reading frames through efficient ribosomal frameshifting (Farabaugh & Björk, 1999; Brierley & Pennell, 2001; Baranov *et al.*, 2002a, 2003), offer a unique tool for the investigation of this question. An understanding of the mechanism of frameshifting could provide an answer to how triplet decoding is controlled by the ribosome.

The first bacterial chromosomal gene that was found to require +1 frameshifting for its expression was the *Escherichia coli* gene *prfB*, which encodes release factor 2 (RF2; Craigen *et al.*, 1985; Craigen & Caskey, 1986). The mechanism suggested for this involves slippage of the P-site $tRNA^{Leu}$ from the codon CUU to the overlapping codon, UUU, in the frameshift site CUU UGA C (Craigen *et al.*, 1985; Weiss *et al*., 1987), followed by binding of a tRNA to the +1-frame A-site codon. Further studies, using artificial constructs based on the RF2 frameshifting cassette, have supported this idea (Curran & Yarus, 1988; Curran, 1993). Efficient frameshifting was seen in those cases where the P-site tRNA was able to form good base pairing with the overlapping +1 codon, for example, UUU or CCC.

The site of the frameshifting required for decoding both the yeast transposable element Ty*1* (Belcourt & Farabaugh, 1990) and the actin-filament-binding protein ABP140 (Asakura *et al.*, 1998) is CUU AGG C. The mechanism originally suggested for this (Belcourt & Farabaugh, 1990) was similar to that suggested for *prfB*: P-site tRNA slippage followed by binding of a tRNA to the +1-frame A-site codon. The frameshifting required for Ty*3* expression occurs at the sequence GCG AGU U (Farabaugh *et al.*, 1993). Its P-site tRNA, decoding GCG, cannot form good base pairs with the +1 codon, CGA, leading to the hypothesis that efficient frameshifting occurs without P-site tRNA slippage, but with out-of-frame binding of tRNA at the A site (Farabaugh *et al.*, 1993; Pande *et al.*, 1995; Stahl *et al*., 2001). Recently, the same group raised the possibility that out-of-frame A-site tRNA binding is responsible for all cases of programmed frameshifting in yeast (Stahl *et al.*, 2001).

However, an alternative explanation has been proposed for the efficient frameshifting that occurs in Ty*1* and Ty*3* (Ivanov *et al.*, 2002; Baranov *et al.*, unpublished data). As described in Sundararajan *et al.* (1999), the P-site codons in these frameshift sites are recognized by tRNAs that lack the ability to form a standard base pair in the wobble position in codon–anticodon duplexes. Accordingly, the rate of dissociation of these tRNAs from their P-site codons should be higher than usual. In addition, these tRNAs cannot form good base pairs with the overlapping +1 codons (especially for Ty*3* decoding) and, therefore, the resulting complex cannot be stable. However, Ty*1* and Ty*3* frameshifting is stimulated by the presence, in the initial frame, of an A-site codon that is decoded by sparse tRNAs (Pande *et al.,* 1995). The relative paucity of the tRNA decoding the zero-frame A-site codon, and the abundance of the tRNA decoding its overlapping +1-frame codon, are crucial for the stimulation of frameshifting (Baranov *et al*., 2003b). Fig. 1 shows a model for +1 frameshifting without out-of-frame tRNA binding.

[1]Department of Human Genetics,University of Utah, 15N 2030E Room 7410, Salt Lake City, UT 84112-5330, USA

[†]Present address: Department of Molecular Cell Biology, University of Copenhagen, Øster Farimagsgade 2A 3. sal, DK-1353 Copenhagen K, Denmark

*These authors contributed equally to this work

[+]Corresponding author. Tel: +1 801 585 3434; Fax: +1 801 585 3910;
E-mail: atkins@howard.genetics.utah.edu

Received 14 January 2003; revised 10 March 2003; accepted 17 March 2003

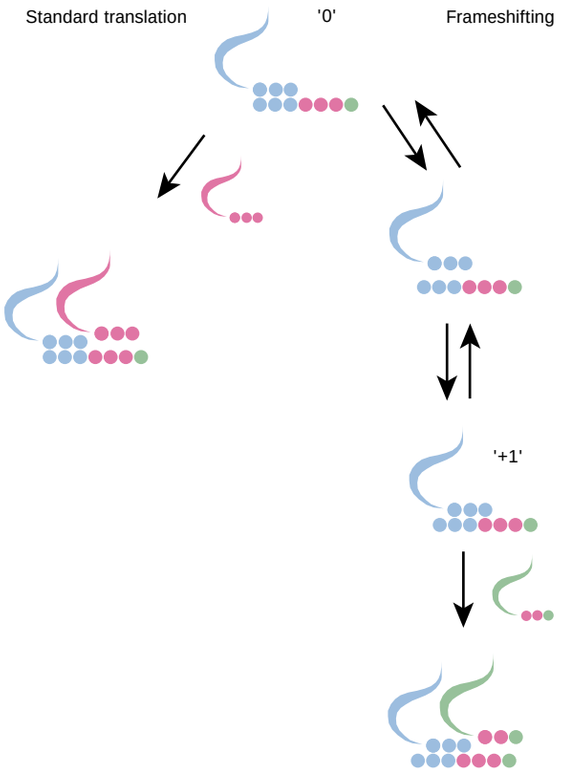

Fig. 1 | Illustration of +1 frameshifting, shown in parallel with the process of standard translation. The kinetic requirement for efficient frameshifting is the commensurability of the rates of the two processes. Usually, the rate of standard translation is significantly higher than that of frameshifting. A low concentration of incoming transfer RNA in the initial frame (magenta) makes standard translation slower than usual. Low stability of the initial P-site codon–anticodon complex ('0'), high stability of the equivalent complex in the new frame ('+1'), and high levels of the incoming tRNA corresponding to the A-site codon in the new frame (green), increase the rate of frameshifting. As a result, a high input of several stimulating factors can compensate for the lack of one of them. In Ty3, it is the lack of stable P-site codon–anticodon duplexes in the +1 shifted frame that is compensated for by three other factors.

If, conversely, frameshifting is limited by binding of the A-site tRNA to the +1-frame codon, then stimulators that promote slippage of the P-site tRNA into the +1 frame should not affect frameshift efficiency. Stimulators of this type have not been identified for +1 frameshifting in yeast; however, they are known in bacteria. We have explored the effect of this type of stimulator on frameshifting in *E. coli* using a model system in which the P-site tRNA cannot form good base pairs with the +1-frame codon, which is analogous to the Ty*1*/Ty*3* situation.

RESULTS AND DISCUSSION

The stimulator used in these experiments was first discovered because of its role in promoting the autoregulatory frameshifting required for synthesis of RF2. It is an internal Shine–Dalgarno (SD) sequence, the precise position of which is crucial for efficient frameshifting (Weiss *et al.*, 1987, 1988; Curran & Yarus, 1988). There are at least two explanations for its action, which are not necessarily mutually exclusive. The short distance between the SD sequence and the P-site codon (three nucleotides) creates a tension between the corresponding parts of the ribosome: the anti-SD region and the decoding centre. This tension causes the P-site tRNA to slip in the +1 direction, so that the distance between the anti-SD region and the decoding centre becomes closer to that used for the 'frame-neutral' role in translation initiation (Atkins *et al.*, 2001; Baranov *et al.*, 2002b). The existence of such tension is supported by the fact that the SD sequence is known to stimulate –1 frameshifting when it is located ~10–14 bases upstream of a frameshift site (discussed in detail in Atkins *et al.*, 2001). In this case, backward movement of the ribosome–tRNA complex, relative to the messenger RNA, helps to achieve a distance between the anti-SD region and the decoding centre and relieves the conferred ribosomal tension. Another explanation is that SD:anti-SD complex clashes with E-site tRNA, promoting its movement towards the P-site tRNA, and also resulting in P-site tRNA slippage (Baranov *et al.*, 2002b; K.H. Nierhaus, personal communication). It is clear that the mRNA–rRNA pairing that involves the SD sequence stimulates peptidyl-tRNA slippage.

The out-of-frame binding model was suggested for Ty*3* frameshifting because tRNA located in the P site, when shifted, cannot form good base pairs with the +1 codon. Farabaugh and colleagues have noted that the P-site tRNAs that promote +1 frameshifting in yeast do not usually form canonical base pairs in the third position of the codon–anticodon duplex (Sundararajan *et al.*, 1999). The tRNAs involved have been termed 'special' or 'near-cognate' tRNAs. Stimulators that are known to promote +1 tRNA slippage in yeast have not yet been discovered. Although a special 3′ context is important for Ty*3* frameshifting (Li *et al.*, 2001), its mechanistic function is unknown. To test the generality of the out-of-frame hypothesis, we modelled conditions of Ty*3* frameshifting in a bacterial system, in which a stimulator, an internal SD sequence that promotes +1 slippage, is used. To model the Ty*3* situation in bacteria, the RF2 frameshifting site was modified so that tRNAs at the P-site satisfied two requirements: first, no canonical base pair could be formed in the wobble position of the zero-frame codon–anticodon duplex. Second, after slippage, the P-site tRNAs cannot form a good base pair with the +1 P-site codon.

We investigated whether a suitably positioned SD sequence had a stimulatory effect on frameshifting at sequences where it was unclear whether out-of-frame binding of an incoming tRNA, or P-site tRNA slippage, have a causal effect. We constructed cassettes that resulted in the positioning of different codons (XYZ) adjacent to the UGA stop codon, on the 5′ side, in the RF2 frameshifting site. The sequence of the wild-type RF2 frameshift site is CUU UGA C (with the first codon in the new +1 frame underlined). The CUU shift codon was replaced by GCG, GGU, GUU, AAU, AAG, GAU, AGU, UGU or CGA. All of these codons are normally recognized by tRNAs sharing two features: they cannot form 'Watson–Crick only' base pairs with the zero-frame codon, and they cannot form more than one Watson–Crick base pair if they are shifted to the +1 overlapping codon (YZU), as in the sequence shown in Fig. 2A. The sequences containing a modified RF2 frameshifting cassette were inserted between the sequences encoding glutathione-*S*-transferase (GST) and maltose-binding protein (MBP), in a *gst–malE* fusion gene on the plasmid GHM53 (see Methods). *malE* is in the +1 frame relative to *gst*, and the complete GST–MBP fusion protein is therefore only translated if +1 frameshifting occurs. Termination at the UGA stop codon results in the

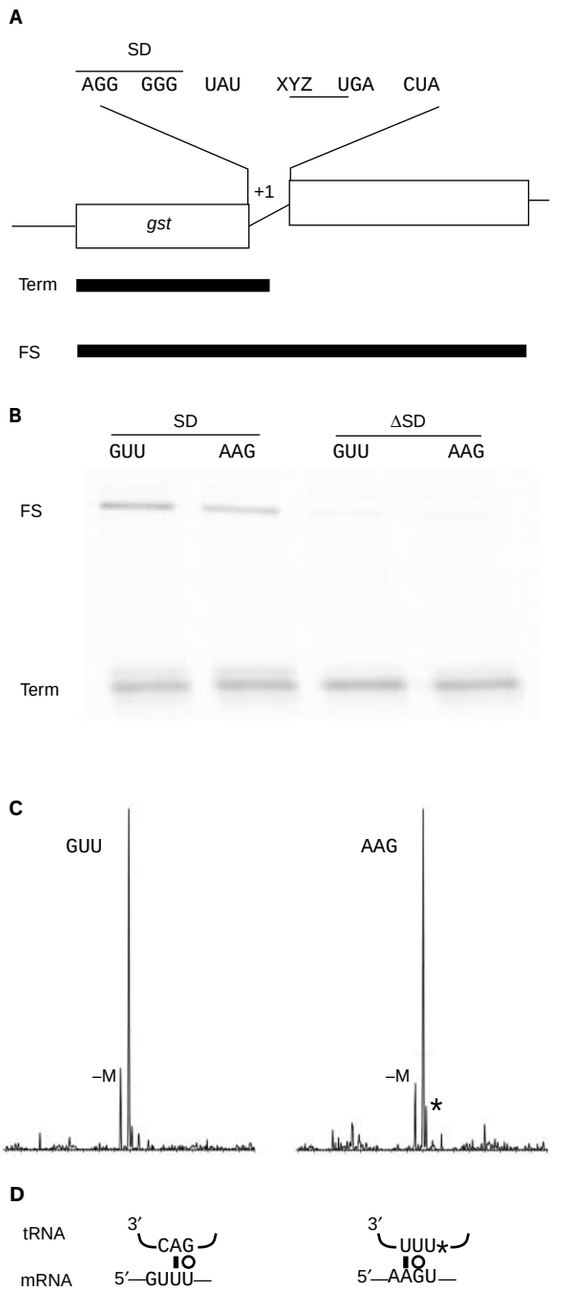

◀ **Fig. 2 |** +1 frameshifting at the gene encoding release factor 2, wherethe CUU shift-site is replaced by GUU or AAG. (**A**) Constructs and their products. XYZ represents the position of CUU, which was replaced in these constructs. (**B**) Pulse–chase experiment. Electrophoretic separation of glutathione-*S*-transferase (GST)-tagged proteins on an SDS gel. The samples electrophoresed on the gel were from constructs containing a Shine–Dalgarno sequence (SD) or lacking this sequence (ΔSD). (**C**) Protein analysis. Mass spectra in the 67,500–71,500 Da range are shown for GST-tagged proteins that were purified from strains expressing constructs containing an SD. The major peaks are at 69,479 Da (GUU) and 69,508 Da (AAG), corresponding to frameshift products with expected masses of 69,479.6 Da (GUU) and 69,508.6 Da (AAG). A minor peak with a mass corresponding to the major product lacking one methionine is indicated (–M). An adduct of the major product is apparent in the AAG spectrum (*). (**D**) Codon–anticodon pairing in the +1 frame. Possible Watson–Crick (bar) and wobble (circle) base pairs are indicated. FS, product of +1 frameshifting in the insert; mRNA, messenger RNA; Term, product resulting from termination at UGA in the insert; tRNA, transfer RNA.

synthesis of a shorter protein (Fig. 2A). The constructs were assayed for frameshifting in pulse–chase labelling experiments. Proteins were purified by affinity chroma-tography using the amino-terminal GST tag, followed by gel electrophoresis. The purification step increases the sensitivity as compared with assays using crude extracts, but is not strictly quantitative (data not shown). The identities of the frameshift and termination protein products were determined by mass spectrometry, after purification using the GST tag. In each case, the mass of the frameshift product corresponded to that expected when the amino acid at the frame junction is specified by the zero-frame codon (Fig. 2C).

Of the nine codons tested, only GUU and AAG resulted in relatively high levels of frameshifting. The fact that detectable frameshifting was not promoted by all nine codons indicates that, in addition to the number of good base pairs in the codon–anticodon duplexes at the P site in the zero and shifted frames, there are other factors that are likely to influence the overall stability of mRNA–tRNA interactions. If frameshifting on these codons occurs due to slippage of the cognate P-site tRNA, the resulting +1 codon–anticodon complex should be relatively unstable, as fewer than two Watson–Crick base pairs can be formed (Fig. 2D). The *E. coli* valine tRNAs have the anticodons 3′-CAG-5′ and 3′-CAV-5′, where V is uridine-5-oxyacetic acid (Yaniv & Barrell, 1971). This is a permissive modification of uridine, and V can pair with U, A or G (Yokoyama *et al.*, 1985). It is likely that both of these tRNAs usually recognize the GUU codon. In both cases, re-pairing to mRNA by the 3′-CAV-5′ or 3′-CAG-5′ anticodons through the +1-frame codon gives a Watson–Crick pair in the second position and a V:U or G:U pair in the third position, but no Watson–Crick or wobble pairing in the first position (Fig. 2D).

Protein analysis (see Methods) showed that AAG is decoded as lysine, and must therefore be decoded by the sole $tRNA^{Lys}$. This tRNA has the anticodon 3′-UUU*-5′ (Chakraburtty *et al.*, 1975), where U* is 5-methylaminomethyl-2-thiouridine (although some of the molecules have selenium instead of sulphur). This restrictive modification probably helps $tRNA^{Lys}$ to distinguish between Lys (AAA and AAG) and Asn (AAU and AAC) codons (Sundaram *et al.*, 2000). Canonical base pairs cannot be formed between the anticodon of this tRNA and the codon in the +1 frame at the third position, and only a G:U pair can be formed at the second position (Fig. 2D). In both of these examples, high levels of frameshifting occur (Fig. 2B, lanes 1 and 2).

The SD sequence (AGG GGG) was destroyed in another set of constructs, in which it was replaced by ACC UCU. No frameshifting was detected when the SD sequence was destroyed, as shown in Fig. 2, lanes 3 and 4. This suggests that P-site tRNA slippage, rather than out-of-frame binding, is the reason for frameshifting in these artificial RF2 constructs. Furthermore, formation of at least two canonical base pairs between the codon and anticodon of the P-site tRNA in the +1 frame is not required for efficient frameshifting.

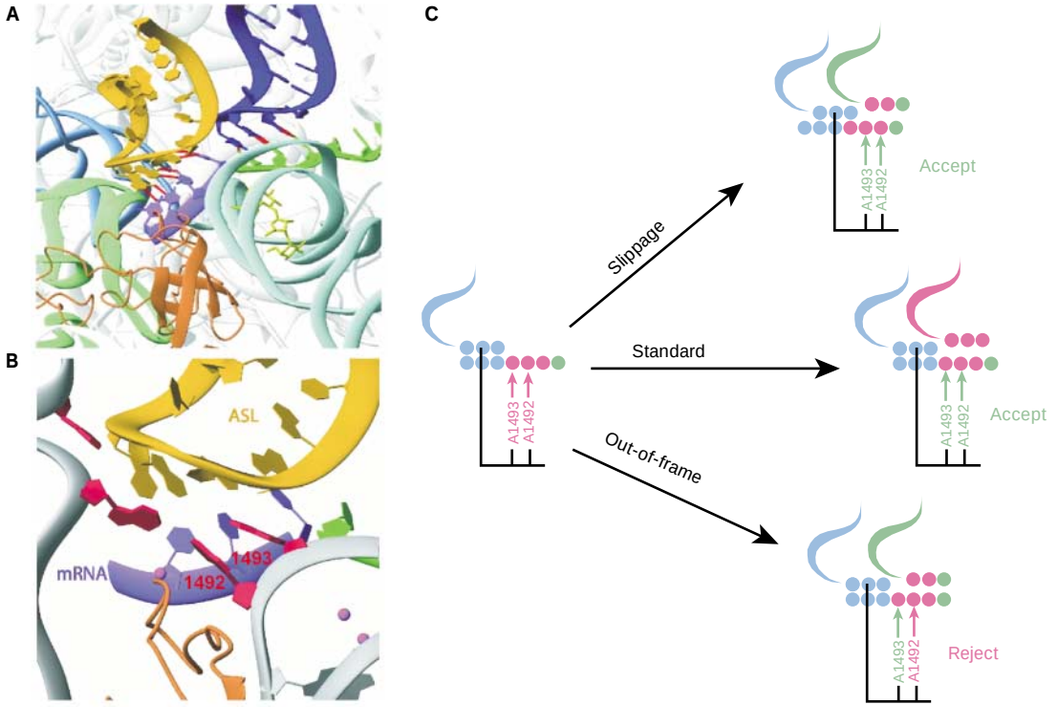

Fig. 3 | Illustration of how ribosomes prevent out-of-frame binding of incoming transfer RNA. (**A**) Details of the A site and P site. The A-site transfer RNA is shown in yellow; helix 6 from the neighbouring ribosome molecule that mimics P-site tRNA is shown in dark blue. (**B**) Details of the ribosomal components surrounding the A-site tRNA; adenosines 1,492 and 1,493 are labelled. (**C**) Schematic illustration of out-of-frame binding at the A site. Magenta arrows indicate that the discriminating adenosines do not sense a correct base pair; green arrows indicate that the discriminating adenosines recognize a correct base pair. Whereas standard translation and P-site tRNA slippage lead to normal recognition at the A site, out-of-frame binding does not. The illustrations in (**A**,**B**) are abstracted with permission from Ogle *et al.* (2001) © (2001) American Association for the Advancement of Science. ASL, anticodon stem–loop; mRNA, messenger RNA.

A similar hypothesis was recently proposed, on the basis of molecular analysis of the +1 frameshifting of eukaryotic antizyme genes (Ivanov *et al.*, 2002). During the initial stages of analysis, it was realized that the tRNA, which is in the P site during antizyme recoding, could not form good base pairs with the overlapping +1 codon. This was even more obvious for several P-site-codon mutants, which otherwise gave almost wild-type levels of frameshifting (Matsufuji *et al.*, 1995). On the basis of these results, it was concluded at first that +1 frameshifting in antizyme genes is due to out-of-frame binding of tRNA at the A-site. Further testing challenged this conclusion; specifically, when a mammalian antizyme 1 (one of several mammalian paralogues of antizyme) frameshift cassette was tested in *Saccharomyces cerevisiae*, it gave high levels of shifting to the +1 frame, but the ribosomes reached this frame mostly (90% of the time) by a –2 shift rather than by a +1 shift (10% of the time; Matsufuji *et al.*, 1996). A similar situation was observed when the same cassette was tested in *Schizosaccharomyces pombe*: the ribosomes reached the +1 frame through a +1 shift 80% of the time, and through a –2 shift 20% of the time (Ivanov *et al.*, 1998). It was clear that the –2 shift occurs only as a result of anticodon re-pairing to mRNA at the P site, and as it seems unlikely that the same sequence can induce two rare and mechanistically different events, it is likely that both shifts are the result of a single P-site re-pairing mechanism.

The examples described above do not support the idea of out-of-frame binding of A-site tRNA. Our understanding of the mechanism of translation has been advanced by recent structural analyses of ribosomes and their functional complexes (Wimberly *et al.*, 2000; Ban *et al.*, 2000; Schluenzen *et al.*, 2000; Yusupov *et al.*, 2001). The data obtained from structural studies, too, do not support the idea of out-of-frame binding. Fig. 3A shows the interactions of mRNA with A-site and P-site tRNAs in the ribosome (Ogle *et al.*, 2001). Fig. 3B illustrates the network of ribosomal components, the decoding centre, that is responsible for the selection of A-site tRNA (Ogle *et al.*, 2001; Lynch *et al.*, 2003). The adenosines at positions 1,493 and 1,492 (here, and later, the *E. coli* numbering is used) are known to be responsible for monitoring the correct conformation of the first two base pairs in the codon–anticodon duplex at the A site (reviewed in Ramakrishnan, 2002). These two adenosines, as well as other components of the decoding centre, have a strict orientation relative to the P-site codon–anticodon duplex. If this was not the case, the ribosome would not be able to discriminate between the zero-frame A-site codon and the +1-frame codon. The 16S rRNA component that is likely to be responsible for the correct positioning of the decoding centre relative to the P-site codon–anticodon duplex is nucleotide 1,401. This nucleotide is flipped into the space between two tRNAs, as seen in the structure obtained by the diffusion of mRNA into ribosome crystals (Yusupova *et al.*, 2001).

In the out-of-frame binding model, the first base of the A-site codon is unpaired. Normally, base pairing at this position is monitored by adenosine 1,493. The lack of correct base pairing in this position is expected to lead to the rejection of tRNAs that recognize the +1 codon. Thus, even if tRNA initially binds at the +1 codon, such binding is expected to be followed by rejection of the tRNA. This is illustrated in Fig. 3C. The recognition of a +1-frame codon is possible only if there are significant structural rearrangements within the 30S ribosomal subunit, leading to relocation of the decoding centre relative to the position of the P-site codon–anticodon duplex. It is unclear as to what forces could lead to such a relocation, but, more significantly, it is unlikely that such repositioning is possible.

A recent review suggested that "the effect of …[tRNAs forming suboptimal codon–anticodon base pairing at the P-site]…is to disrupt the mechanism that the ribosome uses to distinguish an in-frame from an out-of-frame amino-acid–tRNA complex in the A-site." (Stahl *et al.*, 2001). The data presented here suggest that the mechanism of frame control is based on, first, rigid positioning of the decoding centre relative to the P-site tRNA and, second, the stability of the complex formed between the tRNA anticodon and the mRNA codon at the P site. Taking this into account, it is clear why and how tRNAs that form less than optimal codon–anticodon base pairing at the P site disrupt the mechanism of frame control.

METHODS

Plasmids and bacterial strains. A *gst–malE* expression vector (GHM53), containing *Bam*HI and *Eco*RI restriction sites between the coding sequences of GST and MBP has been described previously (Herr *et al.*, 2001). Inserts made from complementary oligonucleotides (containing mutated RF2 frameshifting cassettes) were cloned between the *Bam*HI and *Eco*RI sites. The oligonucleotides were based on the sequences 5′-GATC**AGGGGG**TAT**XYZ**TGACTAC-3′ and 5′-AATTGTAGTCA***ZYX***ATA**CCCCCT**-3′ (italicized letters indicate complementary nucleotides; bold letters indicate nucleotides that are changed, as described in the Results and Discussion section). A derivative of *E. coli* strain SU1675 that lacks the F′ episome was used in all experiments (Weiss *et al.*, 1988).

Frameshifting assay. Overnight cultures of strains expressing the appropriate plasmid were grown in MOPS–glucose (Neidhardt *et al.*, 1974) containing 100 μg ml^{-1} ampicillin and all amino acids (150 μg ml^{-1} each) except methionine and tyrosine, and were diluted 1:50 in 300 μl of this media. After a 2-h incubation at 37 °C, the cultures were induced for 10 min by adding 2 mM isopropyl-D-thiogalactoside (IPTG). Cells were pulsed for 2 min with 7.5 μCi [^{35}S]methionine in 30 μl media, chased for 2 min by the addition of 30 μl of cold methionine (50 mg ml^{-1}), chilled on ice, and harvested by centrifugation. The pellet was resuspended in 100 μl of BugBuster reagent (Novagen), shaken for 10 min and centrifuged at 12,000*g* for 10 min. The supernatant was transferred to 20 μl of 50% GST (AP Biotech) equilibrated in PBS (150 mM NaCl, 16 mM Na_2HPO_4, 4 mM NaH_2PO_4, pH 7.3), 0.5% Triton X-100, and shaken for 10 min. The resin was then washed in 150 μl PBS, 0.5% Triton X-100, followed by washing in 150 μl PBS, and proteins were eluted with 60 μl of 10 mM glutathione in PBS. 10 μl aliquots were loaded onto a 15% Tris–glycine–SDS polyacrylamide gel. Gels were visualized using a Molecular Dynamics PhosporImager.

Protein analysis. Overnight cultures of strains containing the appropriate plasmids were diluted 1:50 in Terrific Broth, grown for 2 h at 37 °C, and induced with 1 mM IPTG for 4 h at 37 °C. Harvested cells were lysed using BugBuster reagent. Recombinant proteins were purified by passaging over glutathionine–sepharose (Amersham Pharmacia Biotech). Purified proteins were concentrated, and washed extensively with Nanopure H_2O using a Centricon 10 unit (Millipore). Final cleanups and mass measurements were performed as described in Herr *et al.* (2001), except that only C4 P10 ZipTips (Millipore) were used for cleanups, and proteins were eluted with 56% (v/v) methanol, 1.5% formic acid, with three aliquots of 2 μl, which were then pooled and introduced into the mass spectrometer by infusion at 3 μl min^{-1}.

ACKNOWLEDGEMENTS

We thank C. Nelson for important help with mass spectra analyses. This work was supported by a grant from the National Institutes of Health (GM48152) to J.F.A. and from the US Department of Energy (DE-FG03-01ER63132) to R.F.G.

REFERENCES

Asakura, T. *et al*. (1998) Isolation and characterization of a novel actin filament binding protein from *Saccharomyces cerevisiae*. *Oncogene*, **16**, 121–130.

Atkins, J.F. *et al*. (2001) Over-riding standard decoding: implications of recoding for ribosome function and enrichment of gene expression. *Cold Spring Harb. Symp. Quant. Biol.*, **66**, 217–232.

Ban, N., Nissen, P., Hansen, J., Moore, P.B. & Steitz, T.A. (2000) The complete atomic structure of the large ribosomal subunit at 2.4 Å resolution. *Science*, **289**, 905–920.

Baranov, P.V., Gesteland, R.F. & Atkins, J.F. (2002a) Recoding: translational bifurcations in gene expression. *Gene*, **286**, 187–201.

Baranov, P.V., Gesteland, R.F. & Atkins, J.F. (2002b) Release factor 2 frameshifting sites in different bacteria. *EMBO Rep.*, **3**, 373–377.

Baranov, P.V., Gurvich, O.L., Hammer, A.W., Gesteland, R.F. & Atkins, J.F. (2003) RECODE 2003. *Nucleic Acids Res.*, **31**, 87–89.

Belcourt, M.F. & Farabaugh, P.J. (1990) Ribosomal frameshifting in the yeast retrotransposon Ty: tRNAs induce slippage on a 7-nucleotide minimal site. *Cell*, **62**, 339–352.

Brierley, I. & Pennell, S. (2001) Structure and function of the stimulatory RNAs involved in programmed eukaryotic –1 ribosomal frameshifting. *Cold Spring Harb. Symp. Quant. Biol.*, **66**, 233–248.

Chakraburtty, K., Steinschneider, A., Case, R.V. & Mehler, A.H. (1975) Primary structure of tRNA-Lys of *E. coli* B. *Nucleic Acids Res.*, **2**, 2069–2075.

Craigen, W.J. & Caskey, C.T. (1986) Expression of peptide chain release factor 2 requires high-efficiency frameshift. *Nature*, **322**, 273–275.

Craigen, W.J., Cook, R.G., Tate, W.P. & Caskey, C.T. (1985) Bacterial peptide chain release factors: conserved primary structure and possible frameshift regulation of release factor 2. *Proc. Natl Acad. Sci. USA*, **82**, 3616–3620.

Curran, J.F. (1993) Analysis of effects of tRNA:message stability on frameshift frequency at the *Escherichia coli* RF2 programmed frameshift site. *Nucleic Acids Res.*, **21**, 1837–1843.

Curran, J.F. & Yarus, M. (1988) Use of tRNA suppressors to probe regulation of *Escherichia coli* release factor 2. *J. Mol. Biol.*, **203**, 75–83.

Farabaugh, P.J. & Björk, G.R. (1999) How translational accuracy influences reading frame maintenance. *EMBO J.*, **18**, 1427–1434.

Farabaugh, P.J., Zhao, H. & Vimaladithan, A. (1993) A novel programmed frameshift expresses the *POL3* gene of retrotransposon Ty*3* of yeast: frameshifting without tRNA slippage. *Cell*, **74**, 93–103.

Herr, A.J., Nelson, C.C., Wills, N.M., Gesteland, R.F. & Atkins, J.F. (2001) Analysis of the roles of tRNA structure, ribosomal protein L9, and the bacteriophage T4 gene 60 bypassing signals during ribosome slippage on mRNA. *J. Mol. Biol.*, **309**, 1029–1048.

Ivanov, I.P., Gesteland, R.F., Matsufuji, S. & Atkins, J.F. (1998) Programmed frameshifting in the synthesis of mammalian antizyme is +1 in mammals, predominantly +1 in fission yeast, but –2 in budding yeast. *RNA*, **4**, 1230–1238.

Ivanov, I.P., Gurvich, O.L., Gesteland, R.F. & Atkins, J.F. (2002) in *Translation Mechanisms* (eds Lapointe, J. & Braker-Gingras, L.) Landes Bioscience, Austin, Texas, USA (http://www.eurekah.com/chapter.php?chapid=841&bookid=59&catid=54).

Li, Z., Stahl, G. & Farabaugh, P.J. (2001) Programmed +1 frameshifting stimulated by complementarity between a downstream mRNA sequence and an error-correcting region of rRNA. *RNA*, **7**, 275–284.

Lynch, S.R., Gonzalez, R.L. & Puglisi, J.D. (2003) Comparison of X-ray crystal structure of the 30S subunit–antibiotic complex with NMR structure of decoding site oligonucleotide–paromomycin complex. *Structure*, **11**, 43–53.

Matsufuji, S., Matsufuji, T., Miyazaki, Y., Murakami, Y., Atkins, J.F., Gesteland, R.F. & Hayashi, S. (1995) Autoregulatory frameshifting in decoding mammalian ornithine decarboxylase antizyme. *Cell*, **80**, 51–60.

Matsufuji, S., Matsufuji, T., Wills, N.M., Gesteland, R.F. & Atkins, J.F. (1996) Reading two bases twice: mammalian antizyme frameshifting in yeast. *EMBO J.*, **15**, 1360–1370.

Neidhardt, F.C., Bloch, P.L. & Smith, D.F. (1974) Culture medium for enterobacteria. *J. Bacteriol.*, **119**, 736–747.

Ogle, J.M., Brodersen, D.E., Clemons, W.M., Tarry, M.J., Carter, A.P. & Ramakrishnan, V. (2001) Recognition of cognate transfer RNA by the 30S ribosomal subunit. *Science*, **292**, 897–902.

Pande, S., Vimaladithan, A., Zhao, H. & Farabaugh, P.J. (1995) Pulling the ribosome out of frame by +1 at a programmed frameshift site by cognate binding of aminoacyl-tRNA. *Mol. Cell. Biol.*, **15**, 298–304.

Ramakrishnan, V. (2002) Ribosome structure and the mechanism of translation. *Cell*, **108**, 557–572.

Schluenzen, F. *et al*. (2000) Structure of functionally activated small ribosomal subunit at 3.3 Å resolution. *Cell*, **102**, 615–623.

Stahl, G., Ben Salem, S., Li, Z., McCarty, G., Raman, A., Shah, M. & Farabough, P.J. (2001) Programmed +1 translational frameshift in the yeast *Saccharomyces cerevisiae* results from disruption of translational error correction. *Cold Spring Harb. Symp. Quant. Biol.*, **66**, 249–257.

Sundaram, M., Durant, P.C. & Davis, D.R. (2000) Hypermodified nucleosides in the anticodon of tRNALys stabilize a canonical U-turn structure. *Biochemistry*, **39**, 12575–12584.

Sundararajan, A., Michaud, W.A., Qian, Q., Stahl, G. & Farabaugh, P.J. (1999) Near-cognate peptidyl-tRNAs promote +1 programmed translational frameshifting in yeast. *Mol. Cell*, **4**, 1005–1015.

Weiss, R.B., Dunn, D.M., Atkins, J.F. & Gesteland, R.F. (1987) Slippery runs, shifty stops, backward steps, and forward hops: –2, –1, +1, +2, +5 and +6 ribosomal frameshifting. *Cold Spring Harb. Symp. Quant. Biol.*, **52**, 687–693.

Weiss, R.B., Dunn, D.M., Dahlberg, A.E., Atkins, J.F. & Gesteland, R.F. (1988) Reading frame switch caused by base-pair formation between the 3′ end of 16S rRNA and the mRNA during elongation of protein synthesis in *Escherichia coli*. *EMBO J.*, **7**, 1503–1507.

Wimberly, B.T., Brodersen, D.E., Clemons, W.M., Morgan-Warren, R.J., Carter, A.P., Vonrhein, C., Hartsch, T. & Ramakrishnan, V. (2000) Structure of the 30S ribosomal subunit. *Nature*, **407**, 327–339.

Yaniv, M. & Barrell, B.G. (1971) Sequence relationship of three valine acceptor tRNAs from *Escherichia coli*. *Nature New Biol.*, **233**, 113–114.

Yokoyama, S., Watanabe, T., Murao, K., Ishikura, H., Yamaizumi, Z., Nishimura, S. & Miyazawa, T. (1985) Molecular mechanism of codon recognition by tRNA species with modified uridine in the first position of the anticodon. *Proc. Natl Acad. Sci. USA*, **82**, 4905–4909.

Yusupov, M.M., Yusupova, G.Z., Baucom, A., Lieberman, K., Earnest, T.N., Cate, J.H. & Noller, H.F. (2001) Crystal structure of the ribosome at 5.5 Å resolution. *Science,* **292**, 883–896.

Yusupova, G.Z., Yusupov, M.M., Cate, J.H. & Noller, H.F. (2001) The path of messenger RNA through the ribosome. *Cell*, **106**, 233–241.

COMBINING OPTICAL TWEEZERS AND MICROPIPETTES FOR DNA STRETCHING: ELASTICITY OF MICROPIPETTE CRUCIAL

Thomas Møller Hansen[1,2], Nader Reihani[1,3], and Lene Oddershede[1*]
[1]*Niels Bohr Institute, Blegdamsvej 17, 2100 Copenhagen, Denmark*
[2]*Institute of Molecular Biology and Fysiology, Øster Farimagsgade 2A, 1353 Copenhagen, Denmark*
[3]*Institute for Advanced Studies in Basic Sciences, PO Box 45195-159, Zanjan, Iran*

1. Introduction

Optical tweezers are often used in connection with other techniques to study physical properties of biological systems. In particular, this combination has often been used to study elastic properties of individual strands of nucleic acids. The DNA used in this study is the shortest so far reported, only 1.1 μm, $\simeq$ 20 times its persistence length. We use two different experimental geometries, one in which the axis of the micropipette is orthogonal to that of the stretched polymer and one where the axis of the micropipette is parallel to the stretched polymer. By comparing the force-extension data to the predictions of the celebrated worm-like-chain model (Marko and Siggia, 1995), we find that the results obtained using the orthogonal geometry have severe problems, the force increases slower than expected with extension of the polymer. Also, the expected plateau at the transition away from the B-form of dsDNA is not horizontal. However, if instead one uses the parallel geometry the data obtained are fit well by the worm-like-chain model. This difference can be explained by the elasticity of the micropipette, which can be crucial to take into account when using micropipettes in connection with optical tweezers.

The elastic properties of DNA are important as it is constantly bend, pushed and pulled inside the living cell by macromolecules working on the DNA. E.g. the DNA is bend when the TATA-box binding protein attaches

* Corresponding author, email: oddershede@nbi.dk

to the promoter during transcription initiation. Also,the RNA-polymerase is capable of exerting consideableforces (up to 15 pN) while transcribing the DNA (Wang et al., 1998). One of the pioneering experimental investigations of the elastical properties of DNA are presented in (Wang et al., 1997). Another impressive *in vitro* study of nucleic acids is that by (Liphardt et al., 2001), who performed a mechanical unfolding of RNA loops using an optical trap in connection with a micropipette. This setup was also used for a test of Jarzynski's equation (Jarzynski, 1997; Liphardt et al., 2002), an important equation dealing with the difficult task of relating the non-equilibrium behavior of a system with its equilibrium behavior.

Such *in vitro* experiments are good because single action-reaction couples can be isolated and understood, but on the other hand, these experiments are not per se biologically relevant as the conditions inside a living cell are totally different from that within a test tube. Recently, effort is also being put into investigating the more complex problem of motion of single molecules *in vivo*, such as e.g. the motion of proteins in the outer membrane of living E. coli bacteria (Oddershede et al., 2002).

2. Methods

2.1. OPTICAL TRAPPING

The optical trap is based on a $NdYVO_4$ laser with wavelength 1064 nm and is implemented in an inverted Leica microscope with a quadrant photodiode back focal plane detection scheme, for a full discription of the equipment see (Oddershede et al., 2001). The water immersion objective (Leica, NA=1.2) allows for optical trapping at any height within the sample and prevents effects of spherical abberations. A laser power of 0.8 W, measured at the output of the laser, was used in all experiments presented here. Data are acquired using a National Instruments card (PCI-MIO-16E-4) and the sample is mounted on a three axis translational piezoelectric stage (Physik Instrumente) with capacitative feedback control and nanometer position resolution. Data aquisition was performed using costum made Labview programs. Simultaneous control over piezo stage and output from the quadrant photodiode allows for accurate measurements of corresponding values of force and distance.

2.2. DNA CONSTRUCT

The DNA is 3256 base pairs long, corresponding to 1.1 μm. It is synthesized by PCR (Polymerase Chain Reaction) using 5' modified primers. In one end of the PCR fragment there is a biotin and the other a digoxygenin. The

biotin is bound specifically to a streptavidin coated bead with diameter 2.1 μm(Bangs Laboratories). The digoxygenin end is specically bound to an anti-digoxygenin coated bead with diameter 2.88μm(Spherotech), to ensure a tight binding between the anti-digoxygenin and the bead this binding is cross-linked with protein C. The bufferused throughout the experiment contained 10 mM Tris-HCl pH 7.9,250 mM NaCl, 15 mM $MgCl_2$, 0.05 weight pct. BSA(Bovine Serum Albumin),and 10 ng/microliter carrier DNA. First, the smaller streptavidin coated beads were incubated with the PCR fragment in buffer C. The number of tethers between beads can be controlled by adjusting the ratio ofPCR fragmentto beads. Just before the experiment, the smaller beads with DNA tethers were mixed with the larger beads and further diluted in the buffer.

2.3. MICROPIPETTES, CHAMBERS

The buffer containing the DNA and beads was flushed into a microfluidic perfusion chamber. Micropipettes (outer diameter approximately 1.5 μm, inner diameter approximately 1 μm) were pointing into the chamber and immobilized with respect to the chamber. Suction could be applied to the pipettes to firmly attach the beads in the pipette. The geometry of the micropipettes with respect to the axis of the propagating laserlight is of extreme importance for this study. Figure 1 shows a schematic drawing of the geometry during a mechanical stretching of a DNA polymer. The left and right parts of Figure 2.3 show scenaria where the micropipette is respectively orthogonal and parallel to the direction in which the polymer is stretched.

2.4. EXPERIMENTAL PROCEDURE

After flushing buffer containing DNA and beads into the microfluidic chamber, one of the larger beads is optically trapped and immobilized on a micropipette. Thereafter, one of the smaller beads with DNA attached is optically trapped and brought into the same height as the larger bead on the micropipette. A timeseries of the thermal fluctuation of the bead inside the trap is monitored to calibrate the optical trap. Then, the smaller bead is brought close to the larger bead and allowed to fluctuate (and rotate) within the trap. When a DNA tether is formed between the two beads, this can be seen on the output from the quadrant photodiode if one tries to move the micropipette away. In the experiment, the optical trap is held fixed and the micropipette attached to the piezostage is moved at a velocity of 1000 nm/s

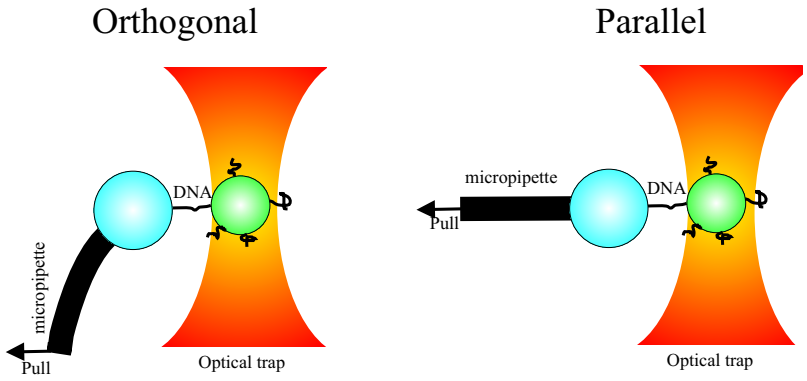

Figure 1. Two different possible geometries for combining optical tweezers with micropipettes for single molecule mechanical studies. The orthogonal geometry, shown to the left, is the most commonly used. The parallel geometry, shown to the right, is the one we suggest to use in the future to avoid bending of the micropipette. The arrow shows the direction of pull. The flexing of the micropipette in the orthogonal geometry is exaggerated.

a distance of 2000 nm away from the trap. For the calibration procedure data is sampled at a 20-50 kHz rate using the quadrant photodiode. In the stretching measurements, data is sampled at 5 kHz.

3. Calibration

When the micropipette is moved that will, in turn, force the bead in the optical trap to be displaced from its equilibrium position. In order to find the forces acting on this bead as a function of its displacement from the center of the optical trap and hence to find the forces acting on the DNA polymer, we need to perform a calibration.

The three coordinates describing the thermal fluctuations of the bead are uncorrelated, and the equation of motion for each of them is the same, but with different parameter values. Therefore we may look at the equation of motion in one dimension, say, for the x-coordinate, only. The optical tweezers exert a harmonic force $-\kappa x$ on the bead. The surrounding liquid exerts a frictional force on the bead, $-\gamma\dot{x}$, with γ the friction coefficient known from Stokes' law $\gamma = 3\pi\eta d$. Here, d is the diameter of the bead and η is the viscosity of the liquid. For beads close to the surface of the coverslip, Faxén's correction to Stokes' law should be invoked too. However, in the results presented here, the bead is far away from any surface. The bead is also subject to a stochastic force $\mathcal{F}(T)$ due to the Brownian motion of the surrounding liquid at temperature T. Since the Reynolds number is very

small, the inertial term can be neglected, yielding the equation of motion

$$0 = -\kappa x - \gamma \dot{x} + \mathcal{F}(t). \tag{1}$$

Upon Fourier transformation of Eq. (1), one obtaines an equation for the Fourier transformed of the position, $\tilde{x}(f)$, and the power spectrum $S_x \equiv \langle |\tilde{x}(f)|^2 \rangle$ for the position x is calculated as

$$S_x = \frac{k_B T}{\pi^2 \gamma (f_c^2 + f^2)}. \tag{2}$$

The characteristic parameter appearing in $S_x(f)$, the corner frequency is given by $f_c = \frac{\kappa}{2\pi\gamma}$, where a typical value of $f(c)$ in our experiments is ~ 1 kHz. Knowing γ, κ can be determined.

The recorded signal, stemming from a quadrant photo diode, gives the position x and y of the bead measured in Volts. We want to determine the factor A, translating the recorded signal, in Volts to a position in meters.

For a bead moving in a harmonic potential, the distribution of positions visited is Gaussian. Thus, from a histogram of the positions measured, we can determine the variance σ_V^2 (subscript V to indicate measured in Volts)

$$\sigma_V^2 = \left\langle x_V^2 \right\rangle - \langle x_V \rangle^2 . \tag{3}$$

In a harmonic potential, the equipartition theorem gives

$$\sigma^2 = \frac{k_B T}{\kappa} \quad . \tag{4}$$

With κ known from the relation $f_c = \frac{\kappa}{2\pi\gamma}$, σ (measured in meters) can be found. Now, A can be determined from σ_V and σ found from Eqs. (3) and (4)

$$A = \frac{\sigma}{\sigma_V}. \tag{5}$$

For a very precise analysis of the fluctuations of a bead in an optical trap, additional terms must be taken into consideration, of which the most severe is the filtering effect of the quadrant photodiode (Berg-Sørensen et al., 2003), but also aliasing must be taken into account and an analytical fit can be performed(Berg-Sørensen and Flyvbjerg, 2004). In our data analyses, we use a program (Hansen et al., 2005) which does all this.

4. Results and discussion

Using the two different geometries shown in Figure 1 yield quite different force-extention curves while stretching 1.1 μ DNA. Figure 2 shows the force

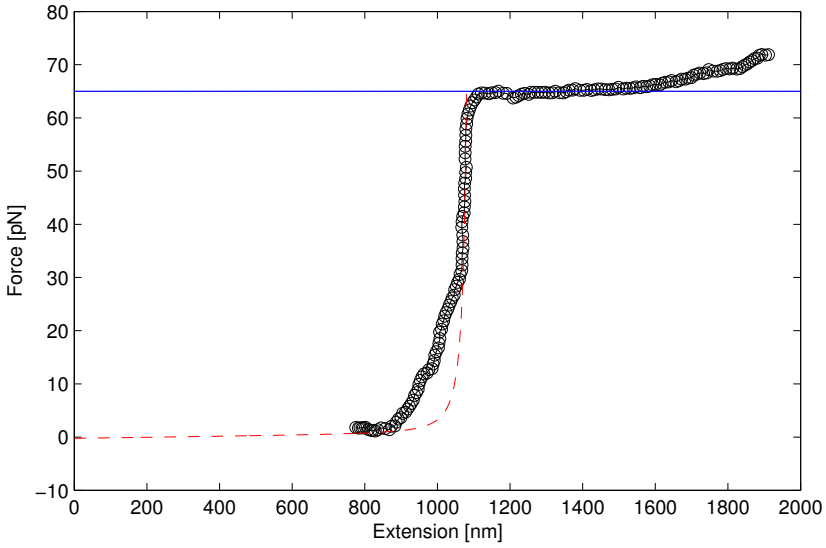

Figure 2. Force versus extention of DNA using the **parallel** geometry. Black circles: Data. Dashed red line: worm-like-chain theory prediction. Full blue line: Expected location of the plateau where dsDNA changes conformation.

extension curve resulting from stretching DNA using a geometry where the axis of the micropipette is parallel with the stretching of DNA (right scenario in Figure 2).

Figure 3 shows the force-extension curve resulting from stretching DNA with a setup where the micropipette is orthogonal to the direction of the stretching.

Numerous models have predicted the force-extension behavior of biopolymers such as DNA. One of the most famous models is the so-called 'Worm-Like-Chain' (WLC) (Marko and Siggia, 1995), predicting that the force F nescessary to extend the polymer to a distance x is given by:

$$F = \frac{k_B T}{\xi_p}\left(\frac{1}{4(1-x/L_0)^2} - \frac{1}{4} + \frac{x}{L_0}\right), \tag{6}$$

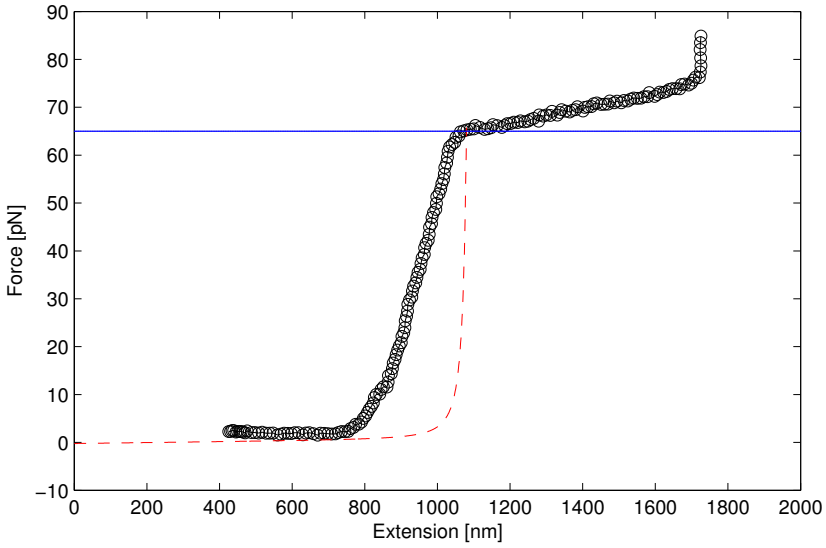

Figure 3. Force versus extention of DNA using the **orthogonal** geometry. Black circles: Data. Dashed red line: worm-like-chain theory prediction. Full blue line: Expected location of the plateau where dsDNA changes conformation.

where ξ_p is the persistence length and L_0 the contour length. In our experiment $L_0 = 1.1\mu$m and we use $\xi_p = 48$ nm as the DNA persistence length under the given electrolyte conditions (Wang et al., 1997). The first quantitative experimental study of the elastical properties of DNA (Wang et al., 1997) showed that the force-extension curve is well fitted by a modified version of the Marko-Siggia WLC. However, for simplicity, and as our goal was not to find the exact elastic properties of the DNA, but rather to make some statement about the equipment, we chose to use the WLC of equation 6, which actually is a good approximation both at high and low forces. At intermediate forces WLC is expected to deviate up to 10 pct.

On both Figures 2 and 3 the prediction of WLC (equation 6) is shown as a dashed red line. It is clear that the increase of the force accordingly to WLC is significantly steeper than that observed with the orthogonal geometry. On the other hand, using the parallel geometry, a much nicer

resemblence is found. It should be noted, that in our experiments only the relative, not the absolute, extension x is known. Therefore, the data has been artificially shiftet horisontally to reach the plateau simultaneously with the predictions of WLC.

It has been shown experimentally (Smith et al., 1996) that exerting a sufficiently large force on DNA will cause the DNA to change conformation and undergo a highly cooperative transition into a stable form which is 70 pct. longer than the usual B-form dsDNA. This transformation happens around F=65 pN. In both Figures 2 and 3 we observe this transformation happening around 65 pN (solid blue line in Figures). Using the orthogonal setup geometry this transition does not appear to happen at a constant force, whereas it does appear to happen at constant force using the parallel setup. In both Figure 2 and 3 we also observe the onset to melting transition which happens at an extension of about 1.8 μm.

If the micropipette is not sufficiently stiff with respect to bending, then in the orthogonal setup, the elasticity of the micropipette might cause the tip of the micropipette to bend when acted upon by a force applied orthogonal to the axis of the micropette (the end of the micropipette is fixed in the perfusion chamber, which is moved by the piezo electrical stage). This would give rise to a behavior as observed in Figure 3, namely that the increase in force is slower than predicted by WLC and that the plateau does not appear horisontal. In the parallel geometry, on the other hand, these deviations are not observed, and largely, the force-extension curve follows WLC and the plateau is horizontal. Of course, in the parallel configuration, the micropipette is stretched lengthwise, but it appears that the micropipette is stiffer in the direction along the pipette than orthogonal to it.

The stiffness of the micropipette used in a setup with orthogonal geometry (Wuite et al., 2000) was estimated on the basis of the thermal fluctuations of a bead attached to the micropipette to be $\kappa_{\mu pipette} \sim 4$ nN/μm. Our measurements give a different number: Judging from Figure 2 and 3, it appears that at a force of F=65 pN, the pipette has been stretched by an additional $\sim$ 200 nm, corresponding to a stiffness of $\kappa_{\mu pipette} \sim$ 0.3 nN/μm. Of course, individual pipettes have varying inner and outer diameters and have differing suspension lengths from their fixed point to the tip, so their flexibility in the orthogonal direction can be expected to vary substantially.

It is important to be aware of this artefact of the micropipette when one uses a micropipette e.g. in connection with optical traps to study mechanical behavior of biological molecules. For longer molecules as λ-DNA it is not so important, but for smaller polymers it becomes increasingly important. Especially when the precision claimed significantly exceeds the

effect brough up here. It should be noted, that a number of experiments reported in literature, e.g. in (Smith et al., 1996) and (Liphardt et al., 2001),(Liphardt et al., 2002) use the orthogonal geometry. A close inspection of the force extension data presented in these papers show that stretching DNA (Smith et al., 1996) does not follow WLC and the plateau is not totally horisontal. Stretching DNA-RNA hybrid handles (Liphardt et al., 2001; Liphardt et al., 2002) does not follow WLC either. One reason for this could be the geometry of the setup as examined in the present paper.

By no means do we claim to have solved the problem, there might be other experimental artefacts that are even more severe. Another issue which we did not consider, but which might be important is that of the pulling speed; the amount of irrevserible work put into the system might change the force-extention relations. However, as our two types of experiments were done with the same pulling speed, they are directly comparable, and our conclusion about the flexibility of the micropipette as crucial, holds.

Our DNA had a contour length of 1.1 μm, and hence it is the shortest so far reported in stretching experiments. The DNA used in (Wang et al., 1997) was 1328 nm and that e.g. in (Smith et al., 1996) was 16 μm λ-DNA. WLC is derived with the assumption that the contour lenght is significantly longer than the persistence length. In our case, this ratio is 23, and one obvious challange would be to go to even shorter DNA's and see the gradual increase in deviation from WLC. Another subject that deserves investigation is whether DNA-RNA hybrids have different force-extension properties than dsDNA.

5. Conclusion

By using optical tweezers we have stretched 1.1μm DNA to its transition point. The DNA was tethered between two beads, one held by a micropipette and the other by optical tweezers. The optical tweezers were equipped such as to enable accurate measurements of corresponding values of force and extension of the DNA tether. We used two different setups: One in which the micropipette was orthogonal to the direction in which the polymer was being stretched, in the other the micropipette was parallel to the stretching direction. Using the parallel setup yielded results where the force-extension data resembled worm-like-chain predictions and a horisontal transion plateau was observed as expected at 65 pN. However, using the orthogonal geometry, which is widely reported in literature, we observed the force to increase slower than expected and the plateau was not horizontal. This can be explained by the fact that the micropipette bends and hence, its elasticity must be taken into account when pulling orthogonal to it at

its tip. Using a setup geometry where the pulling direction is parallel to the micropipette decreases this effect, and is the route we devise out of this problem.

6. Acknowledgements

We acknowledge discussing the biological construct with Michael A. Sørensen, Institute of Molecular Biology and Fysiology, University of Copenhagen, as well as discussions with the other members of the Optical Tweezers Group, Niels Bohr Institute. We acknowledge financial support from the Carlsberg Foundation, the BIOP Graduate School and from the Villum Kann Rasmussen Foundation.

References

Berg-Sørensen, K. and H. Flyvbjerg: 2004, 'Power spectrum analysis for optical tweezers'. *Rev. Sci. Ins.* **75**, 594–612.

Berg-Sørensen, K., L. Oddershede, E. Florin, and H. Flyvbjerg: 2003, 'Unintended Filtering in a Typical Photodiode Detection System for Optical Tweezers'. *Journal of Applied Physics* **93**, 3176–3177.

Hansen, P. M., I. Tolic-Nørrelykke, , H. Flyvbjerg, and K. Berg-Sørensen: 2005, 'Faster version of MatLab package for precise calibration of optical tweezers'. *submitted to Comp. Phys. Comm.*

Jarzynski, C.: 1997, 'Nonequilibrium Equality for Free Energy Differences'. *Physical Review Letters* **78**, 2690–2693.

Liphardt, J., S. Dumont, S. Smith, I. T. Jr., and C. Bustamante: 2002, 'Equilibrium Information from Nonequilibrium Measurements in an Experimental Test of Jarzynski's Equality'. *Science* **296**, 1832–1835.

Liphardt, J., B. Onoa, S. Smith, I. T. Jr., and C. Bustamante: 2001, 'Reversible Unfolding of Single RNA Molecules by Mechanical Force'. *Science* **292**, 733–737.

Marko, J. and E. Siggia: 1995, 'Stretching DNA'. *Macromolecules* **28**, 8759–8770.

Oddershede, L., J. Dreyer, S. Grego, S. Brown, and K. Berg-Sørensen: 2002, 'Motion of a single molecule, the lambda-receptor, in the outer bacterial membrane'. *Biophysical Journal* **83**, 3152–3161.

Oddershede, L., S. Grego, S. Nørrelykke, and K. Berg-Sørensen: 2001, 'Optical Tweezers: Probing Biological Surfaces'. *Probe Microscopy* **2**, 129–137.

Smith, S. B., Y. Cui, and C. Bustamante: 1996, 'Overstretching B-DNA: The Elastic Response of Individual Double-Stranded and Single-Stranded DNA Molecules'. *Science* **271**, 795–798.

Wang, M., M. Schnitzer, H. Yin, R. Landick, J. Gelles, and S. Block: 1998, 'Force and Velocity Measured for Single Molecules of RNA Polymerase'. *Science* **282**, 902–907.

Wang, M., H. Yin, R. Landick, J. Gelles, and S. Block: 1997, 'Stretcing DNA with optical tweezers'. *Biophysical Journal* **72**, 1335–1346.

Wuite, G., R. Davenport, A. Rappaport, and C. Bustamante: 2000, 'An Integrated Laser Trap/Flow Control Video Microscope for the Study of Single Biomolecules'. *Biophysical Journal* **79**, 1155–1167.

Stretching Short DNA Tethers using Optical Tweezers

Nader Reihani, Lana Bosanac, Thomas M. Hansen, and Lene B. Oddershede

Niels Bohr Institute, Blegdamsvej 17, 2100 Copenhagen, Denmark

ABSTRACT

With the evolution of single molecule techniques as force-scope optical tweezers, it has become possible to perform very accurate measurements of the elastic properties of biopolymers as e.g. DNA. Nucleic acid elasticity is important in the interaction of these molecules with proteins and protein complexes in the living cell. Most experimental and theoretical effort has been aimed at uncovering and understanding of the behavior of polymers with contour lengths significantly longer than their persistence length. The well-established Worm-Like-Chain model has been modified such that a satisfactory description of such long biopolymers is available. However, in many single molecule experiments, such as the unfolding of RNA stem-loops[1] and RNA pseudoknots,[2] one is dealing with biopolymers whose contour lengths are comparable to persistence lengths. A full understanding of such curves requires an understanding of the physics of short biopolymers. For such cases, theories are just beginning to emerge and there is hardly any experimental data available. We target this problem by optical tweezers quantitative force-extension measurements on short biopolymers. The biopolymers used are primarily double stranded DNA whose total length (300 nm) is comparable to their persistence length (50 nm). As a control of our equipment and methods, we also stretch longer dsDNA (1100 nm), the force-extension curves of which resemble those in literature.[3] For the short DNA the force-extension curves qualitatively resemble those predicted by WLC theories, but a reasonable fit can only be made if the persistence length is allowed to be a fitting parameter. If made a fitting parameter, the 'apparent persistence length' is found as 8.7±4 nm, a number which is significantly lower than the real physical value.

Keywords: DNA, optical tweezers, force-extension, persistence length, Worm-Like-Chain model

INTRODUCTION

Mechanical properties of the DNA are of importance in many vital cellular functions such as division, folding, packaging, regulation, recombination, replication, and transcription. For a deep understanding of these processes it is crucial to have knowledge about the physical properties, e.g. the elasticity, of nucleic biopolymers. Tools as e.g. optical tweezers have proven very useful in determining the elastic properties of e.g. DNA[3] and the emphasis of such studies has henceforth been on biopolymers which were longer or on the order of tenths of kilo base pairs. The well established biopolymer theories as the Kratky-Porod model, the persistent chain model, the Worm-Like-Chain model or modifications of this are all dealing with biopolymers whose contour length is significantly longer than the persistence length of the biopolymer.

However, as many DNA interactions occur on length scales smaller than or comparable to DNA persistence length, it is also of importance to know the physical properties of DNA, such as its elasticity, on short length scales in comparison to persistence lenght. Another reason is that many biological constructs used in single molecule studies as e.g. in studies of RNA loop structure and stability,[1] or in RNA pseudoknot stability analysis[4] have DNA like handles which are certainly short in comparison to DNA persistence length. Also, seen from a fundamental physics point of view, the question of how to model such short biopolymers where boundary effects become important, is an interesting challenge, which will provide new insights into the world of biopolymers.

In this paper we present optical tweezers measurements of force-extension relationships of long as well as short tethers of dsDNA. The DNA tether is specifically attached in one end to a bead which is held by a micropipette,

Further author information:
N.R.: E-mail: reihani@nbi.dk
L.B.: E-mail: bosanac@nbi.dk
T.M.H.:E-mail: tmhansen@nbi.dk,
L.B.O.: E-mail: oddershede@nbi.dk

the other end is specifically attached to another bead held by the optical trap. First we give a short introduction to WLC theories, then the methods and materials section which provides information about the details of the experiments, and finally, we present the results of stretching the two different lengths of DNA tethers.

THE WLC MODEL

DNA is a double stranded molecule consisting of two polymers of nucleotides that are linked in a double helix by formation of H-bonds between their complementary bases. The molecule possesses some inherent physical advantages for measurement: dsDNA is a very stiff polymer of unusually large persistence length estimated at 50nm by the WLC model and confirmed by measurements.[3] As a consequence, self avoidance is actual, and excluded volume effects are negligible in most conditions - they are minimal for unstretched DNA at $l \leqslant 100kb$ and further reduced under extension.[5]

The persistence length of a polymer, p, is the ratio of its flexural rigidity, κ_f, which contains both information on the material and the geometry of the polymer, to thermal energy:

$$p = \frac{\kappa_f}{k_B T}. \tag{1}$$

Basically, p gives information of the distance over which the biopolymer appears stiff with respect to its thermal motion.

Several mathematical models have been created for the prediction of the overall size of a biopolymer and the determination of a polymers persistence length, The freely jointed chain model predicting non-interacting polymer segments can be used to derive the modified Gaussian model in rubber elasticity and finally extended into the persistent chain model (WLC) of Porod and Kratky.[6] This model has been further perfectionized e.g. by Marko and Siggia.[7]

Physically, the stretching of a DNA polymer can be thought of as divided into regimes: The entropic regime is relevant at lower forces where a stretching basically corresponds to decreasing possible conformational states, thus decreasing entropy. This regime spans the stretching of up to 90% of the entire polymers contour length. The formula given by Marko and Siggia:[7]

$$F(x) = \frac{k_B T}{p} \frac{1}{4(1 - x/L)^2} - \frac{1}{4} + \frac{x}{L} \tag{2}$$

describes the force-extension relation fairly well in the entropic regime.

The second regime, spanning about 90-95% of the DNA contour length is called the enthalpic regime, this is the region of larger forces, where the actual bonds between the molecules are being stretched. This regime is mathematically well described by the 'Extensible Worm Like Chain' (EWLC) model which, in fact, also covers the entropic regime fairly well:[8]

$$F(x) = \frac{k_B T}{p} \frac{1}{4(1 - x/L + F(x)/K)^2} - \frac{1}{4} + \frac{x}{L} - \frac{F(x)}{K} \tag{3}$$

here, K is the elastic modulus of the polymer.

Finally, at around 65-70 pN a force plateau is reached where the DNA molecule can be expanded a significant lenght, beyond its contour length without increasing the applied force.[9] At this force plateau the DNA changes conformation.

Recently, there are theoretical efforts emerging trying to modify the WLC theories to account for finite length of the biopolymer, as well as for various boundary effects such as the bending of the biopolymer. In the work by Kulic et al[10] they theoretically predict that e.g. a bending of a biopolymer will cause the WLC theory still to be a reasonable description, but with the constraint that the persistence length is not any more the true persistence length but rather an 'apparent' persistence length which is significantly shorter than the physical persistence length.

1. MATERIALS AND METHODS

Optical tweezers The optical tweezer setup consists of a single-beam optical trap based on a 1064nm $NdYVO_4$ laser coupled to an inverted Leica microscope. The equipment is described in detail in.[11] The force and position detection system consists of a Si-PN quadrant photodiode (S5981, Hamamatsu) in back focal plane detection scheme and a CCD camera (Sony XC-E150, 25Hz), this particular photodiode is known to perform filtering at high frequencies[12] but this effect is eliminated in the costum made software we use to analyze the data.[13] Spatial resolution is 1-2 nm and temporal resolution up to MHz. A 12-bit A/D board (PCI-MIO-16E-4) digitizes the voltage signals of the photodiode and the piezo stage.

Construction of DNA tether DNA fragments with biotin in one end and digoxygenin in the other were synthesized in PCR reactions using 5' modified primers. For the forward primer, 5' gtatacctctcagttgggtg, the modification was biotin, whereas for the reverse primer, 5' ataattcgcgtctggccttc, it was digoxygenin. pTH401 or pTH419 was used as template. The results were DNA fragments of predicted sizes 942 bp and 3202 bp, corresponding to 320 nm and 1089 nm, respectively. The PCR were done using SUPER TAQ polymerase and reaction buffer from HT Biotechnology, 200 μM dNTPs, 10 pg/μl template DNA, 500 fmol/μl of the primers.

pTH401 and pTH419 were derived from pOFX302.[14] For pTH401 pOFX302 was digested with restriction endonucleases HindIII and ApaI and complimentary DNA oligomeres encoding 5' agctttttaaagcagtaagcgcgcgcacggagcgtcgcgtgcgcgcgcaagctagtggatgtgatcctgatgttgtaaagcgacgcttgggcc, were annealed and inserted between the restriction sites in the plasmid. The identity of the plasmid were checked by DNA sequencing (Big Dye, Perkin Elmer).

For pTH419 DNA fragments from a digestion of bacteriophage λ DNA with restriction endonuclease HindIII were inserted in the HindIII site of pOFX302. Plasmids was checked by agarose gel electrophoresis after digestion with HindIII. One plasmid, showing bands of approximately 8000 bp and 3200 bp was named pTH419.

All enzymes and reaction buffers used in the preparations were from New England Biolabs and molecular cloning methods were as described in.[15]

To bind the DNA to beads, appropriate dilutions of DNA and 2.1 μm streptavidin coated polystyrene beads (Bangs) were mixed and incubated for 1 hr at room temperature with gentle mixing. The ratio of DNA to 2.1 μm beads was chosen so that no more than approximately 4 out of 5 of the beads would later form a tether to the 2.88 μm anti-digoxygenin coated bead. Antidigoxygenin(Roche) was bond to 2.88 μm protein G coated polystyrene beads (Spherotech) and cross-linked by dimethylpimelinediimidate dihydrochloride (Sigma). This procedure insured a low likelyhood of getting tethers of more than one DNA molecule. After binding the DNA to the 2.1 μm beads the mixture was diluted in a dilution of 2.88 μm anti-digoxygenin coated beads and transferred to the sample chamber for the microscope. Experiments were performed in Buffer C: 10 mM Tris-HCl pH 7.9, 250 mM NaCl, 10 mM Mg2Cl, 0.05 % (w/v) BSA at room temperature, 22 C.

Perfusion chambers Perfusion chambers containing approximately 20 μl are constructed by separating two coverglasses by melted and subsequently solidified parafilm. Micropipettes are inserted into the parafilm before melting it and hence, they are immobilized with respect to the sample chamber. It is possible to apply suction to the micropipettes, thus firmly holding beads at the end. The chamber can be flushed with different liquids, if needed. The chamber is mounted onto a piezoelectric stage (PI 731.20) with capacitative feedback control and nano-meter resolution.

Experiments In the experiment, the optical trap is kept fixed with respect to the laboratory frame and the sample is moved. In similar experiments,[16] we have noticed that one has to be careful concerning the direction of the micropipette with respect to the pulling direction: As the tip of the micropipette is rather thin (1.5 μm) and long, the spring constant characterizing the bending of the micropipette in a direction orthogonal to its length is comparable to the spring constant characterizing the optical trap. However, in the parallel direction, the spring constant is considerably stronger. Hence, it is very important to perform the experiments in a geometry where the direction of the micropipette is parallel to the pulling direction as shown in Figure 1.

Buffer C containing the 2.88 μm antidigoxygenin coated polystyrene beads to which the DNA tethers are specifically attached as well as the streptavidin coated 2.1μm polystyrene beads are flushed into the chamber. By the optical trap, a 2.1 μm bead is picked up and by suction in the micropipette firmly placed at its end.

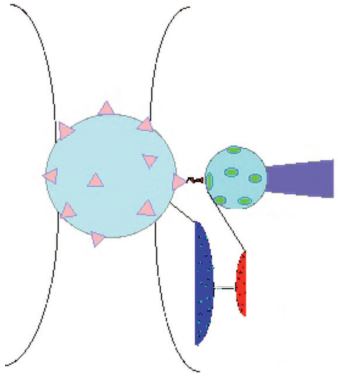

Figure 1. Experimental setup showing e.g. the direction of the micropipette with respect to the tether direction.

Thereafter, a 2.88μm bead with DNA tethers sticking out is picked up by the optical trap. At the laser power used for the force-extension experiments, utilizing the Brownian motion of the bead in the optical trap, it is calibrated and the spring constant describing the optical trap specifically found for each bead used. During the calibration, the bead is held at exactly the same height as the bead in the micropipette and enough far away from the second bead that it does not have any influence. After the calibration procedure, the trapped bead slowly approached the bead held by the micropipette and eventually, the DNA attached to the larger bead is also attached to the smaller bead thus making a tether between the two beads. It is important to have the larger (and not the smaller) bead in the optical trap, because the tether is so short that in the microscope the beads appear as nearly touching, and if the trapped bead is not significantly larger than the focus area of the laser trap, then the adjacent bead would 'cast a shadow' onto the quadrant photodiode, thus obscuring the force measurements. A custom made LabView7.1 based program controls the movement of the stage while acquiring position signals.

DATA ANALYSIS

The calibration procedure was performed ,As earlier described, by means of the Brownian motion of the trapped bead. Since in short DNA experiment the movement of the bead in the trap is comparable with elongation of the DNA having accurate calibration parameters is very important. So, before doing short DNA experiment the accuracy of the calibration has been checked by another method on longer-and well known- DNA as following. Since the force-extension graph at forces about 40pN is almost vertical, one can get the conversion factor β (see below)by simply dividing the slops of the signals read off from photodiode and piezo stage(Figure2). The spring constant, the other calibration parameter, also can be extracted by comparing the plateau voltage with well known force of 68pN for long DNA. Figure 2 shows both signals of piezo stage and photodiode during stretching a 1.1 μ DNA tether. In short DNA experiment only first calibration method is used.

STRETCHING 1.1 μ DNA

The optical tweezers are exerting a harmonic force on the bead in the trap, $F_{trap} = \kappa x_{trap}$, where κ is denoted the trap stiffness and x_{trap} is the position of the bead with respect to the center of the trap. F_{trap} and x_{trap} are found as described in[11] and using the matlab routines described in.[13] To obtain the total extension of the tether, x, at any given time t the voltage signal giving the position of the piezoelectric stage V_s and the corresponding signal from the photodiode V_p, giving the position of the bead relative to the center of the trap, are analyzed in the following way:

$$x(t) = B[V_s(t) - V_s(0)] - \beta[V_p(t) - V_p(0)] + x(0) \tag{4}$$

where the first term describes the distance that the stage has been moved, B (=10,000 nm/v, fixed by company) and β being the conversion factors that translate the voltage signal from the piezoelectric stage and photodiode

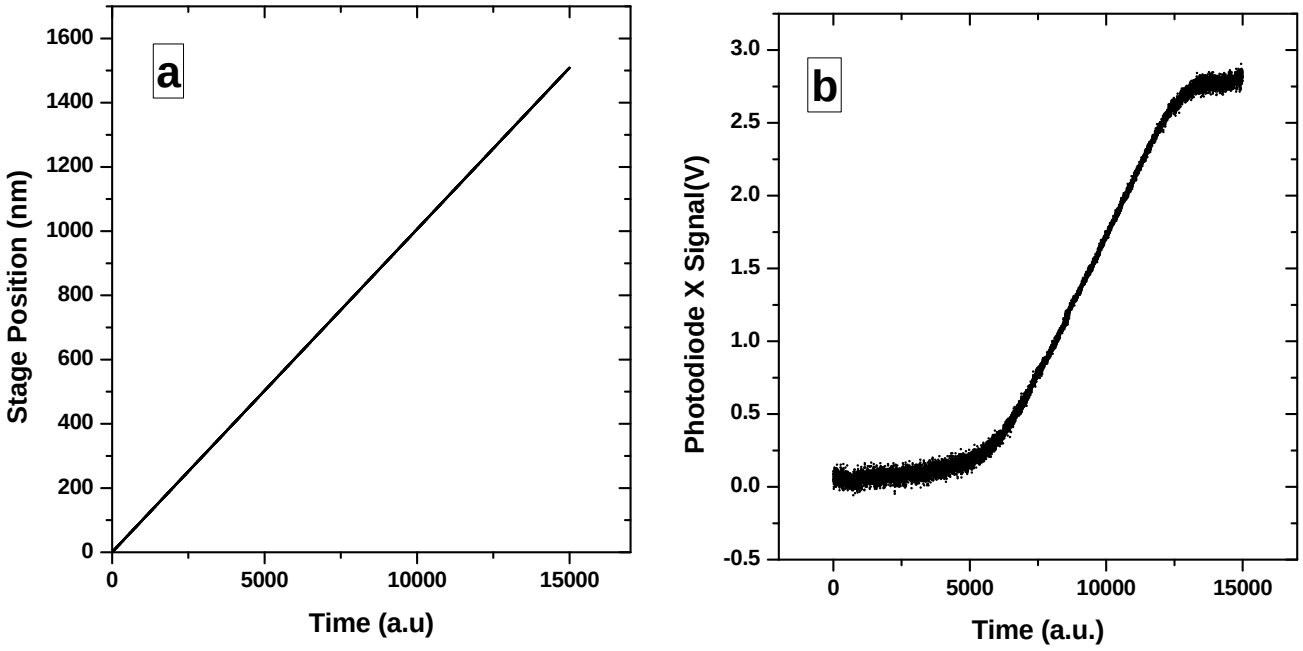

Figure 2. Position signals while stretching a 1.1μm DNA tether read off from piezo stage(a) and photodiode(b), respectively. The ratio of slops at linear rigion of two graph gives the conversion factor of photodiode.

to metric coordinates. The second term is the movement of the bead in trap. However, the starting point is arbitrary and therefore some constant, $x(0)$, is included.

The total force, F, acting on the tethered bead is found in the following way:

$$F = \kappa_{trap} \cdot x_{trap} - \gamma \cdot v \tag{5}$$

where v is the velocity of the fluid relative to the sphere, which equals the velocity of the stage and γ is the friction coefficient. Thus, the last term is the Stokes drag on the sphere which is about 4 orders of magnitude smaller than the first term and hence safely can be neglected. The measured extensions are relative, not absolute.

Figure 3 shows the force-extension relation obtained while stretching a single 1.1 μm dsDNA tether. The full line in the figure shows a fit of the EWLC function to the force-extension curve until point where the plateau begins. If p is allowed to be a free fitting parameter, it comes out as 50 nm, which is as expected.[3] Thus, this curve shows that our equipment and the biological construct is functioning as expected.

STRETCHING 0.3 μ DNA

Figure 4 shows the force-extension curve obtained from stretching the short 0.3 μm DNA tethers. First of all, the resemblance between stretching the 1.1 μm DNA tether and the 0.3 μm DNA tether is very clear. E.g. the force plateau is also present while stretching the shorter DNA, even at an identical force. The data from the shorter DNA has been fit both by the WLC and by the EWLC functions, full and dashed lines, respectively, on Figure 4. The only way the fits can come out with a reasonable resemblance to data is if the persistence length is allowed to be a fitting parameter. Doing this, both WLC and EWLC return values of p close to 5 nm (exact values are given in Figure 4, which is considerably shorter than the physical persistence length of dsDNA which is close to 50 nm. 9 data sets were analyzed by fitting EWLC. Thus the obtained values of p are shown in the histogram in Figure 5. The average value of p is 8.7 nm and the standard deviation is $\pm$ 4 nm.

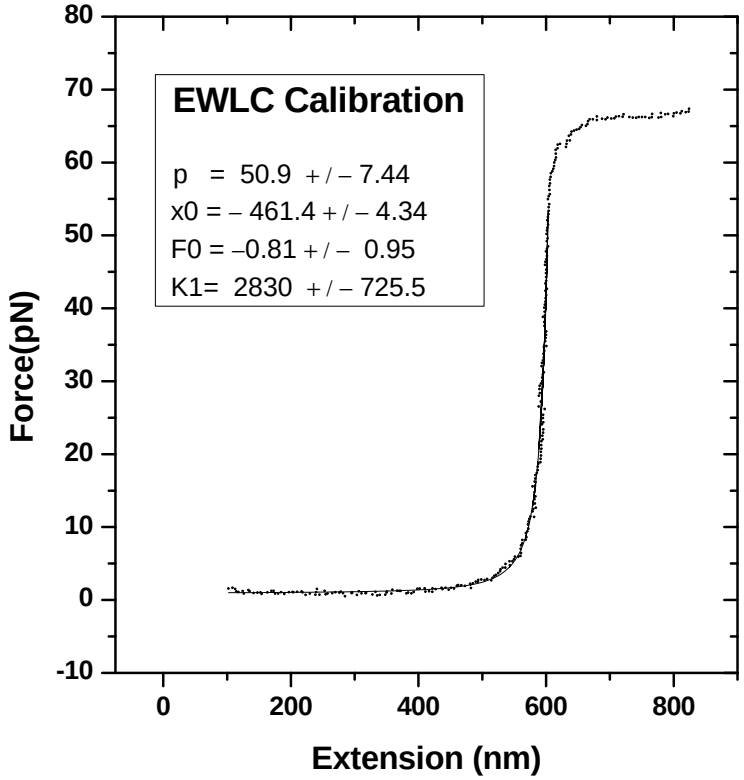

Figure 3. Force-extension curve obtained from stretching 1.1 μm DNA tethers.

CONCLUSION

We have presented the, to our knowledge, first data showing the force-extension relation during stretching of short dsDNA tethers. Stretching was performed using an optical trap. Also, we present an alternative method to perform a calibration yielding the parameters describing the optical trap by comparing readouts from the piezo stage to the readouts from the quadrant photodiode. The equipment and biological construct was tested by stretching longer dsDNA tethers (1.1 μm). The short tethers, the main topic of this investigation, had a length of 300 nm or approximately 6 times the persistence length of dsDNA. Because the contour lenght is comparable to the persistence length, the classical WLC theories cannot be applied in the data analysis. However, if the persistence length is allowed to be a fitting parameter, the fit between the data and WLC theories is satisfying. The value of this 'apparent' persistence length of short DNA is found to be 8.7 pm 4 nm. This is consistent with the theory presented in[10] where e.g. bendings of DNA is supposed to create an 'apparent' and shorter persistence length. However, it still remains unknown why a shorter contour length would have a similar effect.

REFERENCES

1. J. Liphardt, B. Onoa, S. Smith, I. Tinoco, and C. Bustamante, "Reversible unfolding of single RNA molecules by mechanical force," *Science* **292**, pp. 733–737, 2001.
2. T. M. Hansen, "Correlation between mechanical strenght of messenger RNA pseudoknots and ribosomal frameshifting," *Ph.D.thesis* **Department of Molecular Biology and Physiology, University of Copenhagen**, 2006.
3. M. Wang, H. Yin, R. Landick, J. Gelles, and S. Block, "Stretching DNA with optical tweezers," *Biophysical Journal* **72**, p. 1335, 1997.
4. T. M. Hansen, N. Reihani, L. B. Oddershede, and M. A. Sørensen, "Correlation between mechanical strength of messenger RNA pseudoknots and ribosomal frameshifting," *Preprint* , pp. 1–25, 2006.

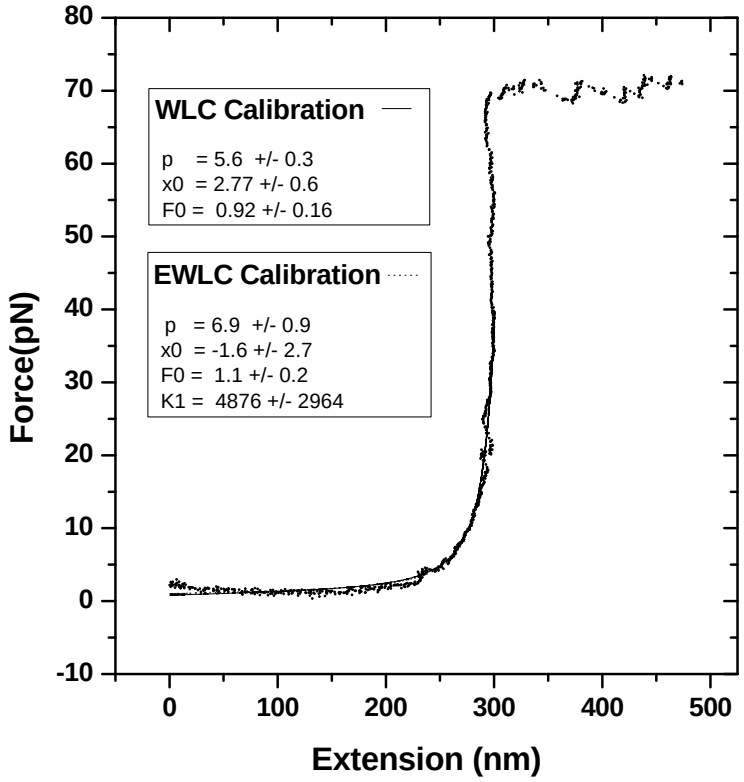

Figure 4. Force-extension curve obtained from stretching 0.3 μm DNA tethers.

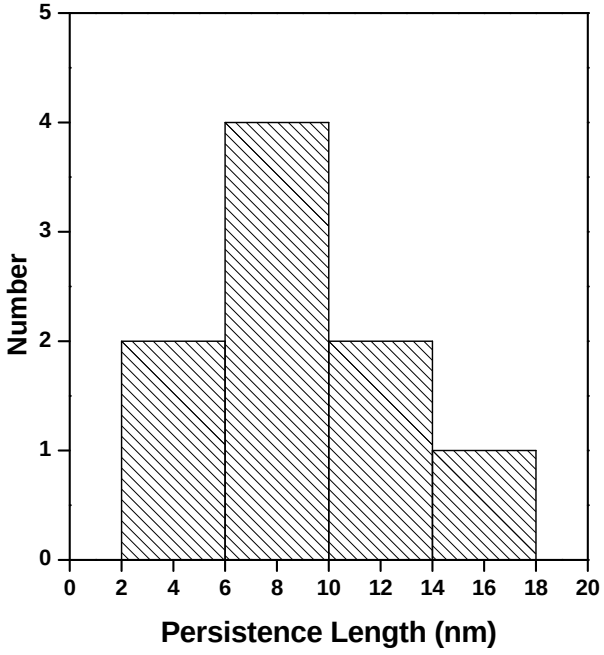

Figure 5. Histogram of persistence length for 9 analyzed experiments on 0.3μm DNA tethers.

5. C. Bustamante, J. Marko, Siggia, and S. Smith, "Entropic elasticity of λ-phage DNA," *Science* **265**, pp. 1599–1600, 1994.
6. O. Kratky and G. Porod, "Rontgenuntersuchung geloster fadenmolekyle," *Recl. Trav. Chim* **68**, p. 1106, 1949.
7. J. Marko and E. Siggia, "Stretching DNA," *Macromolecules* **28**, p. 8759, 1995.
8. T. Odijk, "Stiff chains and filaments under tension," *Macromolecules* **28**, p. 7016.
9. S. Smith, Y. Cui, and C. Bustamante, "Overstretching DNA: The elastic response of individual double-stranded and single-stranded DNA molecules," *Science* **271**, p. 795, 1996.
10. I. Kulic, H. Mohrbach, V. Lobaskin, R. Thaokar, and H. Schiessel, "Apparent persistence lenght renormalization of bent DNA," *Physical Review* **E72**, p. 041905, 2005.
11. L. Oddershede, S. Grego, S. Nørrelykke, and K. Berg-Sørensen, "Optical tweezers: Probing biological surfaces," *Probe Microscopy* **2**, pp. 129–137, 2001.
12. K. Berg-Sørensen, L. Oddershede, E.-L. Florin, and H. Flyvbjerg, "Unintended filtering in a photodiode detection system for optical tweezers," *Journal of Applied Physics* **96**(6), 2003.
13. I. Tolic-Nørrelykke, K. Berg-Sørensen, and H. Flyvbjerg, "Matlab program for precision calibration of optical tweezers," *Computer Physics Communications* **159**, pp. 225–240, 2004.
14. C. Rettberg, M. Prere, R. Gesteland, J. Atkins, and O. Fayet, "A three-way junction and constituent stem-loops as the stimulator for programmed -1 frameshifting in bacterial insertion sequence is911," *Journal of Molecular Biology* **286**, pp. 1365–1378, 1999.
15. J. Sambrook, E. Fritsch, and T. Maniatis, "Molecular cloning: A laboratory manual," *Cold Spring Harbor Laboratory Press NY* , 1989.
16. T. Hansen, N. Reihani, and L.B.Oddershede, "Combining optical tweezers and micropipettes for DNA stretching: Elasticity of micropipette crucial," *NATO Springer proceedings* , 2005.

Correlation between mechanical strength of messenger RNA pseudoknots and ribosomal frameshifting

Thomas M. Hansen*†‡, S. Nader S. Reihani†§, Lene B. Oddershede†, and Michael A. Sørensen*

*Department of Molecular Biology, University of Copenhagen, Ole Maaløesvej 5, DK-2200 Copenhagen N, Denmark; †Niels Bohr Insitute, University of Copenhagen, Blegdamsvej 17, DK-2100 Copenhagen, Denmark; and §Institute for Advanced Studies in Basic Sciences, P.O. Box 45195-1159, Zanjan, Iran

Edited by Peter B. Moore, Yale University, New Haven, CT, and approved February 13, 2007 (received for review September 30, 2006)

Programmed ribosomal frameshifting is often used by viral pathogens including HIV. Slippery sequences present in some mRNAs cause the ribosome to shift reading frame. The resulting protein is thus encoded by one reading frame upstream from the slippery sequence and by another reading frame downstream from the slippery sequence. Although the mechanism is not well understood, frameshifting is known to be stimulated by an mRNA structure such as a pseudoknot. Here, we show that the efficiency of frameshifting relates to the mechanical strength of the pseudoknot. Two pseudoknots derived from the Infectious Bronchitis Virus were used, differing by one base pair in the first stem. In *Escherichia coli*, these two pseudoknots caused frameshifting frequencies that differed by a factor of two. We used optical tweezers to unfold the pseudoknots. The pseudoknot giving rise to the highest degree of frameshifting required a nearly 2-fold larger unfolding force than the other. The observed energy difference cannot be accounted for by any existing model. We propose that the degree of ribosomal frameshifting is related to the mechanical strength of RNA pseudoknots. Our observations support the ''9 Å model'' that predicts some physical barrier is needed to force the ribosome into the −1 frame. Also, our findings support the recent observation made by cryoelectron microscopy that mechanical interaction between a ribosome and a pseudoknot causes a deformation of the A-site tRNA. The result has implications for the understanding of genetic regulation, reading frame maintenance, tRNA movement, and unwinding of mRNA secondary structures by ribosomes.

macromolecular mechanics | optical tweezers | protein synthesis | single molecules | translation

When an mRNA sequence is translated into protein by the ribosome, the nucleotide sequence is read in codons of three nucleotides and hence the mRNA in principle has three reading frames. In the vast majority of mRNAs, only one reading frame, defined by the initiation codon, is exploited and translated into protein. The elongation phase of protein synthesis is a precise process and intrinsic mechanisms exist in the ribosome to enhance translational fidelity (1, 2). The frequency of frameshift errors has been estimated to $<3 \times 10^{-5}$ (3, 4). However, many examples of naturally occurring and highly efficient programmed frameshift sites have been described (5, 6). There is considerable interest in how ribosomal frameshift occurs, as this may provide insight into mechanisms behind reading frame maintenance, tRNA movement, and unwinding of mRNA secondary structures by ribosomes. Typically, a −1 frameshift site comprises two elements, a slippery sequence, X XXY YYZ, where the frameshifting occurs, and additionally, a stimulatory RNA element positioned downstream in the mRNA (7). Frameshifting is thought to happen by dual tRNA slippage. In the original zero reading frame, the P-site tRNA and the A-site tRNA pair to codons XXY and YYZ, respectively, whereas after the shift to the −1 frame they pair to XXX and YYY. At the new position, the tRNAs remain paired to mRNA at the two most upstream XX and YY nucleotides in each codon.

Examples of stimulatory elements include downstream self pairing mRNA sequences called mRNA pseudoknots (Fig. 1). The requirement for these elements to function is a placement at a proper distance from the slippery sequence. In many viral frameshift sites, the stimulatory element is a pseudoknot positioned 6–9 nt downstream of the slippery sequence.

The mechanism of frameshift stimulation by pseudoknots is not well understood. Involvement of protein factors binding to the mRNA seems unlikely because, in a competition experiment, addition of excess RNA pseudoknots did not affect frameshift efficiencies (8). Furthermore, that many pseudoknot-stimulated programmed frameshifts function in heterologous organisms from different kingdoms of life makes it unlikely that the function requires transacting factors. It has been suggested that the stimulatory structure pauses the ribosome while the slippery sequence is positioned in the decoding site of the ribosome, thus increasing the chance of tRNA slippage (9). However, the data from measurements of ribosomal pausing with pseudoknots, mutated pseudoknots, and related stem-loops support the view that pausing alone cannot mediate frameshifting and that additional events are required (10, 11). The programmed frameshift in infectious bronchitis virus (IBV) has been investigated, and it was found that pseudoknots, but not similar stem-loop structures, stimulate efficient frameshifting (10).

As shown in Fig. 1*c*, a pseudoknot can be viewed as a stem-loop where nucleotides in the loop form a second stem with downstream mRNA. This may lock or decrease the rotational freedom of the first stem, and hence induce supercoiling while the ribosome unfolds the first stem. Experimental data support a role for torsional restraint in positioning the ribosome to pause with the slippery sequence in the A- and P-site when unfolding pseudoknots (12). This model makes it clear that an optimal spacing of 6–9 nt between slippery sequence and pseudoknot is crucial and positions the pseudoknot close to the entrance of the mRNA tunnel of the ribosome.

Recently, the ''9 Å model'' was suggested for the mechanism of frameshift stimulation (13). Structural studies have revealed a 9-Å movement by the anti-codon loop of the aminoacyl-tRNA between the state of initial binding and the fully accommodated

Author contributions: T.M.H., S.N.S.R., L.B.O., and M.A.S. designed research; T.M.H. performed research; T.M.H. and S.N.S.R. analyzed data; T.M.H., L.B.O., and M.A.S. wrote the paper; and S.N.S.R. wrote software.

The authors declare no conflict of interest.

This article is a PNAS Direct Submission.

Freely available online through the PNAS open access option.

Abbreviation: IBV, infectious bronchitis virus.

‡To whom correspondence should be addressed. E-mail: tmhansen@nbi.dk.

This article contains supporting information online at www.pnas.org/cgi/content/full/0608668104/DC1.

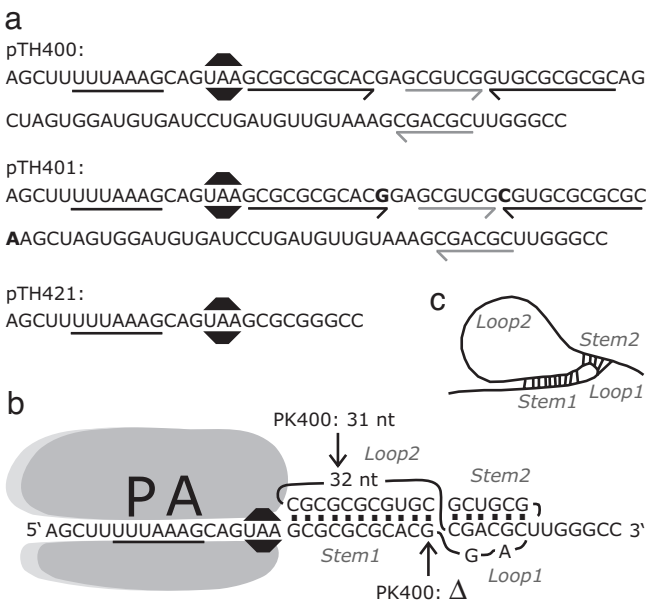

Fig. 1. Pseudoknots and frameshift sites. (*a*) Sequences of frameshift sites encoded in plasmids pTH400, pTH401, and pTH421. The slippery sequence is underlined, and the stop codon UAA is marked by a black ''stop sign.'' pTH400 and pTH401 encode the pseudoknots PK400 and PK401. The nucleotides that can form double-stranded stems are underlined by arrows. Stem1 is indicated by black arrows, and stem2 is indicated by gray arrows. The three nucleotides present only in PK401 are in bold. (*b*) Schematic drawing of an mRNA where the ribosome is positioned with the slippery sequence in its A and P sites. The secondary structure of PK401 is indicated with coaxially stacked stems and single-stranded loops. Differences from PK400 are indicated by arrows. (*c*) A schematic drawing of a pseudoknot.

position (reviewed in ref. 14). It is expected that the codon::anti-codon bound mRNA is pulled a similar distance further into the ribosome (13). The authors suggested that a downstream mRNA pseudoknot would provide resistance to this movement by becoming wedged into the entrance of the ribosomal mRNA tunnel. These two opposing forces result in the creation of a local region of tension in the mRNA between the A-site codon and the mRNA pseudoknot. The tension can be relieved by one of two mechanisms: unwinding of the pseudoknot, allowing the ribosome to move forward, or slippage of the proximal region of the mRNA backwards by one base. Even if it slips backwards one base, then still, afterward, it will have to unwind the pseudoknot to move forward.

In this model, the stability of pseudoknots should play an important role in stimulation of frameshift. Of course, one crucial question is how "stability" is defined. A correlation has not been found between the frequency of frameshifting and the difference in Gibbs free energy between folded and unfolded pseudoknots measured from UV optical melting profiles (15). When the pseudoknot is opened by a ribosome, the action might not be thermodynamically reversible i.e., the work performed by the ribosome might be larger than ΔG, and some fraction of the work might be dissipated irreversibly.

In an attempt to simulate the action of a ribosome, we mechanically unfold the pseudoknot using optical tweezers. By applying a load on the structure, it is forced to unfold. This type of experiment is similar to previous studies on RNA hairpin folding (16, 17). The pseudoknots are unfolded at a nonzero force-loading rate and, hence, in general, do not unfold or refold through an equilibrium process. Here, we first determine the degree of frameshift stimulation effected by two pseudoknots, then focus on the mechanical unfolding and refolding events for the two different pseudoknots and for a control RNA. From the unfolding mechanics, the energetics of the process are considered. Finally, we show how the rates of frameshifting for the two investigated pseudoknots correlate with the mechanical stability of the pseudoknots.

Results

Description of Frameshift Sites. In this work, we investigated an artificial site of programmed ribosomal frameshift resembling that of IBV, which have been studied extensively by Brierley and coworkers (10, 18–20). As a typical natural −1 frameshift site, our site includes a slippery sequence and a stimulatory element, which in this case is a 3′ pseudoknot (Fig. 1). The slippery sequence we used was UUUAAAG rather than UUUAAAC found in IBV, because XXXAAAG is found to be a more efficient slippery sequence in *Escherichia coli* (7), the organism we used for the measurements of *in vivo* frame shift efficiencies.

The choice of model pseudoknot was inspired by the work of Napthine *et al.* (20). They measured frameshift efficiencies in rabbit reticulocyte extracts of a series of IBV-derived pseudoknots with different lengths of stem1 sequences. Remarkably, frameshift efficiencies decreased 7-fold when the length of stem1 was reduced from the wild-type length of 11 bp to 10 bp. However, when the Napthine *et al.* (20) performed a structure probing analysis, both RNAs formed pseudoknots and appeared indistinguishable in conformation. Also, the predicted ΔG for stem1 of the wild-type IBV and IBV-derived pseudoknots with 11 bp and 10 bp stem1 did not correlate with the differences in frameshifting efficiency (20). In this work, we chose to compare two IBV-like pseudoknots with 11 bp and 10 bp in their stem1 (see Fig. 1 and *Materials and Methods*). For those two pseudoknots, we examined the frameshift efficiency *in vivo* and the mechanical stability in single molecule experiments. Rather than using the exact same structures as Napthine *et al.*, the pseudoknots in this work have longer loop2 sequences, as in the wild-type IBV pseudoknot. Apart from making our experiments closer to the wild-type situation, this also increased the difference in length for folded and unfolded pseudoknots for easier spatial detection.

Pseudoknot Stimulated Frameshifts in *E. coli*. Three plasmid constructs were made for measurements of frameshift efficiencies. All three encode the slippery sequence and a 6-nt spacer (Fig. 1). This sequence is followed by either a pseudoknot with 11 bp in stem1, a pseudoknot with 10 bp in stem1, or no pseudoknot as a control. The shortest pseudoknot is henceforth named "PK400," the longer pseudoknot is named "PK401," and the control is named "PK421." DNA oligonucleotides encoding these elements were inserted in the end of an *orf* that originates from bacteriophage T7 *gene10* (see *Materials and Methods*). Translation of the *gene10 orf* and the slippery sequence without frameshift will lead to termination at a UAA stop codon in the spacer between slippery sequence and the pseudoknot. The result is the release of a 28-kDa termination product. If the ribosomes shift to read the −1 frame at the slippery sequence, the UAA stop codon is out of frame, and translation continues through the pseudoknot and into a *lacZ orf*. The −1 frame shift allows continuous translation to the end of the *lacZ orf* and results in a 147-kDa frameshift product. The relative amounts of termination and frame shift products were used to estimate the frameshift frequencies. The proteins were metabolically labeled by addition of [^{35}S]methionine in pulse–chase experiments with cultures of *E. coli* expressing the individual constructs (see *Materials and Methods*). After harvesting the cultures, the proteins were separated by gel electrophoresis and visualized by autoradiography (Fig. 2). Prominent bands corresponding to the termination and frameshift products were identified by comparison of proteins harvested from IPTG-induced and uninduced

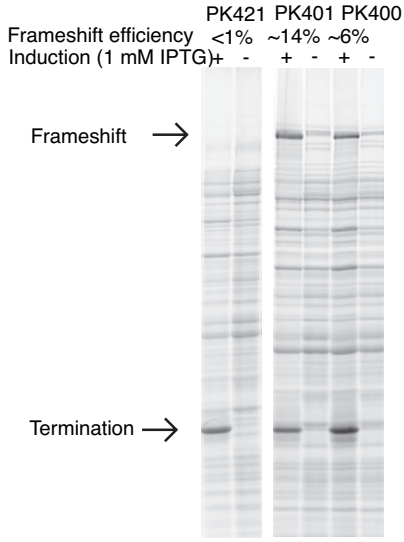

Fig. 2. Frameshift assay. Autoradiogram of SDS-polyacrylamide gel showing proteins metabolically labeled by [^{35}S]methionine. Expression from plasmids of genes encoding frameshift sites are induced by the presence of IPTG. For the constructs encoding pseudoknots, PK400 or PK401, induction leads to synthesis of two proteins (see arrows): one protein from ribosomes terminated at the zero frame stop codon, which follows the slippery sequence, and another protein from ribosomes which frameshifted to the −1 frame. Only the termination product is detected for the construct with no pseudoknot, PK421. Percent frameshift is given above each lane.

cultures. IPTG is a specific inducer of transcription from the *ptac* promoter driving the expression of the plasmid encoded hybrid T7 gene*10*::*lacZ* gene fusions. The presence of the frameshift products in cultures of PK400 and PK401 indicates efficient ribosomal frameshift with the pseudoknots encoded in the construct. However, for the control culture, containing the gene fusion without a pseudoknot, only the shorter termination product could be detected thus confirming the dependency of frameshifting at slippery sequences on the presence of stimulatory pseudoknots. The frameshift frequencies were quantified by measuring the relative amounts of frame shifted and terminated proteins in the individual lanes (see *Materials and Methods*). We found that the PK401 construct, encoding the pseudoknot with an 11-bp stem1, as in the wild-type IBV pseudoknot, gave the highest frequency of frameshift, namely 14 ± 1.5% (mean ± SEM). The pseudoknot with the shorter 10-bp stem1 yielded 5.9 ± 0.40% frameshift, a >2-fold reduction caused by a difference by a single base pair in stem1. The PK421 control construct, which does not contain a pseudoknot, yielded a frameshift frequency below our detection limit of ≈0.5% frameshift.

Mechanical Unfolding and Refolding of Pseudoknots. The mechanical unfolding of pseudoknots was performed with an optical trap by exerting a stretching force on individual mRNA molecules containing the structure-forming sequences.

Tethers of RNA pseudoknots PK400 or PK401 with DNA handles were formed (see *Materials and Methods*) with one end of the tether specifically attached by a biotin–streptavidin bond to a bead held by an optical trap while the other end of the tether was specifically attached by a digoxygenin–antidigoxygenin bond to another bead held by a micropipette (Fig. 3). The optical trap and the detection system has been described (21, 22) and were used to measure the forces acting on the bead in the trap. The optical tweezers exert a harmonic force, F_{trap}, on the trapped particle, $F_{trap} = k_{trap}\, x$, where x is the deviation from the equilibrium position and k_{trap} is denoted the trap stiffness. For

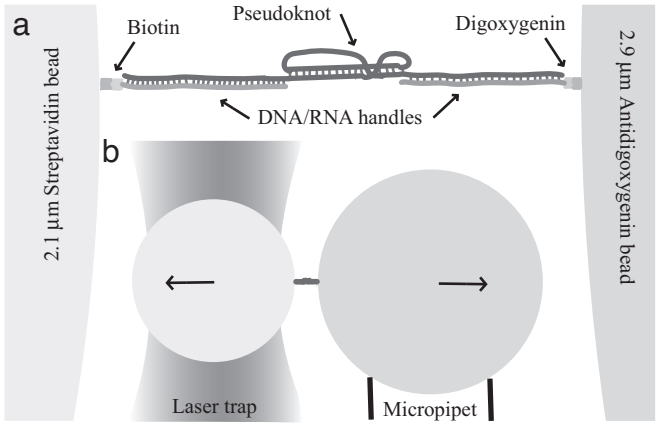

Fig. 3. Mechanical stretching setup. Schematic drawing of the experiment. (*a*) The RNA with complementary DNA handles is attached to beads with biotin-streptavidin and digoxygenin-antidigoxygenin bonds. The RNA/DNA heteroduplexes are 426 and 415 bp, respectively, and leave the middle region of the RNA free to form tertiary structures. The possible nucleotide sequences of the middle region are listed in Fig. 1*a*. (*b*) One bead is placed in the force measuring laser trap, whereas the other bead is attached to a micropipette. The micropipette was moved with respect to the laser trap to stretch and relax the molecule. The image is drawn to scale.

the positions visited by the bead in the trap, k_{trap} can be considered constant and found by proper calibration (22, 23). Hence, with x measured F_{trap} is also known. During a stretching or relaxing experiment, the trap was stationary while the micropipette was moved by a piezo electric stage. Several cycles of stretching and relaxing were performed for each molecule.

Fig. 4 shows typical force-extension curves from stretching and relaxing cycles of the two pseudoknots PK400 and PK401 as well as of the PK421 control. However, the stretching–relaxing curves can have quite different appearances, and more curves are shown in supporting information (SI) Figs. 6 and 7. For PK400, the rip-data presented stems from 32 stretching curves and for PK401 100 rip events were analyzed. For both PK400 and PK401, a sudden elongation of the molecules is observed in the stretching curve at 31 ± 1.9 pN and 39 ± 1.5 pN (mean ± SEM),

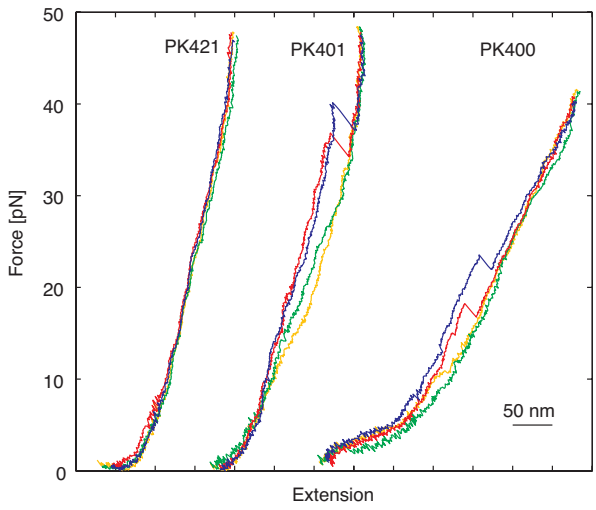

Fig. 4. Stretch and relax curves of single molecules. Force and change in extension were measured in several cycles of stretching and relaxing of a single molecule. Here, data from two cycles are shown for pseudoknot containing RNA, PK400 and PK401, and for the no-pseudoknot control PK421. Red, first stretch; yellow, first relax; blue, second stretch; green, second relax.

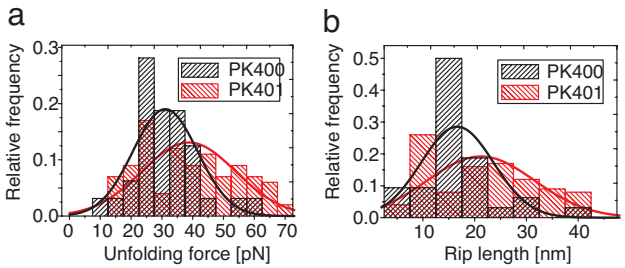

Fig. 5. Histograms of unfolding forces and rip lengths. The distributions of unfolding forces (*a*) and rip lengths (*b*) are shown in histograms. The values were estimated from individual stretching curves of PK400 and PK401 RNAs. Also, Gaussian curves are drawn by using the calculated mean and standard deviation from the data sets.

respectively, corresponding to an unfolding of the pseudoknot. The distributions of unfolding forces are shown in Fig. 5*a*. Henceforth, this sudden elongation will be termed a rip. A Student's *t* test showed that the rupture force of PK400 is significantly lower than the rupture force of PK401. At the loading rate used (≈10 pN/s), the variation in unfolding forces was relatively broadly distributed with standard deviations of 10 and 15 pN for PK400 and PK401, respectively. We used only two criteria to determine whether the structure being stretched was, indeed, an RNA tether containing a pseudoknot; however, other criteria were also tested (see *Materials and Methods*). The final numbers of the average unfolding forces depended slightly on the chosen criteria, but regardless of the criteria used, the unfolding force of PK400 was always significantly lower than the unfolding force of PK401.

Most often, only one rip is observed in the stretching and relaxing curves, thus indicating that the pseudoknots seemed to unfold in a single step. Only in 4 of the 32 analyzed stretching traces originating from PK400 a close inspection of the force versus time traces shows an intermediate state (SI Fig. 6). For these traces, it is noteworthy that, consistently in all data sets, the first unfolding part is longer (12 nm ± 2.4 nm) than the second (9 nm ± 2.8) (mean ± SD), although the difference is not statistically significant. None of the 100 analyzed traces from unfolding of PK401 showed an intermediate state.

Qualitatively, the relaxation curves differ substantially. For both pseudoknots, we grouped the relax traces into five categories, depending on how the relax curve fitted with the corresponding stretching curve: (*i*) One clear re-folding transition, (*ii*) one smaller refolding event plus a gradual refolding (SI Fig. 7*a*), (*iii*) two clear refolding events (SI Fig. 7*b*), (*iv*) only gradual and slow refolding (SI Fig. 7*c*), and (*v*) none of the others. The distribution of relaxation curves into these categories is given in Table 1.

Clearly, the category *iii* in Table 1 shows that in a substantial fraction of the refolding traces, there are two distinguishable events. For PK401, these two distinguishable events happen at 9 ± 4 pN and 19 ± 4 pN (mean ± SD), respectively. This might originate from a two step refolding of the pseudoknot, folding, e.g., stem 1 first and then stem 2. The refolding data from PK400 was too sparse to allow for a similar analysis of the forces.

Rip Lengths. Fig. 5*b* shows the distribution of riplengths during unfolding of the pseudoknots. The mean rip lengths were 17 ± 1.2 nm for the PK400 and 21 ± 1.0 nm (mean ± SEM) for the PK401 pseudoknots. These values are also given in Table 2 in the R_{exp} column. A Student's *t* test shows that these numbers are significantly different.

Because the standard worm like chain (WLC) model (24) only holds for the forces below 10 pN, the extensible worm like chain (EWLC) model inspired by Odijk (25) was used in this analysis. According to the EWLC model, the force-extension relation can be written as (26)

$$F = \frac{k_B T}{L_P}\left(\frac{1}{4(1 - x/L + F/K)^2} - \frac{1}{4} + x/L - \frac{F}{K}\right), \quad [1]$$

where k_B, T, K, L_P, x, and F are Boltzmann constant, absolute temperature, stretch modulus, persistent length, end to end distance, and stretching force, respectively. A theoretical estimation of rip length was calculated from Eq. **1**, setting the stretch modulus K to 1 nN (26), the persistence length L_P to 1 nm (27) and the contour length of single-stranded RNA L to 0.59 nm/nt (27). The original spatial extension of the pseudoknots was calculated by approximating their 3D structure as helixes of 16 and 17 bp with a rise of 0.28 nm/bp as in a canonical RNA A-helix (28). The pseudoknots and RNA/DNA duplex handles are much stiffer than the rest of the structure and were treated as nonelastic. Based on these approximations, the predicted rip lengths, R_{theory}, are 27.8 and 30.1 nm for pseudoknots PK400 and PK401, respectively. Thus, the observed rip length is substantially shorter than the predicted rip length.

Discussion

In this work, two pseudoknots, differing only by 3 nt, have been compared by single-molecule stretching experiments and a ribosomal frameshift assay in living cells. The pseudoknots efficiently stimulated frameshift *in vivo* with a 2-fold difference in frequency. It seems reasonable that frameshifting efficiency does not depend on the pseudoknot only, but also on the primary sequence and the context, e.g., the slippery sequence, the spacing, and the translation system including ribosomes and tRNAs. Thus, a 7- to 8-fold difference was observed when a set of pseudoknots, resembling PK400 and PK401, was tested by *in vitro* translation in a mammal (rabbit) reticulocyte lysate (20).

In an attempt to mimic the action of a ribosome, RNA tethers including one of the two pseudoknots were mechanically unfolded using optical tweezers. The unfolding happened most often in a single step and the unfolding forces were found to be significantly different for the two pseudoknots. The pseudoknot giving rise to the highest degree of frameshifting (PK401) also demanded for the largest unfolding force. Hence, the unfolding force appears to correlate with the degree of frameshifting that the pseudoknot gives rise to. The "looser" pseudoknot, PK400, was seen occasionally (in 12.5% of the cases) to unfold through an intermediate step. The unfolding distances of the two steps were almost equal and in

Table 1. Nature and distribution of refolding traces

Type of knot, no. of traces	One clear step, %	One smaller step plus gradual refolding, %	Two clear refolding steps, %	Only gradual refolding, %	None of the other categories, %
PK400, $n = 22$	5.7	26	8.0	39	22
PK401, $n = 73$	25	20	18	28	8.9

Table 2. Experimental and calculated thermodynamical parameters for mechanical unfolding of the two RNA pesudoknots

Pseudoknot	ΔG^0_{theory}, kJ/mol	$W_{str,theory}$, kJ/mol	$\Delta G_{total,theory}$, kJ/mol	R_{theory}, nm	R_{exp}, nm	W_{total}, kJ/mol
PK400	151	111	262	27.8	17 ± 1.2	317 ± 48
PK401	165	127	292	30.1	21 ± 1.0	501 ± 36

ΔG^0_{theory} is the standard Gibbs free energy of unfolding the pseudoknot at 37°C in 1 M Na^+ obtained from http://bibiserv.techfak.uni-bielefeld.de/pknotsrg/. $W_{str,theory}$ is the calculated work it takes to stretch the RNA tether from zero to the unfolding force using Eq. **1**. $\Delta G_{total,theory} = \Delta G^0_{theory} + W_{str,theory}$. R_{theory} is the calculated change in length of the RNA tether during the unfolding process, and R_{exp} is the similar value experimentally measured. W_{total} is the area underneath the $F - x$ curve during unfolding.

accordance with, for example, first the unfolding of stem2 and thereafter stem1. For PK401, the mechanically "stronger" pseudoknot, no similar intermediates were observed in the rip characterizing the unfolding. More often, the refolding traces, of both PK400 and PK401, showed intermediate steps.

The control molecule with no pseudoknots encoded was found to yield stretch and relax curves without rips but otherwise identical to the pseudoknot containing RNAs (Fig. 4). Seen from a polymer physics point of view, the force-extension behavior of the control tether is nontrivial, as it consists of two DNA–RNA hybrid handles with a small section in the middle consisting of ssRNA (27 nt). The contour lengths of the DNA–RNA handles are only a few times their persistence lengths, and hence, it does not make sense to fit worm-like chain or similar theories to this part of the data.

Thermodynamics. The total work of unfolding the pseudoknot was found from the experimental data as the area under force-extension curve at the unfolding region, the obtained values are given as W_{total} in Table 2. During the process, the pseudoknot is both unfolded and somewhat stretched by the applied force. W_{total} includes both the irreversible and reversible parts of the work of the unfolding process as well as the work of stretching the single-stranded RNA segment at that particular force. This experimentally obtained total work can be compared with the theoretically predicted estimates of the free-energy cost of unfolding a pseudoknot plus stretching it; theoretical estimates of the change in free energy of unfolding the structures, $\Delta G°_{theory}$, were calculated by the *pknotsRG* algorithm (ref. 29 and http://bibiserv.techfak.uni-bielefeld.de/pknotsrg/), which works at 37°C and 1 M Na^+ (results are shown in Table 2). The experimental conditions were somewhat different, namely, 20°C, 10 mM Tris·HCl (pH 7.5), 250 mM NaCl, and 10 mM Mg_2Cl. A theoretical estimate of the work of stretching the unfolded RNA tether, $W_{str,theory}$, from zero to it's extension at the unfolding force was calculated by integration of Eq. **1** with respect to extension (27) (see Table 2 for results). The $\Delta G_{total,theory}$ column of Table 2 shows the total energy, $\Delta G°_{total,theory} = \Delta G°_{theory} + W_{str,theory}$, which on theoretical grounds is expected to go into the unfolding and stretching process. Comparing $\Delta G°_{total,theory}$ to the experimentally obtained W_{total}, it is clear that the latter is much larger, thus implying that a significant amount of the performed work is dissipated irreversibly under the unfolding/stretching process where the loading rate was ≈10 pN/s. It is striking that the measured W_{total} (Table 2) is the only parameter in Table 2 that yields a difference between the two pseudoknots that is comparable to the 2-fold difference between the *in vivo* frame shifting effects of the same pseudoknots.

Models for Pseudoknot-Stimulated Frameshifting. The fact that the difference in unfolding forces correlates positively with frameshift frequencies for the two pseudoknots investigated is consistent with the 9 Å model of frameshift stimulation. This model builds on the possible resistance of the pseudoknot to unfold at its entrance into the mRNA channel of the ribosome. The pseudoknot is thought to block the translation pathway and force the ribosome to slip one base downstream at the slippery sequence to adapt to the physical obstacle. This step normally causes a 9-Å allosteric-induced movement in the ribosome upon GTP hydrolysis at the incoming ternary complex in the translational cycle (13). Recently, this model has found support from structural cryo-electromicroscopic observations that interaction between a ribosome and a pseudoknot causes a deformation of the A-site tRNA (30).

Indeed, the work we found necessary to unfold our pseudoknots by stretching (see Table 2) was much greater than the energy that can be obtained by hydrolysis of GTP into GDP + Pi (≈35 kJ/mol). Thus, we expect that unfolding the pseudoknot can be an energetic barrier to the movement of the ribosome, and that this is the reason why the frequency of frameshifting positively correlates to the mechanical strength of the tertiary structure. In comparison to a simple hairpin structure, the pseudoknot has lost its rotational freedom in the stem1 helix due to the "locking" via base pairing in stem2. This locking may cause a need for more base pairs to be broken simultaneously, probably in stem2, before the structure resolves. This process may involve ribosome associated RNA helicases (30, 31) at least in some organisms.

Opposed to the suggested pausing at pseudoknots, hairpin structures have been shown not to slow down ribosome movement *in vivo* (32) and unable to assist frameshifting in IBV (13). Nevertheless, the downstream stimulatory structure in the *E. coli dnaX* frameshift is a hairpin, and a correlation between frameshift efficiency and the predicted strength ($\Delta G°$) of different mutant hairpins have been found (34). Presently, theoretical estimates of hairpin stability might be more precise than those of the more complex pseudoknots. Indeed, for a hairpin, $\Delta G°$ values from reversible mechanical unfolding matched theoretical estimates (16). Regardless of the extent and role of pausing in frameshifting, the results of Larsen *et al.* (34) support the finding that downstream mRNA structure strength correlates with the ability to stimulate frameshift on a slippery sequence.

Naptine *et al.* (20) investigated the effect on frameshifting on shortening the length of stem1 of a pseudoknot, and they found the frameshifting efficiency to be closely related to the length of this stem, if shorter than 11 bp, essentially no frameshifting was observed. Among other effects investigated (e.g., slippery sequence-pseudoknot spacing distance), they found the length of stem1 to be most important. This finding is in accordance with our observations, where we postulate that the mechanical stability of the pseudoknot, which is also determined by the length of, for example, stem1, is crucial for the degree of frameshifting.

In another class of frameshift-stimulating pseudoknots, the stem1 is as short as 5–7 bp. The function of these pseudoknots in frameshifting seems to depend on an extra loop2–stem1 interaction that facilitates a special kinked tertiary structure (19). To our knowledge, it remains to be determined whether this extra loop2–stem1 interaction increases the physical strength of this particular class of pseudoknots.

In conclusion, we find that two pseudoknots stemming from the frameshifting site in IBV and differing only in 3 of 68 nucleotides give rise to a factor of 2 difference in frameshifting frequencies. Unfolding the structure by optical tweezers shows that the two structures unfold at forces that are different; the pseudoknot giving rise to the lower degree of frameshifting is easier to unfold than the pseudoknot giving rise to the higher degree of frameshifting. This finding leads us to propose that the frameshifting efficiency of a given pseudoknot is correlated to its mechanical strength. In the future, this postulate should be supported with similar experiments on a variety of pseudoknots. Our observations and postulates are in accordance with the 9 Å model (13) and with the mechanical explanation of pseudoknot function suggested by recent cryoelectronmicroscopy observations (30).

Materials and Methods

Plasmids and Frameshift assay. Plasmids encoding the sequences shown in Fig. 2 were made by inserting synthetic DNA oligomeres, containing the sequences, between unique HindIII and ApaI restriction endonuclease sites in pOFX302 (33) and verified by DNA sequencing.

The frequencies of ribosomal frameshifting were estimated in protein extracts from cells labeled in pulse labeling experiments. See *SI Text*.

Preparation of the Samples for Single-Molecule Experiments. RNA was synthesized *in vitro* by T7 RNA polymerase as recommended by the manufacturer (Promega). First, DNA templates for the RNA synthesis were produced by PCR. Plasmids pTH400, pTH401, or pTH421 served as template in the PCRs. Primers were TH412: ATAATTCGCGTCTGGCCTTC and TH414: TAATACGACTCACTATAGGGAGAGTATACCTCTCAGTTGGGTG. The 5′ end of TH414 contains the T7 promoter (underlined). Run-off RNA synthesis are expected to produce 939-, 942-, or 876-nt RNA strands from the three templates.

Upstream and downstream handles DNA were each synthesized by assymetric PCR. The downstream handle DNA had a digoxygenin group on its 5′ nucleotide, and the upstream handle was labeled with biotin in its 3′ end enzymatically (see *SI Text* for details). Handles were annealed to RNA by mixing approximately equal amounts of the nucleotide species in buffer R (10 mM Tris·HCl, pH 7.5/250 mM NaCl/10 mM Mg_2Cl) or in 10 mM sodiumphosphate (pH 6.0), 250 mM NaCl, and 10 mM Mg_2Cl. The mixture was heated to 65°C for 8 min and allowed to cool down to room temperature for >30 min. Annealed RNA and handles were stored at −70°C until usage. To bind the handle/RNA to beads, appropriate dilutions of the handle/RNA mixture and 2.1-μm streptavidin-coated polystyrene beads (Bangs) were mixed and incubated for 1 h at room temperature with gentle mixing. The ratio of handle/RNA to 2.1-μm beads was chosen so that no more than approximately four of the five beads would later form a tether (see *SI Text*) to the 2.88-μm anti-digoxygenin-coated bead. This criterion insures a low likelihood of getting tethers of more than one handle/RNA molecule. After binding the RNA to the 2.1-μm beads, the mixture was diluted in a dilution of 2.88-μm anti-digoxygenin-coated beads and transferred to the sample chamber for the microscope. Experiments were performed at 22°C.

Data Analysis. The stage signal was smoothed with a sliding window 3,000 data points wide, before the time series were averaged in 10-ms nonoverlapping windows. The force exerted on the bead in the trap and its position were calculated by using both coordinates of the quadrant photodiode, whereas the first point of the time series was defined as origin for the coordinate system. The change in tether length was calculated by subtraction of the movement of the bead in the trap from the stage movement.

Due to the short overall length of the tether, it is difficult by eye to decide whether an RNA tether is present between the two beads; if the beads are connected, this could also be due to the van der Waals attraction between them, caused by a polystyrene "hair" sticking out of one of the beads or simply some kind of dirt in the sample. To avoid "false" tethers/attractions between the beads in our data set, all data sets were subject to two filtering criteria: (*i*) The first part, i.e., the first 250 ms, of the force-extension curve needs to be flat (slope less than ± 50 nm/s). This filter would remove tethers that were too short. (*ii*) The "noise" of the first part (250 ms), of the curve should not be zero, more precisely, traces for which the standard deviation was between 3.5 and 7 nm passed this filter. These criteria made sure that the cases where the two beads were attached to each other did not pass. Other filters were also tested (e.g., only using data showing rips, only using data where we had force measurements >70 pN), but regardless of how these criteria were chosen, the rupture forces of the two different pseudoknots were consistently significantly different. Thus, this is a very robust result. The presented data represent repetitive pulls of at least eight individual molecules of each of the pseudoknots PK400, PK401, or the control PK421.

We thank Stanley Brown for suggestions and helpful discussions and John Atkins for comments on the manuscript. This work was supported by grants from the Carlsberg Foundation, BioNET sponsored by the Villum Kann Rasmussen Foundation, and the Faculty of Science, University of Copenhagen.

1. Ninio J (1975) *Biochimie* 57:587–595.
2. Rodnina MV, Gromadski KB, Kothe U, Wieden HJ (2005) *FEBS Lett* 579:938–942.
3. Atkins JF, Elseviers D, Gorini L (1972) *Proc Natl Acad Sci USA* 69:1192–1195.
4. Kurland CG (1979) in *Nonsense Mutations and tRNA Suppressors*, eds Celis JE, Smith JD (Academic, London), pp 98–108.
5. Farabaugh PJ (1996) *Microbiol Rev* 60:103–134.
6. Gesteland RF, Atkins JF (1996) *Annu Rev Biochem* 65:741–768.
7. Weiss RB, Dunn DM, Shuh M, Atkins JF, Gesteland RF (1989) *New Biol* 1:159–169.
8. ten Dam E, Brierley I, Inglis S, Pleij C (1994) *Nucleic Acids Res* 22:2304–2310.
9. Rice NR, Stephens RM, Burny A, Gilden RV (1985) *Virology* 142:357–377.
10. Kontos H, Napthine S, Brierley I (2001) *Mol Cell Biol* 21:8657–8670.
11. Tu C, Tzeng TH, Bruenn JA (1992) *Proc Natl Acad Sci USA* 89:8636–8640.
12. Plant EP, Dinman JD (2005) *Nucleic Acids Res* 33:1825–1833.
13. Plant EP, Jacobs KL, Harger JW, Meskauskas A, Jacobs JL, Baxter JL, Petrov AN, Dinman JD (2003) *RNA* 9:168–174.
14. Noller HF, Yusupov MM, Yusupova GZ, Baucom A, Cate JH (2002) *FEBS Lett* 514:11–16.
15. Giedroc DP, Theimer CA, Nixon PL (2000) *J Mol Biol* 298:167–185.
16. Liphardt J, Onoa B, Smith SB, Tinoco IJ, Bustamante C (2001) *Science* 292:733–737.
17. Onoa B, Tinoco I, Jr (2004) *Curr Opin Struct Biol* 14:374–379.
18. Brierley I, Digard P, Inglis SC (1989) *Cell* 57:537–547.
19. Liphardt J, Napthine S, Kontos H, Brierley I (1999) *J Mol Biol* 288:321–335.
20. Napthine S, Liphardt J, Bloys A, Routledge S, Brierley I (1999) *J Mol Biol* 288:305–320.
21. Berg-Sorensen K, Oddershede L, Florin EL, Flyvbjerg H (2003) *J Appl Phys* 93:3167–3176.
22. Oddershede L, Grego S, Nørrelykke SF, Berg-Sorensen K (2001) *Probe Microscopy* 2:129–137.
23. Hansen P, Tolic-Norrelykke I, Flyvbjerg H, Berg-Sorensen K (2006) *Comput Phys Commun* 174:518–520.
24. Marko JF, Siggia ED (1995) *Macromolecules* 28:8759–8770.
25. Odjik T (1995) *Macromolecules* 28:7016–7018.
26. Vanzi F, Takagi Y, Shuman H, Cooperman BS, Goldman YE (2005) *Biophys J* 89:1909–1919.
27. Tinoco I, Jr (2004) *Annu Rev Biophys Biomol Struct* 33:363–385.
28. Holbrook SR, Kim SH (1997) *Biopolymers* 44:3–21.
29. Reeder J, Giegerich R (2004) *BMC Bioinformatics* 5:104.
30. Namy O, Moran SJ, Stuart DI, Gilbert RJ, Brierley I (2006) *Nature* 441:244–247.
31. Takyar S, Hickerson RP, Noller HF (2005) *Cell* 120:49–58.
32. Sorensen MA, Kurland CG, Pedersen S (1989) *J Mol Biol* 207:365–377.
33. Rettberg CC, Prere MF, Gesteland RF, Atkins JF, Fayet O (1999) *J Mol Biol* 286:1365–1378.
34. Larsen B, Gesteland RF, Atkins JF (1997) *J Mol Biol* 271:47–60.

Supporting information for paper IV published on www.PNAS.org.

(Fig. 6-9 are printed after the Suppoting information text).

Fig. 6. Intermediate steps in the unfolding pathway of PK400.

Fig. 7. Examples of qualitatively different force-extension graphs showing both unfolding (black) and refolding traces (red).

Fig. 8. Distribution of experimentally obtained unfolding and refolding work distributions for 19 cycles from PK401 which refolded in a single step. Accordingly to Crooks theorem, the crossing point of the work distributions is identical to ΔG of the process.

Fig. 9. Fits to a kinetic equation. Function of fraction of pseudoknots which are unfolded below a particular force, P, plotted as a function of force accordingly to the kinetic equation (Eq. **2**). Full line shows a fit of Eq. **2** to the data, circles represent experimental values, dashed lines indicate 95% confidence intervals.

Table 3. Experimental and calculated thermodynamical parameters for mechanical unfolding of the two RNA pesudoknots

RNA	ΔG^0_{theory} kJ/mol	$W_{str,theory}$ kJ/mol	$\Delta G_{total,theory}$ kJ/mol	R_{theory} nm	R_{exp} nm	W_{total} kJ/mol	$\Delta G_{Jarzynski}$ kJ/mol	ΔG_{Crooks} kJ/mol
PK400	151	111	262	27.8	17±1.2	317±48	77.6	------
PK401	165	127	292	30.1	21±1.0	501 ± 36	94	104

ΔG^0_{theory} is the standard Gibbs free energy of unfolding the pseudoknot at 37 C in 1M Na+ obtained from http://bibiserv.techfak.uni-bielefeld.de/pknotsrg/. $W_{str,theory}$ is the calculated work it takes to stretch the RNA tether from zero to the unfolding force using equation 1. $\Delta G_{total,theory} = \Delta G^0_{theory} + W_{str,theory}$. R_{theory} is the calculated change in length of the RNA tether during the unfolding process, R_{exp} is the similar value experimentally measured. W_{total} is the area underneath the F-x curve during unfolding. $\Delta G_{Jarzynski}$ and ΔG_{Crooks} are the Gibbs free energies found by Jarzynski's and Crooks methods, respectively.

Discussion

Thermodynamics

A deeper understanding of the thermodynamics involved in the process is non-trivial. Firstly, because the unfolding happens as a non-equilibrium process with irreversibly dissipated energy, and secondly, because the recently developed methods for dealing with such systems (1-4) have not yet been reported successfully applied to systems which unfold through visible intermediate

conformations. In our case, a few percent of the unfolding and refolding events do exhibit the presence of such intermediate states. If we ignore this second problem and apply the method suggested by Jarzynski (3), we find the predicted free energy change of the process, $\Delta G_{Jarzynski}$, by an exponential weighing of individually found values of the total work going into the process. The result for PK400 and PK401 is shown in Table 3. Comparing $\Delta G_{Jarzynski}$ to ΔG^0_{theory} it is clear that the latter is largest. There can be several causes of this discrepancy: First, ΔG^0_{theory} is underestimated as it has been calculated for higher temperature and salt concentration. Second, due to the exponential weighing in Jarzynski's method, the left tail of the work distribution basically determines the value of $\Delta G_{Jarzynski}$. Invoking now the problem of the intermediates which are occasionally observed in the unfolding and refolding process, the fact that we use the first observed rip for our data analyses, might mean that we occasionally by chance use the work which only went into unfolding part of the structure, e.g., into unfolding stem 2, and as this work is lower than the work going into unfolding the total structure. This low work is dominating the outcome of Jarzynski's equation, it is likely that the value we see for $\Delta G_{Jarzynski}$ really only is the free energy going into unfolding part of the structure, e.g., stem 2. Also, we invoked Crooks method (2) which uses the distribution of the work from both unfolding and refolding curves to calculate ΔG_{Crooks}. Fig. 8 shows the distribution of work for 19 unfolding and refolding cycles of PK401 which refold in a single well defined step. ΔG_{Crooks} is determined as the crossing point of the folding and unfolding work distributions. Data were too sparse for a similar analysis of PK400. For PK401 $\Delta G_{Crooks} \sim \Delta G_{Jarzynski}$, but it must be emphasized that the employment of any of these methods for systems, where intermediates are observed, is at present not established and is awaiting further development of the theoretical tools. The ΔG's of unfolding RNA loops corresponding to the stems in the two pseudoknots at 37 C and 1M NaCl are: PK400 stem1 88.2 kJ/mol, PK400 stem2 25.6 kJ/mol, PK401 stem1 97.4 kJ/mol, and PK401 stem2 29.8 kJ/mol (using mfold v3.2 (5)). Comparing these numbers to first column of Table 3 (ΔG^0_{theory}) it is clear that unfolding a pseudoknot does not simply correspond to unfolding the two loops. Unfolding a tertiary structure craves more energy than unfolding the involved secondary structures.

In conclusion, it seems that none of the theoretical methods available for calculation of the pseudoknot stability can account for the amount of energy we found was needed to unfold the knots by stretching. It is striking, however, that the measured W_{total} is the only parameter in Table 3 that yields a difference between the two pseudoknots that is comparable to the two fold difference between the *in vivo* frame shifting effects of the same pseudoknots. Future experiments may show if this correlation between unfolding energies and stimulatory effects on framshifting is universal.

Kinetics

Kinetic parameters can be extracted from the repetitive unfolding of a single molecules at constant loading rate, r, as described in refs. 6 and 7. To do this, the probability, P, that the unfolding reaction has not occurred at forces lower than a particular force, F, was calculated from the distribution of unfolding forces. The relation between P and r is:

$$r \ln(1/P) = [k(0)k_BT / X^{\ddagger}][\exp(FX^{\ddagger}/k_BT)-1] \quad (2)$$

where k(0) is the apparent rate constant at zero force and $X^{\ddagger}$ being the distance to the transition state. Fig. 9 shows plots of r ln(1/P) versus F from the experimental unfolding of PK400 and PK401 as well as a fit of the above equation. For the pseudoknots we find very similar values of $X^{\ddagger}$,

namely $X^{\ddagger} = 0.18 \pm 0.06$ nm for PK400 and $X^{\ddagger} = 0.19 \pm 0.01$ nm for PK401. Comparing to literature, these values are rather low, thus implying that both pseudoknots are "brittle" structures which resist mechanical deformation but once they are deformed they easily fracture. Previously, secondary structures such as stem loops were shown to be compliant with $X^{\ddagger}$ values of 5-10 nm, whereas tertiary structures are brittle with $X^{\ddagger}$ values close to 1 nm (8, 9). Therefore, the pseudoknots resemble tertiary structure more than the related stem-loop secondary structures. The fitted values of the rate constant at zero force are $k(0) = 0.16 \pm 0.08\ s^{-1}$ for PK400 and $k(0) = 0.074 \pm 0.007\ s^{-1}$ for PK401. Employing a students *t* test, we found no significant difference between the k(0) for the two pseudoknots in our data sets.

Materials and Methods

Plasmids and Frameshift assay

The frequencies of ribosomal frameshifting were estimated in protein extracts from cells labeled in pulse labeling experiments. The strains used in these assays were derived by transformation of strain MAS90 (*E. coli* K-12, *recA1 Δ(pro-lac) thi ara F': lacI^{q1} lacZ::Tn5 proAB^{+}*) with pTH400, pTH401 and pTH421, respectively. Cultures were grown in Mops minimal media at 37°C for at least 8-10 generations in the log phase (10). Expression of transcription from the constructs was induced by addition of Isopropyl beta-D-Thiogalactopyranoside (IPTG). IPTG was added to 1 mM final concentration when the cultures reached a density of $0.4 - 1.6 \times 10^8$ cells/ml. The time of induction defines t = 0. At t = 15 min 10 μCi ^{35}S methionine were added to 1 ml culture. After 20 s, 100 μg of unlabeled methionine was added per ml culture, which is $\approx 10^5$ times molar excess to the previously added ^{35}S methionine. At t = 2 min the culture was moved to 0°C. The cells were harvested by centrifugation, boiled with SDS-sample buffer and the samples were analyzed with 8.75 or 10% SDS-PAGE. The gels where exposed to a Phosphor imager screen (Molecular Dynamics). ImageQuant software (Molecular Dynamics) was used to measure amounts of ^{35}S radioactivity in the bands. Counts found in bands induced by IPTG were normalized to the number of methionine residues expected in the products. The frameshift frequency was calculated as the ratio of frameshift product to the sum of frameshift product and termination product.

Preparation of the samples for single molecule experiments

Upstream and downstream handles DNA were each synthesized in a two step reaction. Primers for the upstream handle were TH416 GTATACCTCTCAGTTGGGTG and TH407 TGAATCCGCGGTACCAGCAC, whereas for the downstream handle they were TH415 CTAATTCACTGGCCGTCGTT and TH408 dig-ATAATTCGCGTCTGGCCTTC. For each handle, the first step was an asymmetric PCR reaction in the sense that the concentration of one of the primers, TH415 and TH416, was ten times reduced. In the second step the first step reaction was mixed with an equal volume of reaction mixture containing only one primer, TH407 or TH408. Otherwise the reactions were done at standard PCR conditions. The downstream handle DNA had a digoxygenin group on it's 5' nucleotide, since primer TH408 was synthesized with a digoxygenin on the 5' terminal nucleotide. The upstream handle was labeled with biotin in its 3' end enzymatically. For this terminal-deoxynucleotide-transferase and biotin-N4-CTP were used as recommended by the manufacturer (Pierce).

In the sample chamber for the microscope, the beads concentrations were adjusted to make sure, that the beads not used for the current experiment and hence free to move around in the chamber,

would not interfere with the measurements. Still it was possible to find enough beads in the chamber for several experiments. Dilutions were in buffer R.

Procedure

To form a tether between the two beads, first a 2.88 μm bead was trapped, then the pipette tip was moved near the bead, which was then released and attached to the pipette. Then a 2.1 μm bead was trapped. The beads were positioned about 10 μm apart but in the same depth by adjusting the stage position and microscope focus. A timeseries of the thermal fluctuation of the bead inside the trap was monitored to calibrate the optical trap. To form a tether between the two beads they had to be moved into close proximity of each other. First the centres of the beads were aligned on an axis parallel to the *x* axis of the piezo stage. To achieve that, the bead in the pipette was moved by manual control of the piezo stage's position while watching the images of the beads. The precision of this alignment was probably down to a hundred nanometers. The next step was to bring the beads in close distance, 50 nm or less, to make the formation of a tether likely within a few minutes. Distortion of the diode signal indicated close proximity of the beads. When a tether was formed this could be observed by an increase in the voltage signal from the quadrant photodiodes if one tried to move the pipette away. The RNA/DNA hybrid tether was stretched and relaxed in consecutive cycles. In one cycle the pipette was moved 600-800 nm at 100 nm/s and reverse while the quadrant photodiode signal and the stage position were sampled at 5 kHz. In the force range of pseudoknot unfolding the loading rate is nearly constant at about 10 pN/s.

Optical tweezers equipment

The optical trap equipment is based on a 1,064-nm $NdYVO_4$ laser and is implemented in an inverted Leica microscope with a quadrant photodiode back focal detection scheme, for a full description see (11). The water immersion objective (Leica, NA = 1.2) allowed for optical trapping at any depth within the sample. A laser power of 0.8 W, measured at the output of the laser, gave a trap stiffness in the range of 0.1-0.2 pN/nm. The trap stiffness and the conversion factor between the distance traveled by the bead in metric measured and the voltage output from the quadrant photodiode were estimated using a Matlab program (12), which takes into account aliasing and the filtering effect of the quadrant photodiode (13).

A micropipette with a tip diameter of ≈1 μm was pointing into the sample chamber. Suction could be applied to the pipette to firmly attach a bead to the tip. The pipette was immobilized with respect to the chamber, which was mounted on a two-dimensional translational piezoelectric stage (Physik Instrumente) with capacitive feedback control and nanometer position resolution. Data acquisition and control of the stage were performed using custom made Labview programs. Simultaneous control over piezo stage and output from the quadrant photodiode allowed for measurements of corresponding values of force and distance.

1. Collin, D., Ritort, F., Jarzynski, C., Smith, S. B., Tinoco, I., Jr. & Bustamante, C. (2005) *Nature* 437, 231-4.

2. Crooks, G. E. (1999) *Phys. Rev. E* 60, 2721-2726.

3. Jarzynski, C. (1997) *Phys. Rev. Lett.* 78, 2690-2693.

4. Liphardt, J., Dumont, S., Smith, S. B., Tinoco, I., Jr. & Bustamante, C. (2002) *Science* 296, 1832-5.

5. Zuker, M. (2003) *Nucleic Acids Res.* 31, 3406-15.

6. Evans, E. & Ritchie, K. (1997) *Biophys J* 72, 1541-55.

7. Tinoco, I., Jr. (2004) *Annu Rev Biophys Biomol Struct* 33, 363-85.

8. Liphardt, J., Onoa, B., Smith, S. B., Tinoco, I. J. & Bustamante, C. (2001) *Science* 292, 733-7.

9. Onoa, B. & Tinoco, I., Jr. (2004) *Curr Opin Struct Biol* 14, 374-9.

10. Rettberg, C. C., Prere, M. F., Gesteland, R. F., Atkins, J. F. & Fayet, O. (1999) *J. Mol. Biol.* 286, 1365-78.

11. Oddershede, L., Grego, S., Nørrelykke, S. F. & Berg-Sorensen, K. (2001) *Probe Microscopy* 2, 129-37.

12. Hansen, P., Tolic-Norrelykke, I., Flyvbjerg, H. & Berg-Sorensen, K. (2006) *Comput. Phys. Commun.* 174, 518-520.

13. Berg-Sorensen, K., Oddershede, L., Florin, E. L. & Flyvbjerg, H. (2003) *Journal of Applied Physics* 93, 3167-3176.

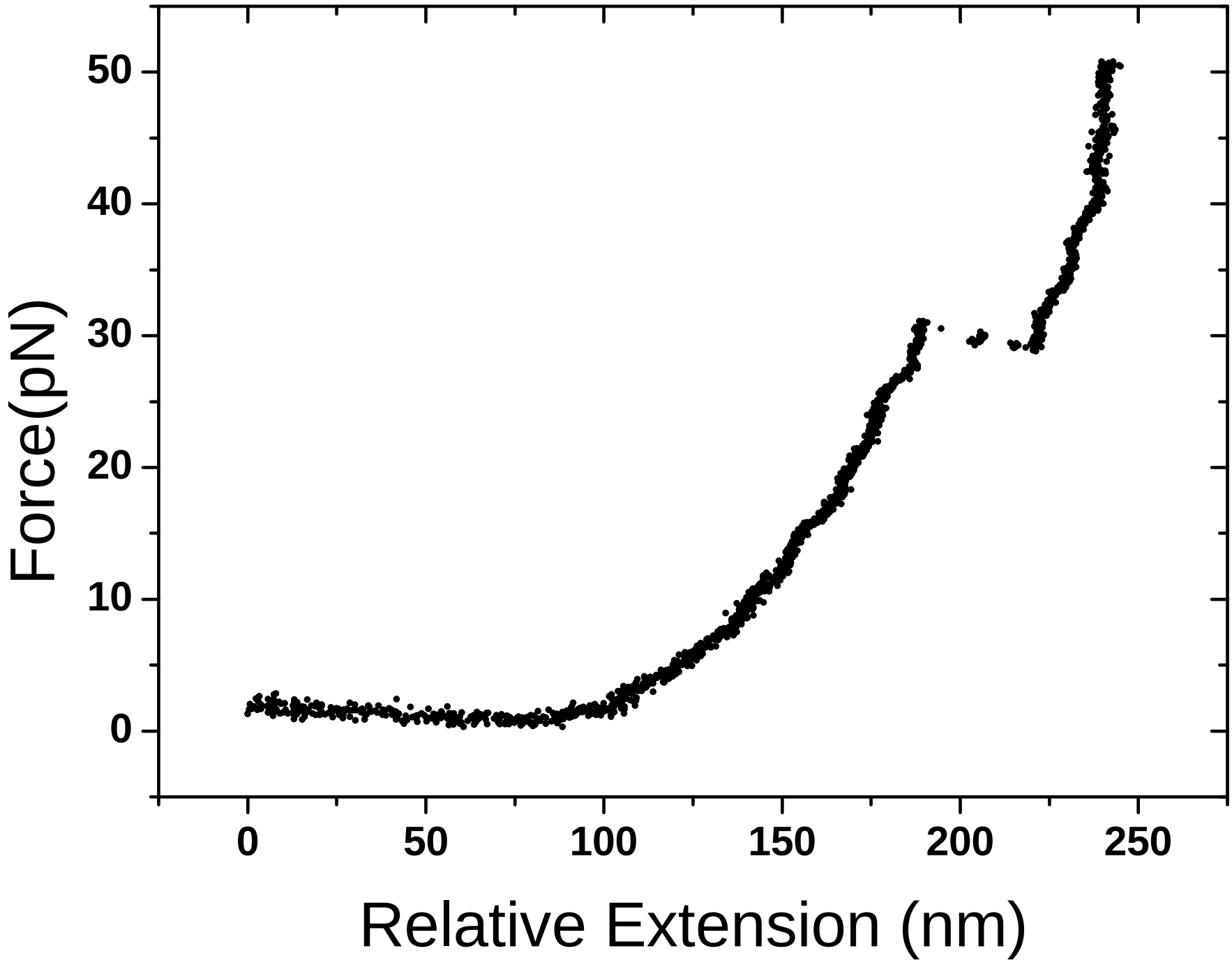
Force(pN)
50
40
30
20
10
0
0
50
100
150
200
250
Relative Extension (nm)

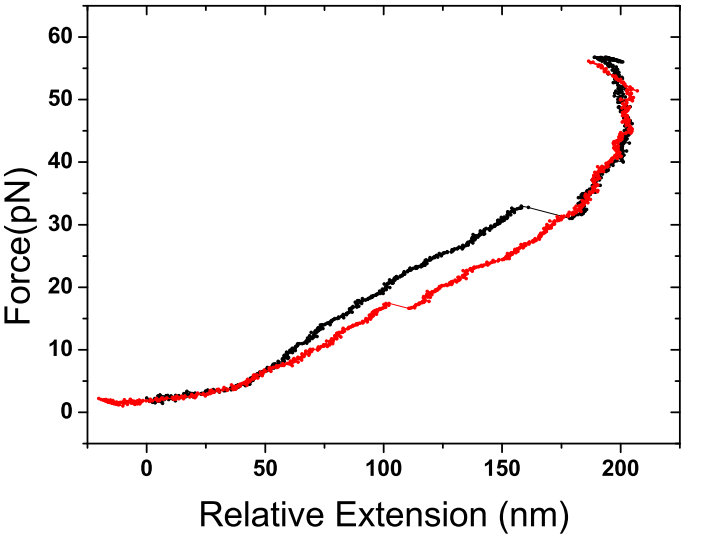
Force(pN)
0
10
20
30
40
50
60
0
50
100
150
200
Relative Extension (nm)

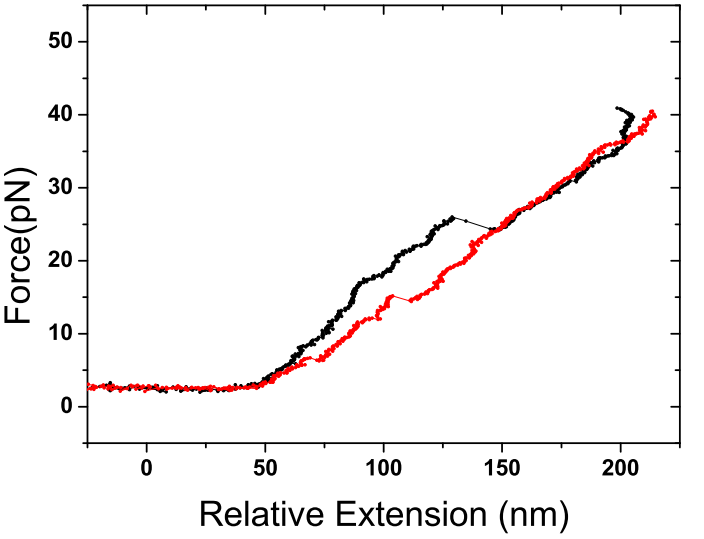
Force(pN)
0
10
20
30
40
50
0
50
100
150
200
Relative Extension (nm)

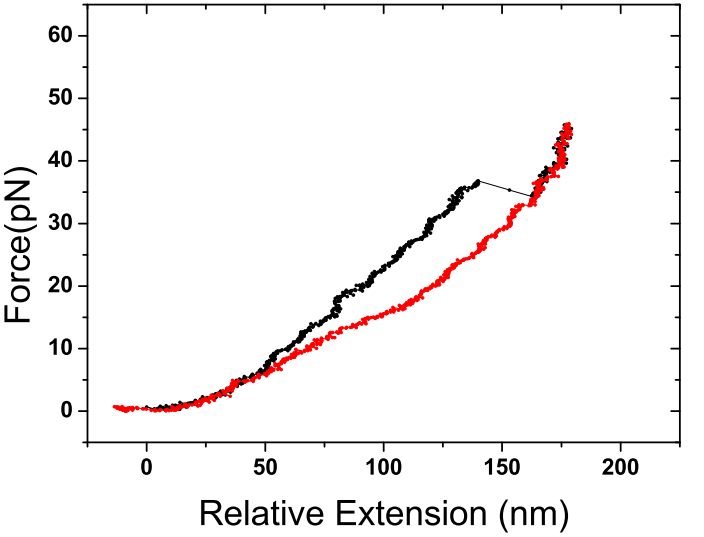
Force(pN)
0
10
20
30
40
50
60
0
50
100
150
200
Relative Extension (nm)

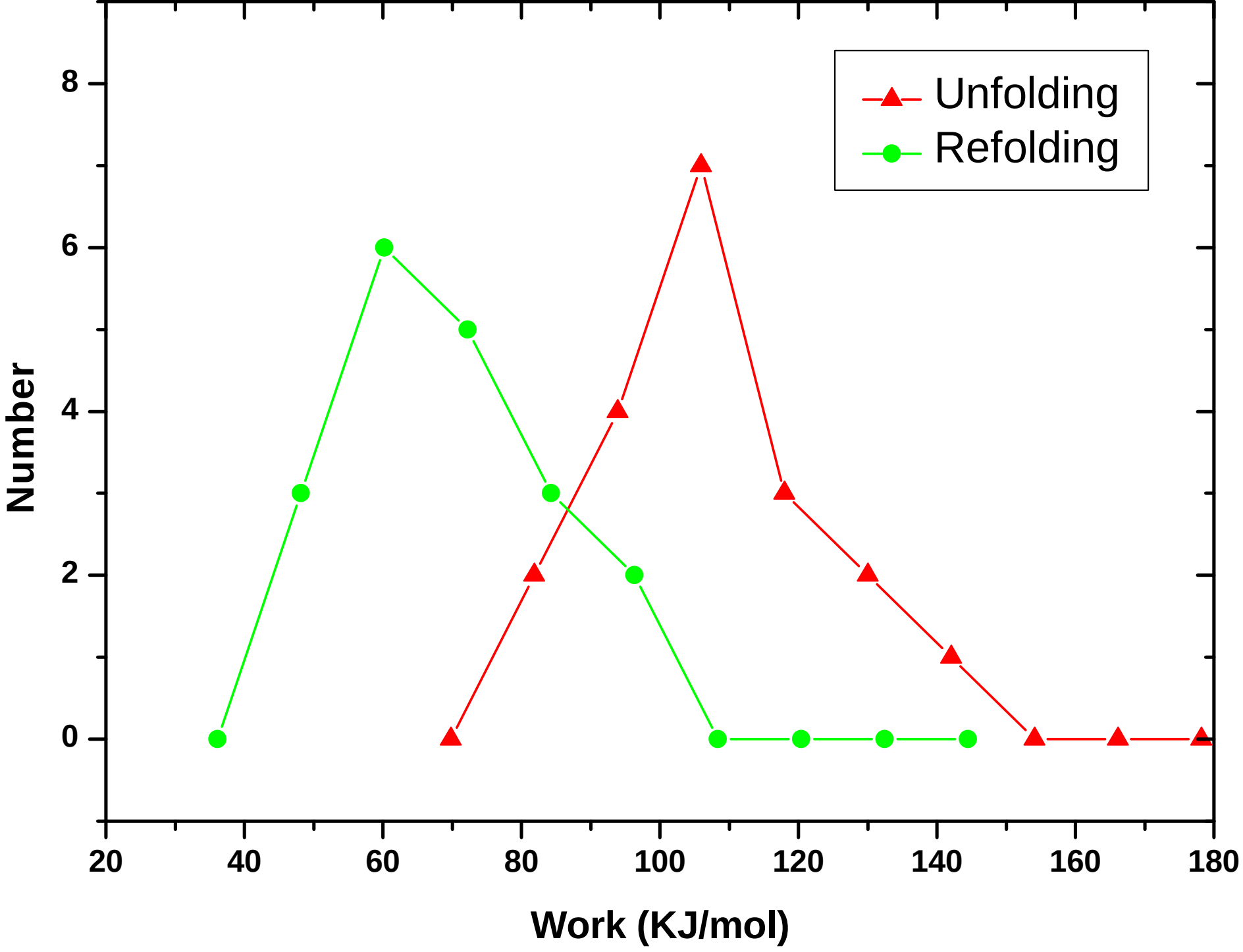
Unfolding
Refolding
Number
Work (KJ/mol)
0
2
4
6
8
20
40
60
80
100
120
140
160
180

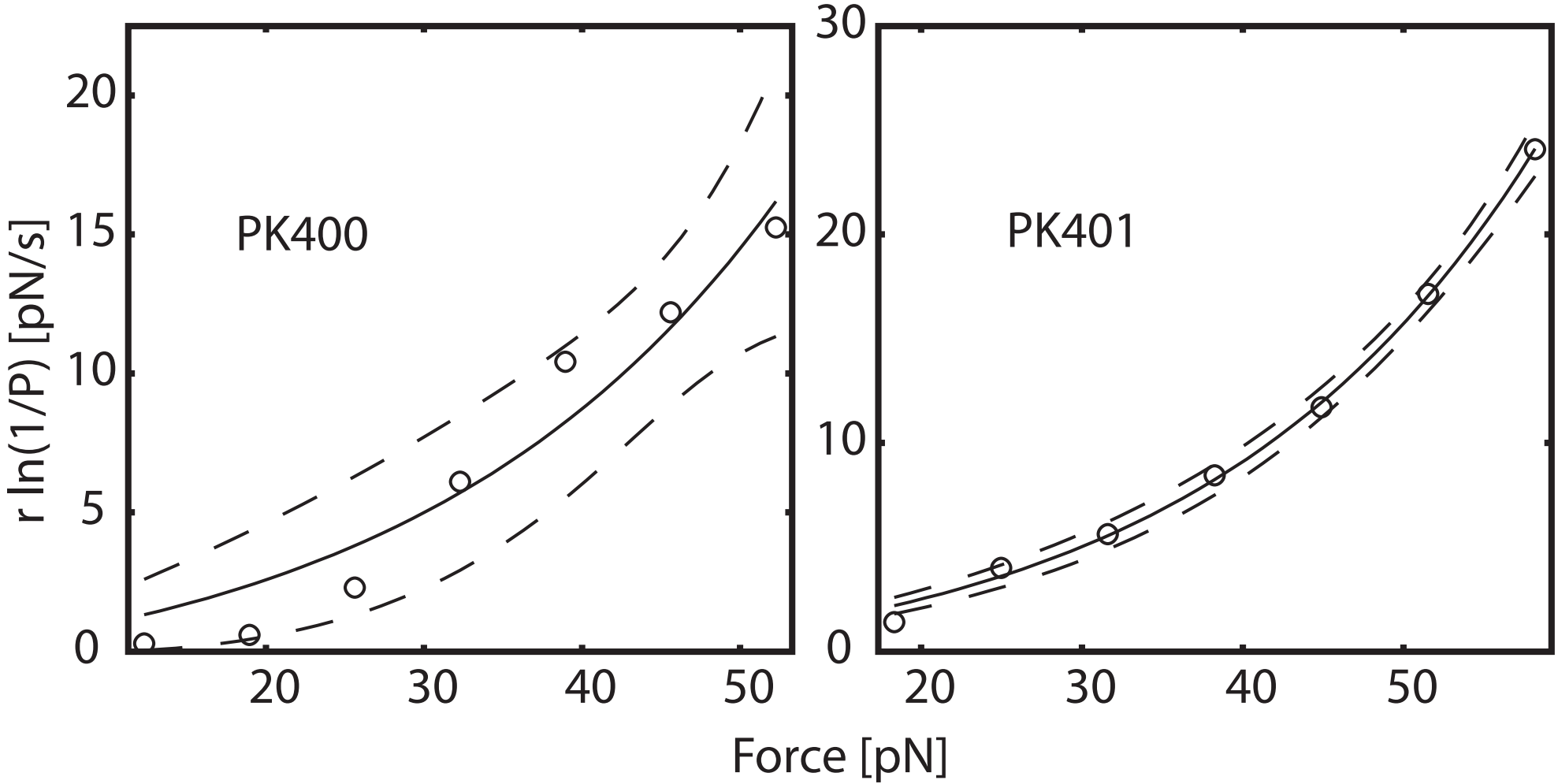
PK400
PK401
r ln(1/P) [pN/s]
Force [pN]
0
5
10
15
20
30
40
50